Targeting Glioblastoma Cells with Drug-Loaded Targeted Nanocarriers

Thesis

School of Life, Health and Chemical Sciences

Targeting glioblastoma cells by drug-loaded targeted nanocarriers

Marco Pizzocri

A Thesis submission to The Open University for the degree of Doctor of Philosophy
February 2021

Internal Supervisors:
Lorena Passoni, PhD
Proff. Michela Matteoli

External Supervisor:
Paul Mulholland, MD PhD

Abstract

Glioblastoma (GBM) is the most common and aggressive primary human brain tumor associated with very poor prognosis and survival (Stupp and Hegi, 2019). Despite ongoing research, the outlook on GBM remains quite disappointing with a median survival of ~15 months and 5-year survival rate less than 5%. The fact that treatment and prognosis have remained unchanged for fifteen years leads to the realization that there are major challenges that we have not been able to overcome. Challenges are fundamentally represented by (*i*) the tumor itself, (*ii*) the anatomic localization, and in particular the presence of the Blood Brain Barrier (BBB), and (*iii*) the toxicity of current treatments.

Nanotechnology can be instrumental for all of these issues. The ultimate goal of this project is the development of multi-task targeted, drug-loaded Nanovectors (NVs) able to cross the BBB and target GBM, release chemotherapeutics and induce tumor cell death and disease regression.

Liposome (LIPs) incapsulating Doxorubicin (DOXO) and functionalized with a peptide derived from the ApoE lipoprotein (mApoE), mApoE-DOXO-LIPs, demonstrated the ability to cross BBB and target the Glioblastoma Stem-like cells (GSCs) both *in vitro* and, especially, *in vivo* reducing the tumor growth in PDX mice cotreated with radiation (2Gy dose). Moreover, the histological analysis demonstrated that 2Gy/mApoE-DOXO-LIPs treatment induced apoptosis in tumor cells preventing side effects on healthy brain parenchyma, reducing the toxicity of the drug. Interestingly, morphological and histological analysis on $Iba1^{+}$ cells suggested that GSCs apoptosis could induce Immune cell death (ICD) activation with in turn could activate the immune system against GBM.

However, LIPs treatment still induced systemic toxicity in treated mice, probably due to the high accumulation of the NVs in the liver (approximately 40% of injected LIPs), causing a body weight loss of approximately 12%. To reduce the LIPs side effect different polymeric NVs were tested. Poly(lactic-co-glycol acid) (PLGA) and poly(ε-caprolactone) (PCL) NVs functionalized with a MMP2 Activatable Low Molecular Weight Protamine (ALMWP) were chosen to reduce NVs side toxicity. While linear PLGA NVs wasn't

effective due to their fast drug release, star shaped PCL NVs (ALMWP-DOXO-PCLs) were able to induce *in vitro* GSCs death at a extremely low DOXO concentration (approximately 10 time lower than LIPs) without affecting healthy cells like the endothelial cells.

The work of this thesis demonstrates that drug-loaded targeted nanovectors can function as a delivery strategy to specifically and effectively drive chemotherapeutics into GBM tumor microenvironment and cells and could represent a key technology to treat GBM.

Acknowledgement

Almost five years ago I started my PhD program complaining: I didn't want to have a PhD, it was too much. I believe that my master of science would be enough to me or, maybe, I was just scared. With the benefit of hindsight I know that I have been lucky to have undertaken this path.

Among all, the first person I have to thank is my wife Angela, in particular for her patience and for all the self-denial she has done to support me.

I would like to thank my supervisors Lorena for her everyday help, in particular during the thesis period, Michela because she has given me the possibility to work in her lab and because she has believed in my abilities, and Paul for his kindness and his suggestions.

I really want to thank all my labmates of the pharmacology and brain pathology lab for these incredible years, with them it has been all easy and crazy. A particular thank to the boss of the lab technician Faggiani, to branchy and the GBM group component Matteo, Betta, Valentino and Milly.

Finally I want to thanks all my parents and my friends for their support and friendship.

“Fletto i muscoli e sono nel vuoto”

Introduction

1. CNS tumor

Tumors of the central nervous system (CNS) comprise a heterogeneous group of neoplasms that vary in location, age at onset, histologic features, tendency for progression and migration, and response to therapy (Louis et al., 2007). These tumors exhibit a wide spectrum of histologic subtypes reflecting their potential cell of origin, local microenvironments and clinical outcome (Gutmann et al., 2006).

Historically, CNS tumors were classified mainly based on histogenesis, according to their similarities with the putative cells of origin and their levels of differentiation (Louis et al., 2016). The largest group of primary brain tumors (42% of total events) is represented by gliomas, that have many histologic features in common with glial cells (astrocytes, oligodendrocytes and ependymal cells) (Louis et al., 2007). Other brain tumors arise from ectodermal structures related to the brain (meningioma), from lymphocytes (CNS lymphoma), or from precursor neuronal elements (neuroblastoma, medulloblastoma), germ cells (germinoma, craniopharyngioma, teratoma), or endocrine elements (pituitary adenoma).

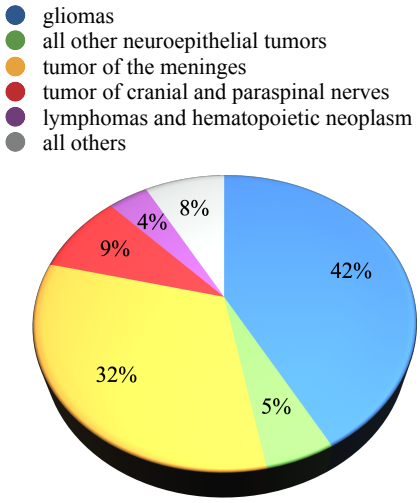

Fig. 1: Relative Frequency of primary CNS tumors. Adapted from Weller et al., 2015.

In 2016 the World Health Organization (WHO) updated the classification by combining histopathology with the genetic molecular characteristics of the CNS tumor. Nowadays, histology, WHO grade (I to IV, with IV grade representing the most malignant behavior) assigned based on the presence or absence of anapestic features, and molecular profile are considered as different layer that define the final integrated diagnosis of the CNS tumor (**Fig. 2**) (Weller et al., 2015).

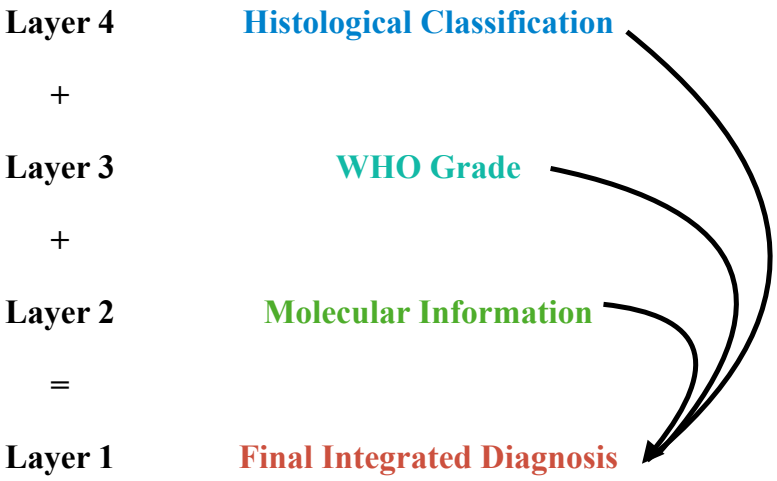

Fig. 2: Layered diagnosis of CNS tumors. Integrated diagnosis (layer 4) comes last, when layers 1–3 are defined. WHO grading criteria (layer 3) and relevant molecular information (layer) are separately defined for different histologic tumor types. Adapted from Johnson et a., 2016.

Among all the molecular alteration that accord in CNS tumor two of them were selected for their pivotal biological and clinical relevance in diagnosis determination:

1. Isocotrate dehydrogenase 1 (IDH1) mutation: the wild-type (wt) form of these gene confers a worse prognosis respect the mutated (Hartmann et al., 2010)
2. Translocation of the p-arm chromosome 1 with the q-arm of chromosome 19 (1p/19q codeletion): improved prognosis and response to chemotherapy (Weller et al., 2013)

The 2016 classification underline the importance of the molecular "layer" and prompted a lot of new discover on this aspect. Therefore, the Consortium to Inform Molecular and Practical Approaches to CNS Tumor Taxonomy (cIMPACT-NOW) was created to disseminate the updates and to direct the future WHO classification. Recently, a new WHO classification of the CNS tumor has been announced to be edited in the second part of the

2021. In this new classification the molecular alterations will be the main elements that will drive to the final diagnosis, definitively overturning the importance of the paradigma histology/molecular features.

1.1 Glioblastoma

GBM (designated WHO grade IV) is the most common malignant primary brain neoplasm in the adults, accounting for approximately 20% of all intracranial tumors and more than 80% of gliomas of the cerebral hemispheres (Hanif et al., 2017). GBM incidence is 5-7 cases per 100 000 people per year worldwide (Thakkar et al., 2014), with a peak incidence between 55 and 60 (Hanif et al., 2017) and a slightly higher prevalence in men compared to women, with a ratio of 1.6:1 (Davis., 2016). Until now, GBM doesn't have an etiology correlation with typical environmental factors such as smoking, diet or cell phone use and the only known risk factor is the exposure to ionizing radiation (Alexander and Cloughesy, 2017; Davis., 2016).

GBM represents one of the deadliest tumors with a 5-year survival rate of <10%, and a mortality rate close to 100% (Taylor et al., 2019). Its unfavorable prognosis is mainly due to its high propensity for tumor recurrence that inevitably occurs after 6-9 months after diagnosis.

1.1.1 Histopathology

Generally, GBM arise in the supratentorial region. Only 5% of the cases are located in the cerebellum, brainstem and spinal cord (Nakada et al., 2011). Usually, GBM appear as a single and large lesion with irregular shape (Nelson and Cha., 2003) composed by several regions that differ for their histological appearance (Smith and Ironside, 2007; Agnihotri et al., 2013):

1. Necrotic area
2. Multifocal hemorrhage area
3. Cystic and gelatinous area

Histologically, GBM is composed by either a pleomorphic small cell population poorly differentiate or large multinucleate cells with multifocal necrosis and the presence of pseudopalisanding nuclei (Nelson and Cha, 2003; Frosch, 2013). Another characteristic of GBM is the presence of vascular endothelial cell proliferation (Smith and Ironside, 2007; Agnihotri et al., 2013) (**Fig. 3**).

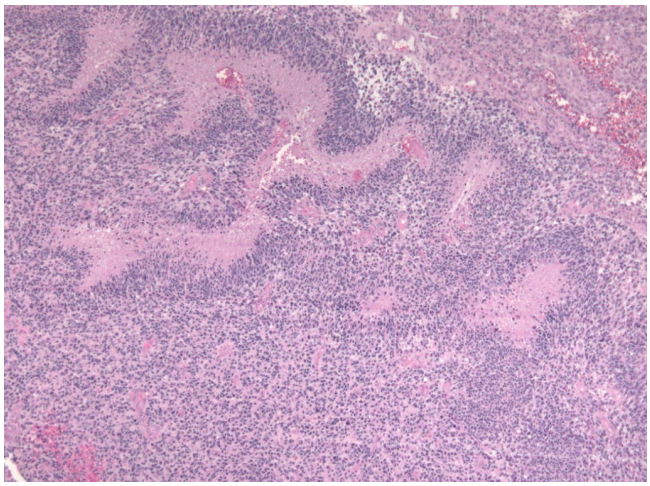

Fig. 3: GBM histology. Foci of necrosis with pseudopalisading of malignant nuclei and endothelial cell proliferation.

1.1.2 Molecular pathology

GBM represents one of the most comprehensively genetically characterized cancer types, leading to recognition of groups defined by transcription profile. Multi-dimensional and comprehensive characterization of more than 500 GBM sample have demonstrate how each GBM represents an unmatched set of genomic alteration, marker expression and pathway activation (Brennan et al., 2013).

According to the 2016 WHO classification, GBM is now subdivided into two types on the basis of the presence or absence of IDH mutation (Yan et al., 2009): wt IDH1 is present tumor diagnosed as GBM (primary GBM) while mutated IDH1 is generally associated to GBM derived from lower grade glioma (secondary GBM). Harbouring IDH mutation has been found to confer an increased survival compared to *wild-type* GBMs. Primary and secondary GBM have different pathogenesis that confer them a specific molecular pattern

(Ohgaki and Kleihues, 2007; Agnihotri et al., 2013; Ohgaki and Kleihues, 2013; Liu et al., 2012; Cloughesy et al., 2014):

- **Primary GBM**: Epidermal Growth Factor Receptor (EGFR) mutation, overespression of Mouse Double Minute 2 (MDM2), deletion of p16 and loss of heterozygosity of chromosome 10q holding phosphatase and tensing homologue (PTEN) and mutation in the promoter of TERT
- **Secondary GBM**: overexpression of platelet derived growth factor a and platelet derived growth factor receptor alpha (PDGFA/PDGFRα), retinoblastoma (RB), loss of heterozygosity of 19q and mutation in IDH1/2, TP53 and ATRX.

In addition to IDH status, other two molecular features are routinely used in the clinic for GBM prognosis (**Fig. 4**):

1. O−6−methylguanine−DNA methyltransferase promoter methylation (MGMT) - MGMT function as a dealkylating agent (Lee, 2016). The interest in this gene has increased considerably since the publication that GBM patients with methylated, and consequently inhibited, MGMT promoter had more prolonged survival when treated with temozolomide (TMZ) than patients with unmethylated MGMT promoter (Weller et al., 2015).

2. 1p/19q co−deletion - One study demonstrated that the presence of complete or partial co-deletion of 1p and 19q conferred a significantly increased response to chemotherapy, and prolonged disease-free survival time, compared to tumors of only one or the other chromosomal arm, regardless of histologic subtype (MnNamara et al., 2017). Due to the significant clinical implications for the presence of this gene, 1p/19q co-deletion testing should be performed on all glial tumors, included GBM, with or without oligodendroglial features, since a small percentage (5%)

of morphological astrocytomas are with 1p/19q co-deletion, which may confer a slightly better prognosis for the patients (Shan et al., 2019).

In 2010, for the first time, Verhaak et al. (Verhaak et al., 2010) classified GBM subtypes based on specific gene expression signature. They identify four different subclasses reminiscent of distinct neural cell of origin, associated with different incidence and clinical outcome (**Fig. 4**):

1. **Proneural (PN)** highly enriched in oligodendrocyte signature;
2. **Classical** expressing an astrocytic signature;
3. **Neural** associated with oligodendrocytic and astrocytic but also enriched in neurons genes;
4. **Mesenchymal (MES)** associated with an astroglial signature.

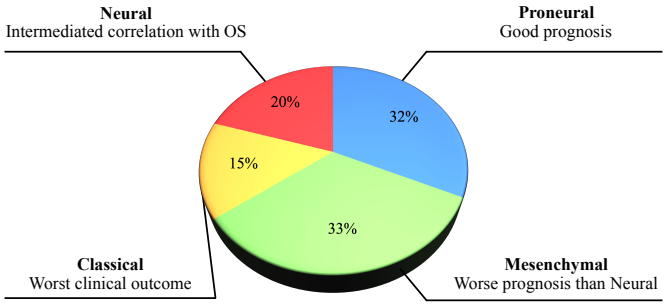

Fig. 4: GBM subtypes and their incidence and malignancy. Adapted from Fedele et al., 2019.

Since then, many studies enforced and amplify this classification, defining a specific set of genes for each signature. This allow to established the presence of two main GBM subset (PN and MES) and an intermediated one (Classical) (Bath et al., 2013; Halliday et al., 2014; Moreno et al., 2017; Rooj et al., 2017; Minata et al., 2019) since the Neural subset probably arise from the neuronal tissue that surround GBM margins (Wang et al., 2017) Among them, mesenchymal subtype results the more aggressive, invasive, angiogenic,

hypoxic, necrotic, inflammatory, and multitherapy-resistant features than other transcriptional subtypes (Kim et al., 2021).

2. Clinical features and therapy

GBM patients present a short clinical history in more the 50% of the cases (3-6 months) while could be spans over years for the GBM developed from low-grade tumor (secondary GBM) (Clarke, 2005; Salah Uddin and Jarmi, 2015). Symptoms could arise suddenly and often can be confused with symptoms of other disease (like stroke). The more frequent symptoms are slowly progressive neurologic deficit, usually motor weakness (10 to 40%), headache (50 to 60%), headaches, nausea, vomiting and cognitive impairment seizures (20 to 50%). These sing or symptoms are generated by three different mechanism (Clarke, 2005; Salah Uddin and Jarmi, 2015):

1. Brain tissue damage and necrosis provoked by the tumor generate specific deficit based on the region where GBM is located;
2. Increased intracranial pressure due to the increase of the tumor mass and the edema surrounding the tumor. A typical symptoms caused by the increase pressure is headache;
3. Brain area where GBM arise is the main cause of the presence of seizure.

Despite the enormous effort oft he international community, GBM remains an incurable disease, with a median survival of just 15 months. The most consistently reported and best-established prognostic factors include (Xavier-Magalhães et al., 2013):

1. Age of the patient
2. Tumor location
3. Who grade
4. Performance status of the patient
5. Extent of surgical resection

Recently molecular stratification with biomarkers (IDH1, MGMT status, 1p/19q) have been recognized as predictive of patient response and outcome, proving crucial in rationalizing treatment decisions in addition to the classical histological prognostic factors.

Currently, the most efficient and standardly used protocol for GBM treatment is the one proposed in 2005 by Stupp et al. (Stupp et al., 2005), basically composed of two steps:

1. **Surgery.** Surgery is the principal component of GBM standard care. Tumor mass removal can lead to many benefits including reduction of tumor burden, reduce seizure, limit and abolish the neurological deficit. Surgery carries also a diagnostic roles since it provides tissue specimen for histologic and molecular diagnosis. Notably, during surgery it is also possible to introduce local therapeutic agent in order to improve the efficacy of the resection and quality of life (Newton et al., 2007) However, the high degree of GBM invasion often in eloquent areas makes extensive and complete resection impossible (Iacob and Dinca, 2009). Therefore, GBM recurrence occurs in 80% of the cases within 2-3 cm from the original tumor (Mrugala, 2013).

2. **Radiation and Chemotherapy.** In order to kill the invading cells that have not been removed by the resection, surgery is followed by radiotherapy (RT) and chemotherapy with TMZ cotreatment. Different RT protocol tested (fractionated, brachytherapy or stereotactic radiosurgery) have shown to be effective against GBM relapse improving life expectancy of patients (Hanif et al., 2017). However, some limitation and side effect are associated with RT. Among them are radio necrosis and permanent neuronal damage (Iacob and Dinca, 2009). Moreover, GBM react to RT with enhanced invasiveness and tumor cell radio resistance (Iacob and Dinca, 2009).

   As adjuvant of RT, TMZ is currently used as standard treatment of GBM patients (Reardon and Wen, 2006; Iacob end Dinca, 2009). TMZ is an alkylating agent. Its toxicity is related to the DNA methylation at the N7 and O6 position on the guanine in replicating cells. The guanine methylation leads to DNA miss match repair failure and consequent cell death (Scott et al., 2011). However, likewise RT also TMZ have limitation and side effect, in particular hematologic toxicity (Chang et al., 2007).

Despite surgery and radio- chemotherapy, GBM inevitably recurs after 6-9 months from diagnosis and only approximately 3-30% of the patients are eligible for re-operation or re-irradiation (Robin et al., 2017). Mostly, patients are treated with chemotherapy as second-line treatment. Antiangiogenics, inhibitors of the epidermal growth factor receptor, nitrosoureas, and re-treatment with TMZ have been studied in the second line, but a standard therapy has not yet been established. In the last years, many attempts have done to develope new efficient therapy. The more promising admitted to clinical trials are based on (Mohtashami et al., 2020):

1. **Molecular signaling.** In GBM context, many signal pathway are altered causing uncontrolled proliferation, neoangiogenesis, cell migration and differentiation (Preusser et al., 2015; Soukhtanloo et al., 2020). Many attempts have been done to developed **tyrosine kinase inhibitor** targeting specific pathway extremely important in GBM and in tumor in general. Among them are the pathways involving the Epidermal Growth Factor Receptor (**EGFR**), overexpressed in 60% of the primary GBM (Xu et al., 2017), the mammalian Target of Rapamicine (**mTOR**) and the Vascular Epithelial Growth Factor (**VEGF**) (Mohtashami et al., 2020).
   Another important target is the Nuclear factor kappa-light-chain-enhancer of activated B cells (**NF-κB**), a transcription factor that regulates many mechanism like cell growth, invasion, radioresistance and survival (Srivastava et al., 2017; Duerinck et al., 2015). Inhibit NF-κB in GBM could be crucial also for its ability to mediate TMZ resistance through the MGMT regulation (Qian et al., 2015).

2. **Monoclonal antibodies (mAbs).** In spite of significant results obtained in different cancers such as hematological, renal and breast (Lim et al., 2018), trials using mAbs against GBM didn't show the expected results (Mohtashami et al., 2020). The main target of this mAbs is EGFR since is overexpressed in GBM and is located on the cell membrane. Nevertheless, a mAbs against CD95 used in a phase II trial was able to extend the survival of recurrent GBM patients (Blaes et al., 2018), switching on again the research on immunetherapy against GBM.

3. **Immune check point inhibitors.** A particular class of mAbs targets the immune check point inhibitors such as Programmed cell Death 1 (PD-1) and its Ligand (PD-L1) and Cytotoxic T-Lymphocyte Antigen 4 (CTLA-4). The inhibition of these molecules should reactivates the T-Cell enhancing the tumor cell immune response (Caccese et al., 2019). The efficacy of these mAbs have been evaluated in different trials and different combination among them or other kinds of treatment, suggesting that the use of these mAbs could represent an important step forwards in GBM treatment (Lowther, et al., 2016; Reardon et al., 2016; Reardon et al., 2017; Omuro et al., 2018).However, the inhibition of the check points in GBM didn't demonstrate sufficient efficacy in clinical trials, failing to improve the survival of the patients (Brahm et al., 2020). A possible way to ameliorate the efficacy of these therapies could be the employment of multi-modal approach to activate local and systemic tumor-specific immune responses.

4. **Vaccines.** Vaccination stimulates the body's tumor-specific immune response by the injection of foreign antigens. Vaccines against GBM are primarily of two categories: **peptide** and **cell-based vaccines.** Peptide vaccines involve the injection of tumor specific antigens. The characterized targets for GBM peptide vaccines are EGFRvIII, Survivin and the Heat Shock Protein (HSP) (Mohtashami et al., 2020). However, despite good results of phase I/II clinical trials, no successful phase III clinical trials have been reported to date. Cell-based vaccines (dendritic and/or tumor cell vaccines) are based on the injections of ex vivo-modified cells (Kong et al., 2017).

5. **Adoptive cell therapy and CAR T.** Adoptive cell therapy aims at infusing immune cells with direct anti-tumor activity in order to reestablish the anti tumor activity of the immune systems (Wang et al., 2020). The most promising approach of adoptive cell therapy is the use of genetically modified T cells with chimeric antigen receptors (CARs). To

generate CAR T cells, T lymphocytes are transduced with CAR constructs containing a Tumor-Associated Antigen (TAA) recognition domain linked to the constant regions of a signaling T cell receptor (Land et al., 2020). In GBM treatment, CAR T cells are still at the early phase of development. The more promising CAR T targets are Interleukin-13 receptor alpha 2 (IL13Rα2), EGFRvIII and HER2. So far, clinical trials have demonstrated the safety of these approaches (Land et al., 2020), encouraging to keep on the research on CAR T lymphocyte.

6. **Oncolytic virotherapy.** This therapeutic option is based on the ability of viruses to infect and selectively replicate in cancer cells. Their infection should lead to tumor cell death without harming healthy cells (Chen et al., 2012). Oncolytic therapy has been applicator in different trials in GBM treatment and, in some cases, has shown amazing results, prolonging the OS of many months respect the conventional therapy (Mohtashami et al., 2020). A particular aspect of oncolytic virus is the possibility to be engineered in order to express immunemodulatory transgenes able to enhance the immune infiltration and response against GBM. Open studies are trying to determine the efficacy as immunomodulatory of cytokines (IL-4, IL-12 or IL-15), immune checkpoint inhibitors (Anti PD-1) or oncogenes (PTEN, p53) (Zhang et Liu, 2020)

2.1 GBM challenges

Despite ongoing research, the outlook on GBM remains quite disappointing. The fact that treatment and prognosis have remained unchanged for fifteen years leads to the realization that there are major challenges that we have not been able to overcome. Among all the difficulties on GBM management, there are three main challenges that lead to treatment failure:

1. The presence of the Blood-Brain Barrier
2. The tumor itself
3. the toxicities of current treatments

2.1.1 The Blood Brain Barrier

The CNS required a high controlled microenvironment to guarantee the normal functioning of the brain. CNS isolation from the rest of the body is protect by the presence of three biological barrier composed of different cell types and established at three pivotal interfaces: i) the Blood-Brain Barrier (BBB), created by the endothelial cells of the vessel to separate the brain from the blood component, ii) the Blood-Cerebrospinal Fluid Barrier (BCSFB), formed by the epithelial cells of the choroid plexus to separate the CSF from the brain, and iii) the arachnoid barrier, provided by the avascular arachnoid epithelium to enwrap the CNS under the dura madre (Abbott et al., 2013) (**Fig. 5**).

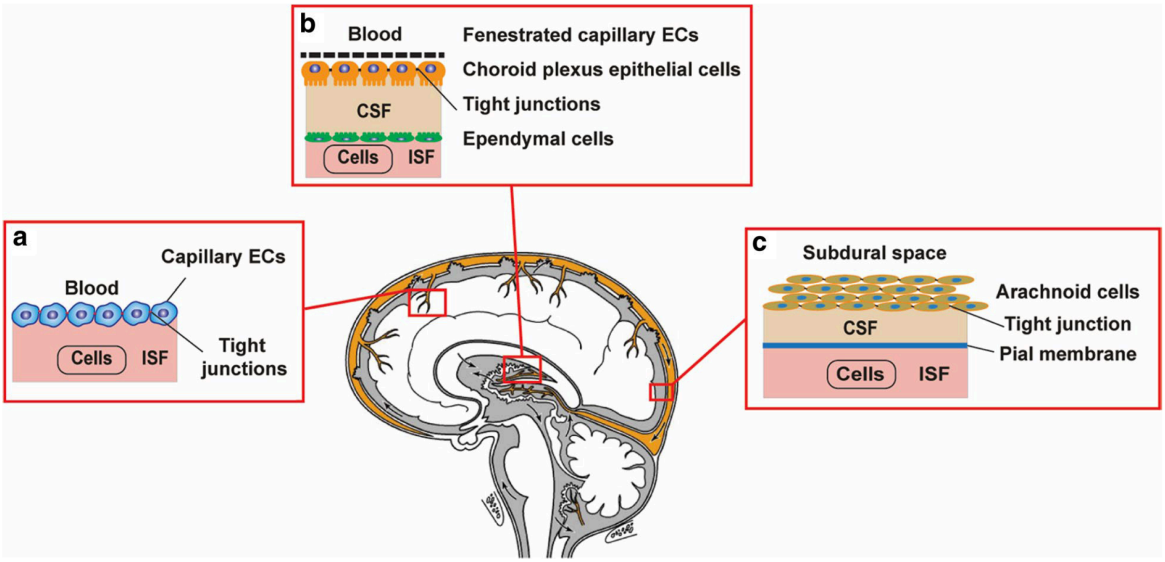

Fig. 5: Biological barriers that protect the brain. The brain is protected by biological barrier at three different levels. **a)** Blood–brain barrier protect the brain from the blood component and regulate nutrients and molecules passage; **b)** blood–CSF barrier separate the brain from the cerebrospinal fluid; **c)** the arachnoid barrier. ISF Interstitial Fluid. Adapted from Kadry et al., 2020.

Due to its peculiar structure, BBB is the main responsible for CNS protection and homeostasis maintenance. Brain microvascular endothelial cells have peculiar characteristics that make them different from the vessel located in other parts of the body. Among them, three are the most important (Kadry et al., 2020):

1. The presence of **Tight Junctions** (TJ) between the cells that prevents the passive passage of polar molecules between blood and brain
2. The absence of fenestration between the cells
3. The regulation of the passage of the essential molecule with specific transporters and the presence of the efflux mechanisms.

Beyond the endothelial level, the BBB is organized with other cell types in a Neurovascular Unit (NVU). Indeed, the endothelial cells are cover by the pericytes with in turn are embedded by the basal lamina. Finally, the endfeet of the astrocytes enwrap the vessels establishing the NVU (Zlokovic, 2011) (**Fig. 6**).

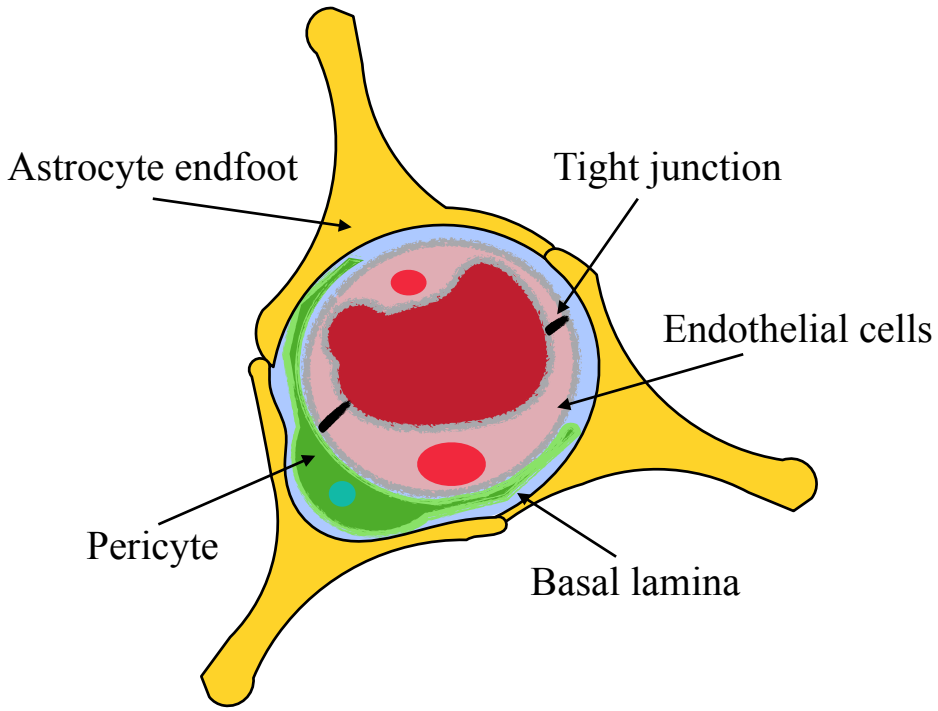

Fig. 6: Neurovascular unit structure. The blood vessels of the brain are organized with other cells in structure named neurovascular unit. The endothelial cells, strictly bind each other by the TJ, are surrounded by the pericytes and the basal lamina. Finally, the astrocytes covered the entire structure with their endfeet and ultimate the highly impermeable structure of the BBB.

BBB free diffusion is possible only for lipophilic molecules smaller than 400 Da that can passively cross trough the BBB and gases, in particular diffusion of O_2 from blood to brain

and CO_2 diffusion in the opposite direction is extremely rapid in order to maintain normal brain metabolism and regulate the pH in the Interstitial Fluid (ISF) and other cells (Kadry, 2020). The involvement of a ligand specific transporter is needed to regulates the passage of nutrients, metabolites, energy molecules, such as glucose cholesterol, and other molecules from blood vessel into the brain parenchyma. In the same way, metabolic waste products are transported from brain parenchyma into the blood (Zhao et al., 2015).

The main mechanism that regulates macromolecules crossing through the BBB is transcytosis that allow the transport of macromolecules from the apical to the basolateral plasma membranes of endothelial cells.

There are two main categories of transcytosis in the CNS (**Fig. 7**) (Ayloo and Gu, 2019):

1. **Adsorptive transcytosis:** charged molecules, like albumin, interact with the plasma membrane and this facilitate the transport across the endothelial cell;
2. **Receptor Mediated Transcytosis (RMT)**: ligands, including transferrin, and macromolecules like lipoproteins bind their receptors on cell membrane and this assure the BBB crossing.

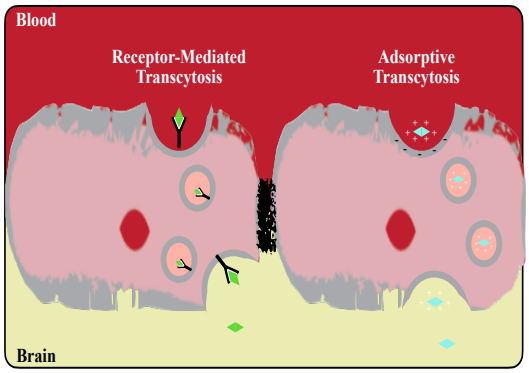

Fig. 7: Transcytosis in CNS endothelial cells. RMT and adsorptive transcytosis. In both mechanism, the molecules are internalized into an endosome and transported through the cell to the basolateral cell membrane. Adapted from Ayloo and Gu, 2019.

An example of RMT is represented by lipoproteins and their receptors. Among them, Apolipoprotein E (ApoE), a multifunctional protein with central role in CNS lipid metabolism (Pirmoradi et al., 2019). By binding to the Low Density Lipoprotein Receptor (LDLR) expressed on the luminal membrane of the endothelial cells ApoE allows the transport and the regulation of cholesterol homeostasis in the brain (Pirmoradi et al., 2019).

Once the molecules interact with the endothelial cell by both RMT or charge interaction, they are internalized by endocytosis. Cell membrane invagination and cargo internalization are regulated by different proteins and pathways:

1. **Clathrin-dependent endocytosis:** clathrin-coated pits generates at the level of molecule/cell membrane interaction; the GTPase dynamine facilitates the invagination release from the membrane and the formation of clathrin-coated vesicle (Sweitzer and Hinshaw, 1998)
2. **Caveolae-dependent endocytosis:** plasma membrane invaginations called caveolae are formed by caveolins binding to cytosolic cavins. This interaction leadsendosomal vesicle formation (Hill et al., 2008).

In the cytoplasm, endocytic vesicles are sent trough tubules pathways to the basolateral membrane (Villaseñoret al., 2017), where vesicle membrane fuses with cell membrane allowing the release of their cargo to conclude the transcytosis (Pulgar, 2019) (**Fig. 8**).

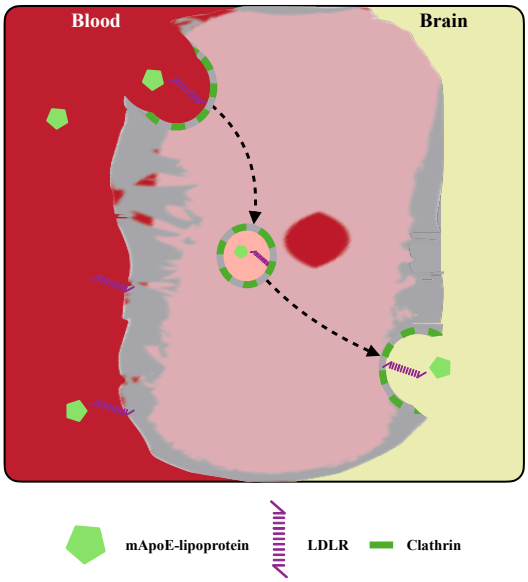

Fig. 8: Receptor Mediated Transcytosis of mApoE-lipoprotein. Schematic representation of ApoE-lipoprotein transcytosis from blood vessel to brain parenchyma. Adapted from Pulgar 2019.

The BBB protective nature acts also in the case of drugs. In addition, the effectiveness of CNS targeted drugs is further limited by the presence of the efflux transport system (Loscher and Potschka, 2005). Adenosine Triphosphate Binding Cassette (ABC) and

Solute Carrier (SLC) are the two main classes of drug transporter present on BBB. ABC biological function is the active transports against concentration gradients of hydrophobic compounds, and consequently hydrophobic drugs, by ATP hydrolysis with P-glycoprotein (P-gp) (Mahringer and Fricker, 2016), encoded by multi drug resistance gene 1 (MDR1). SLC instead actively transports energetic substrates, amino acids, neurotransmitters and organic ions (Nałęcz, 2016), driving the resistance of small molecule and peptide (Sanchez-Covarrubias et al., 2014).

Drug efflux mechanisms are at the basis of many drug delivery failure in GBM. Among them is Doxorubicin (DOXO), an anthracycline antibiotic with antineoplastic activity isolated from the bacterium Streptomyces peucetius. DOXO functions primarily intercalating between base pairs in the DNA helix interfering with its uncoiling. Additionally, DOXO inhibits topoisomerase II which results in an increased and stabilized cleavable enzyme-DNA linked complex during DNA replication and subsequently prevents the ligation of the nucleotide strand after double-strand breakage. DOXO also generate oxygen free radicals that contribute to the toxicity of the anthracycline antibiotics, namely the cardiac and cutaneous vascular effects (PubChem [Internet]. Bethesda (MD): National Library of Medicine (US), National Center for Biotechnology Information; 2004-. PubChem Compound Summary for CID 31703, Doxorubicin; [cited 2021 Feb. 26]. Available from: https://pubchem.ncbi.nlm.nih.gov/compound/Doxorubicin). DOXO is currently used in the treatment of many tumor like non-Hodgkin's and Hodgkin's lymphoma, multiple myeloma, as well as lung, ovarian, gastric, thyroid, breast, sarcoma, and pediatric cancers (Cortés-Funes and Coronado, 2007). Its effectiveness has been demonstrated also against GMB cells *in vitro* but has poor efficacy *in vivo* due to extrusion by multidrug resistance-related proteins present on BBB (ABCB1/MDR1, ABCG2/BCRP, ABBC1/MRP1, ABCC2/MRP2, ABCC3/MRP3 and ABCC6/MRP6) that reduce the amount of drug that can reach the GBM cells. Moreover, also GBM cells express multidrug resistance-related proteins (ABCB1/P-gp, ABCG2/BCRP, ABCC1/MRP1, ABCC4/MRP4, and ABCC5/MRP5) further reducing the active drug inside tumor cells (Gomez-Zepeda et al., 2019).

2.1.2 GBM itself

Cellular hierarchies related to the developmental programs of tissue stem cell and their lineage differentiation play a central role in many cancers. In GBM different cell sub-populations can be isolated within the same lesion. Results obtained with single cell RNA sequencing strongly suggest that GBM intra cellular heterogeneity is due to gene expression programs that are normally active during neurodevelopment and are differently active in GBM cells (Darmanis et al., 2017; Neftel et al., 2019; Patel et al., 2014; Wang et al., 2019; Bhaduri et al., 2020). In this cellular heterogeneity the GBM Stem Cells (GSCs), also known as tumor-initiating cells, play a pivotal role in tumor progression and outcome due to their intrinsic refractoriness to conventional therapy and ability to invade the surrounding healthy tissue. Their malignancy is enhanced by their self-renewal ability, pluripotency, multilineage differentiation, high rate of proliferation, angiogenetic and immune response modulation capacity (Lathia et al., 2015). GSC typically growth in specific tumor compartments named niches. Three main niches has been histopathologically recognized: the perivascular niche near the brain vessel or in proximity of neoformed vessel (1); the hypoxic niche in the inner part of the tumor mass, far from vessel and, consequently, oxygen (2); the invasive niche in the outer part of the tumor in close contact with the brain parenchyma (3) (Hambardzumyan and Bergers, 2015) (**Fig. 9**).

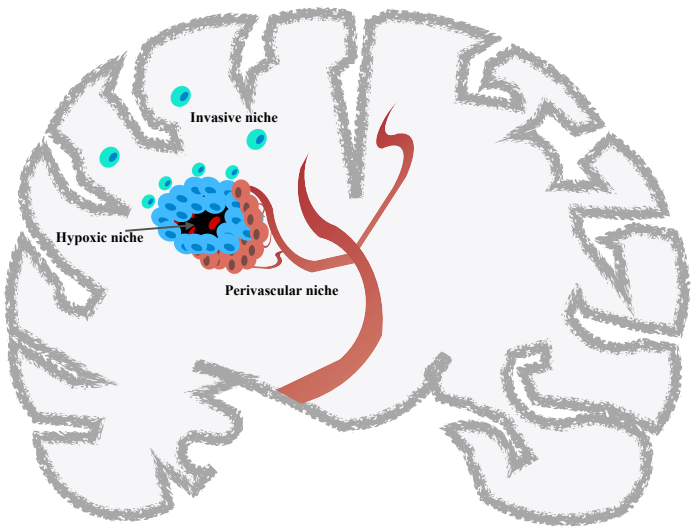

Fig. 9: GSCs niches. GBM are extremely heterogeneous tumor, composed by different cell subpopulations. Among them, GSCs represents one of the most abundant subpopulation. GSCs usually growth in specific tumor compartments called niches. Three different niches can be identify: the **perivascular niche** near the blood vessels; the **hypoxic niche** in the inner part of GBM core characterized by low nutrients and oxygen amount; and the **invasive niche**, corresponding to the outer part of the GBM where GSCs migrate and invade the brain parenchyma and originate new GBM lesion.

GBM heterogeneity can be described with different molecular signature. Similarly, GSCs can be identify by unique molecular signature. In the last 10 years the gene expression of specific markers has been largely investigated, focusing the attention on PN and MES subtype (Bath et al., 2013; Halliday et al., 2014; Moreno et al., 2017; Rooj et al., 2017; Minata et al., 2019):

1. **Pro Neural** (PN): GSCs sharing some characteristics of the fetal Neural Stem Cells (NSCs). Among PN markers the most characterized are CD133, SOX2, SOX9, OLIG2 and ADGRG1
2. **Mesenchymal** (MES): GSCs sharing characteristics of adult NSCs. Some of the most characterized MES marker are CD44, CTGF, FN1, CHI3L1, ALDH1A3.

These signature of the GSCs is not fixed and invariable but could evolve in time from PN to MES in the so called Proneural to Mesenchymal transition (PMT), a change in molecular characteristics allowed by a high permissive epigenetic status (Banerji et al., 2013; MacArthur et al., 2013) that makes GSC a cell population constantly evolving in a continuous dynamic flux (Chang et al., 2008). Multitherapy used to treat GBM in patients forced the PMT transition enriching the GSCs in MES signature. MES GSCs have been demonstrated to be extremely radio and chemo resistance and are the main cause of the recurrence unresponsiveness to therapy (Segerman et al., 2016). PMT and the high GSCs variability within the tumor could be explain by the plethora of stimuli that these cells receive like alteration in the microenvironment, drug treatments and GSC interaction with other cells, both GBM cells and not (Pisco et al., 2013).

In a recent model, Prager et al. described these stimuli as “attractors” able to generate local microenvironment different from that of the original tumor. The high stemness and entropy of GSCSs make these cells more prone to react and change in response to surrounding stimuli, generating new signature and sub-population. In this prospective, therapeutic treatments could not only select a GSCs resistant to treatment but they could also generate new GSCs sub-populations able to generate different lineages (Prager et al., 2020) (**Fig. 10**).

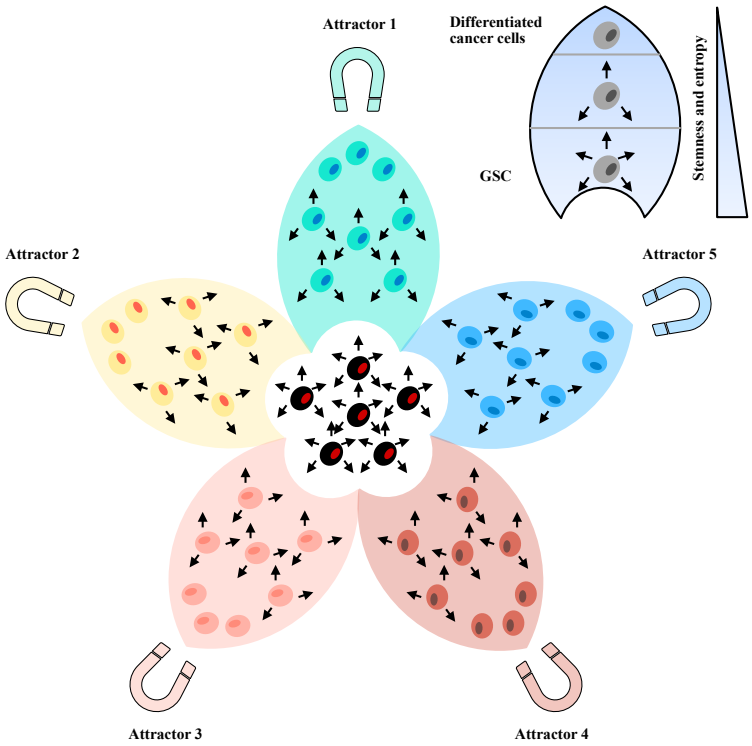

Fig. 10: Attractor state model. Multipotent GSCs have the highest level of entropy and ability to differenziate in response to different attractors (e.g. genetic mutation, therapeutic treatments, oxygen or nutrient level). Different attractor states induce the development of different population. Adapted from Prager et al., 2020

GSCs are the subpopulation with key role in tumor growth and recurrence (Singh et al., 2004; Bao et al., 2006; Chen et al., 2012) and their increased resistance to chemo- and radio-therapies (Bao et al., 2006; Chen et al., 2012; Cheng et al., 2011) is directly related to refractoriness to conventional therapy. Known mechanism subtending drug resistance in GSCs included:

1. Drug efflux by ABC transporters express on GBM cells including ABCB1/P-gp, ABCG2/BCRP, ABCC1/MRP1, ABCC3, ABCC4/MRP4, ABCC5/MRP5 and ABCC6 (Gomez-Zepeda et al., 2019; Jeon et al., 2011);
2. DNA repair mechanisms such as DNA mismatch repair (MMR), base excision repair (BER) or by the action of a demethylating enzyme such as MGMT (Lee, 2016) or KDM5 (Banelli et al., 2015). The inhibition of MGMT through promoter methylation has been largely studied in the last years (Hegi. Et al., 2005; Park et al., 2011; Binabaj et al., 2018) and is currently considered one of the GBM prognostic factor;

3. Selection of chemo- and radio-resistance subpopulation by cotreatment of TMZ and RT (Bao et al., 2006; Chen et al., 2012). These resistant GSCs are the main cause of GBM recurrence

2.1.3 Current treatment toxicities

Since 2005 the Stupp protocol is stably used for GBM treatment (Stupp et al., 2005). This protocol is set on maximal surgical resection followed by RT (usually 60 Gy in 30 fractions of 2 Gy, Dhermain, 2014) and adjuvant chemotherapy with TMZ (**Fig. 11**). Tis protocol allow to extend the median survival of the patient to 15 months. However, the prognosis remain unfaithful and since then no significant step forward have been done.

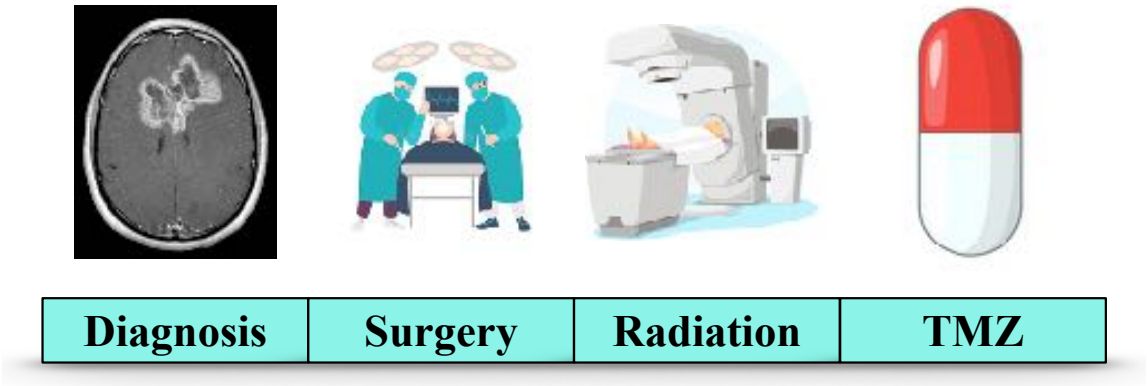

Fig. 11: GBM treatment protocol. Schematic representation of GBM treatment. After diagnosis, patients undergo GBM maximal resection by surgery. Then, they are treated with radiotherapy plus TMZ as adjuvant.

CNS is generally resistant to radiation but the high dosage used in GBM treatment can lead to brain damage both in the acute and long term phase (Dropcho, 1991). Radio-induced brain damage is related to the dose administered, the dose per fraction and the duration of the treatment, the volume of the GBM and is dependent to the interaction of the brain cells that composed the tumor microenvironment (Cuccurullo et al., 2019). Indeed, besides the fixation of the DNA double strand brakes that principally hit the tumor cells, other mechanisms of radio-toxicity damage the the brain tumor, such as oxidation of the lipid bilayer, microvascular permeability, rearrangement of the cell-cell junctional complexes and mitochondrial alteration (Cuccurullo et al., 2019).

The neuro-inflammation induced by the RT is particularly critical for the brain cells. The H_2O free radicals generated by RT induced the production of Tumor Necrosis Factor α (TNFα) and Interleukin 1β (IL-1β) by the glial cells (Kam and Banati 2013). The absence of endogenous anti oxidant and the high metabolism of the brain cells make this cells particularly sensible to the oxidative stress (Grunert et al., 2018)

Another severe local tissue reaction to RT is the Radiation Necrosis (RN) that appears 3-12 months after the treatments with a not well understood pathophysiology. RN is characterized by necrosis of blood vessel walls and the presence of adjacent perivascular parenchymal coagulative necrosis , while the change in the white matter observed are mainly focal and diffuse demyelination (Zikou et al., 2018).

Along with RT, patients receive the administration of the chemotherapy agent TMZ. TMZ is an adjuvant drug TMZ and, as a chemotherapy agent, is obviously related to severe side effect. Patients receiving TMZ are at risk for hematologic toxicity and should be monitored with weekly complete blood counts (CBCs). At least 15% and up to 75% of the patients suffer of moderate to severe lymphopenia and neutropenia, showing an extremely low CD4+ T cell counts after six weeks of daily TMZ with concurrent radiotherapy (Grossman et al., 2011). A mild and self-limited aminotransferase elevations occur in up to 12% of patients 2-8 weeks after the start of the treatment but several patients had received multiple courses before the onset of liver injury. In addition, TMZ has been associated with several cases of reactivation of chronic hepatitis B in patients who were hepatitis B surface antigen (HBsAg) positive at the start of chemotherapy. (PubChem [Internet]. Bethesda (MD): National Library of Medicine (US), National Center for Biotechnology Information; 2004-. PubChem Compound Summary for CID 5394, Temozolomide; [cited 2021 June 25]. Available from: https://pubchem.ncbi.nlm.nih.gov/compound/Temozolomide).

Many other undesired reactions to TMZ may occur during assumption including:

3. Bruising, bleeding gums or nose bleeds
4. Loss of appetite
5. Headache

6. Feeling or being sick
7. Tiredness
8. Seizures (fits)
9. Weakness on one side of the body
10. Hair loss
11. Skin rash

Due to these side effects, the use and dosage of RT and TMZ must be limited to avoid excessive toxicity. Consequently, the efficacy of the Stupp protocol cannot be modify even if we know that is still insufficient to treat GBM.

3. Nanomedicine

In the last two decades, Nanomedicine shows great promise in the treatment of tumor. The delivery of drugs via nanoparticles helps to improve the performance of anti-cancer drugs in terms of bioavailability, safety and specificity. Taking advantage of molecular markers over-expressed on tumor tissues compared to normal cells, an “active” molecular marker targeted approach should increase drug concentration at the tumor site, improving efficacy, reducing chemo-resistance and off-target side effect.

In GBM, the first and probably most complicated issue that nanomedicine have to face is the cross of the BBB, in particular in the peripheral region of the tumor.

3.1 The Blood-Brain Tumor Barrier

In the GBM context the BBB shows different states and BBB impairment is not uniform. The interface between BBB and the tumor is called Blood-Brain Tumor Barrier (BBTB) (Khan et al., 2021). At the level of the core tumor mass, BBB is heavily altered and its impermeability is impaired by the down regulation of claudin-1, a pivotal component of the TJ in endothelial cells (Khan et al., 2021). However, at the interface with the tumor edge, characterized by the presence of invasive GSCs, BBB maintains intact its structure and permeability (Costas D. Arvanitis et al., 2020, Jann N. Sarkaria et al., 2018) (**Fig. 12**):

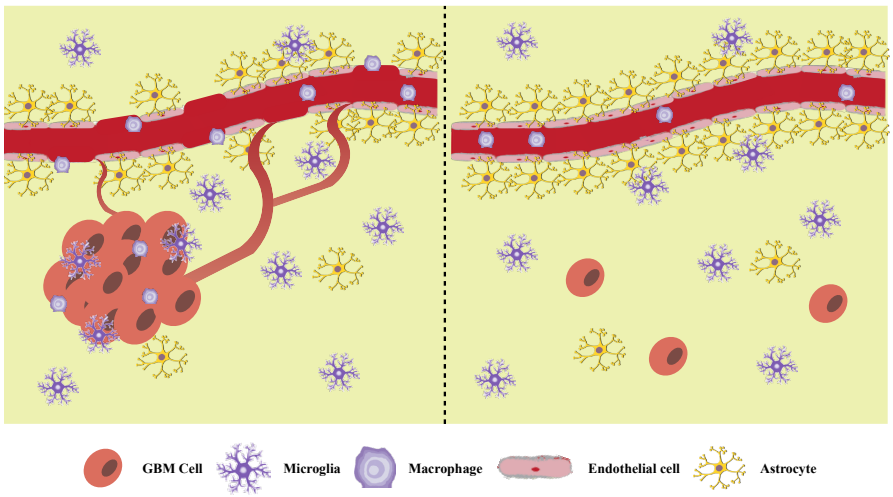

Fig. 12: heterogeneous disruption in GBM. Significant BBB breakdown seen in the bulk tumor region (left panel) allows drugs and cells extravasation. Regions with infiltrating GBM and GSC cells show less or no breakdown of the BBB (right) preventing therapeutics to reach these cells.

As complete tumor resection is impossible to achieve, reaching GBM cells remaining after surgery at the periphery of the tumor where an intact and still impermeable BBB represents the main obstacle to GBM treatment (Costas D. Arvanitis et al., 2020).

Several efforts are currently under study to bypass this problem. One of the most promising is the specific targeting of GBM cells with drug loaded nanoparticles.

3.2 Nanoparticles

Nanoparticle (NP) is defined as a particle of matter that is between 1 and 100 nanometres (nm) in size. NPs can be divided into three main groups: organic (lipids, proteins or polymers); carbon-based; and inorganic (metals or salts) (Buzea et al., 2007). The multi-faceted physiochemical properties of these materials allow NPs to be suitable for the most diverse applications at the molecular level. Because of their characteristic ultra-small dimensions, their ratio surface-area to volume is rather high, giving the possibility of ultimately refining the size, shape, chemical properties, surface functionalization and biologic capacities based on the specific application (**Fig. 13**) such as diagnosis, gene and drug delivery, vaccines and tissue engineering (Soares et al., 2018).

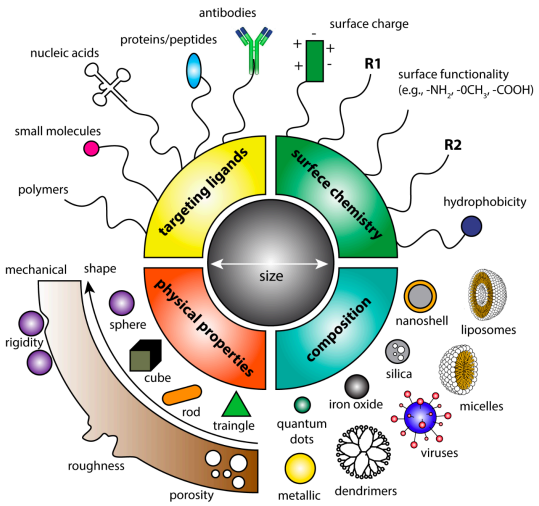

Fig. 13: Designing nanoparticles for intracellular applications. NPs can be synthesized varying their composition (organic, carbon based or inorganic core), physical properties (shape, size, porosity,…), targeting ligand and surface chemistry in order to obtain the best drug delivery system for each specific necessity. Adapted from Adikhari et al., 2019

One of the most promising field of nanomedicine is the treatment of cancer. Indeed, the delivery of drugs via NPs helps to improve the performance of anti-cancer drugs in terms

of bioavailability, safety and specificity. Accordingly, NPs can improve drug's therapeutic effectiveness while reducing adverse side effects associated with high dosage.

3.3 Drug-loaded nanocarriers

A nanocarrier is a NP used as a transport module for another substance including chemotherapeutics, nucleic acid and other active molecule. Among the most commonly used nanocarriers are lipid bilayer vesicle (liposome), and polymeric web composed of repeated self-assembling polymer chain (Jain and Thareja 2019).

The first FDA approved nanovector for drug-delivery was Doxil®, a liposomal form of DOXO for the treatment of ovarian and breast cancer (Song et al., 2012; Schwendener 2007; Torchilin 2005; Maurer et al., 2001). DOXO is one of the most commonly used chemotherapeutic agent for the treatment of a broad range of cancers but cardiotoxicity and myelosuppression limit its use. Liposome encapsulation constrains DOXO severe adverse effects (Rafiyath et al., 2012). However, liposomal DOXO has been shown to be inefficient against GBM in patients (Ananda et al., 2011). The poor clinical outcomes were presumably the result of the limited BBB crossing and other challenges inherent in tumor drug delivery (Lockman et al., 2010) .

The main strategies used in tumors targeting by nanocarriers are:

1. **Passive targeting** based on the Enhanced Permeability and Retention effect (EPR), firstly described by Matsumura end Maeda in 1986 (Matsumura end Maeda, 1986). NPs accumulate in tumor tissue thanks to the presence of fenestrated blood vessels and an inadequate lymphatic drainage (Moghimi et al., 2001; Fang et al., 2011). Passive targeting works at the level of GBM core, where the BBB structure is highly compromised and fenestrated but it is not efficient to reach peripheral tumor cells that invade the healthy parenchyma where the BBB structure is preserved. Here, the EPR effect is insufficient to allow nanocarriers targeting of GSCs responsible for cancer recurrence (Lemée et al., 2015).

2. **Active targeting** is achieved through the decoration of the nanocarrier surfaces with ligands binding to receptors over-expressed on the tumor cells and their microenvironment. This strategy will improve the affinities of the nanocarriers for the surface of cancer cell and thus enhance the drug penetration. Moreover, in the case of GSC invading cells, active targeting can help nanocarriers to cross the BBB and GBM cells targeting.

The major challenge of a nanocarrier-based therapy for GBM is the finding of the best targeting strategy for BBB crossing and drug delivery at the specific site.

3.4 Active targeting strategies

It is well recognized that active targeting is essential for the efficient delivery of drugs, genes and theranostics to the location of interest avoiding normal tissues and thereby enhancing therapeutic efficiency and limiting side effects. Active targeting is able to significantly increase the quantity of drug delivered to the target cells compared to free drug or passively targeted nanosystems.

3.4.1 Ligand-modified nanocarriers

Coating specific targeting ligand(s) on the surface of nanoparticles is the most common strategy of active targeting. These targeting ligands could be in the form of small molecules, peptides, antibodies, designed proteins, and nucleic acid aptamers (Liu et al., 2009; Friedman et al., 2013). The main goals of active strategy in GBM are (I) BBB targeting and crossing, in order to accumulate a higher drugs amount at tumor site respect passive targeting, and (II) specific tumor targeting, in order to reduce drug delivery to non-cancer, healthy cells.

BBB crossing by active targeted nanocarrier can be achieved by Receptor Mediated Transcytosis (RMT) (Jones and Shusta, 2007). After ligand/receptor binding, nanocarriers are internalized into endothelial cells by endocytosis.

One of the most studied ligands used to take advantage of RMT in nanocarriers delivery to the brain is Transferrin (Tf). For example, the presence of Tf receptor at the BBB allows Tf-liposome to accumulate 13 times more in the brain respect to unconjugated liposome (Soni et al., 2005). Similarly, cyclic Arg-Gly-Asp (cRGD) enhanced tumor uptake of micelles loaded with oxaliplatin in a orthotopic mouse GBM model, reducing tumor growth, thanks to cRGD binding of αvβ3 and αvβ5 integrins overexpressed on tumor vasculature and tumor cells (Miura et al., 2013).

Due to its capability to interact with the lipoprotein receptor-related protein (LRP), which is highly expressed on the BBB, it has been already reported that the use of Angiopep-2 enhances the delivery of genes into the brain through the BBB (Ke et al., 2009). Since LRP is also overexpressed in human GBM cells, Angiopep-2 can be used as a dual targeting agent, enhancing both endocytosis across the BBB and a successful targeting of GBM cells (Xin et al., 2011).

Thanks to an extensively reprogrammed cellular metabolism, tumor cells survive and proliferate under nutrient and oxygen deprivation. In this context, GBM cells are highly dependent on cholesterol supply for survival (Geng et al., 2016) and rely on exogenous cholesterol uptake, mediated by the Low-Density Lipoprotein Receptor (LDLR) (Villa et al., 2016). Indeed, LDLR is expressed in GBM and its upregulation correlates with tumor progression and drug resistance (Geng et al., 2016; Guo et al., 2011; Maletinska et al., 2000). LDLR expressed at the BBB (Wagner et al., 2012) is crucially involved in the transport of macromolecules from the blood stream to the brain by RMT (Fung et al., 2018; Pulgar 2018). LDLR binds and internalizes Apolipoprotein E (ApoE)-containing lipoproteins which mediate the brain metabolism of cholesterol (Pirmoradi et al., 2019). Several nanoscale drug delivery systems involving ApoE-conjugated nanoparticles are currently under investigation as potential vectors to deliver pharmacological agents across the BBB for the treatment of central nervous system disorders (Dal Magro et al., 2017).

3.4.2 Activatable nanocarriers

One of the most recent and promising targeting strategies aims to create nanovector that maintain the stealth property during circulation and then transform to a more cell-

interactive form (active targeting) upon arrival at the target tumor sites (Gullotti and Yeo, 2009). This strategy aims to mitigate the side effect of the treatments by localizing the drug release. Moreover, this localized release could increase the drug concentration at the tumor site, enhancing the drug effective dose.

Nanocarrier activation could be achieved by two main mechanisms (White et al., 2019):

1. **Extrinsic activation:** takes advantage of external physical stimuli including ultrasound, magnetic field, light and X-ray to active the nanocarriers
2. **Activation by altered cancer cell metabolism:** it takes advantage of the unique characteristics of tumor microenvironment.

In the last years ultrasounds have been largely studied as extrinsic nanovectors activation. Circulating microbubbles hit by Focus Ultrasound (FUS) can effectively increase the permeability of BBB by stretching the blood vessel and creating transient opening of the of the tight junction (Deng et al., 2019). Dual administration of microbubbles and nanocarrier could effectively increase the accumulation of drugs at tumor site (Fisher and Price, 2019). However, despite the promising results, more detailed studies are required to prove the efficacy of this mechanism.

Tumors develop unique microenvironments such as slightly acidic pH (Gerweck and Seetharman, 1996) and an a high level of proteinases (Egeblad and Werb, 2002). The tumor extracellular pH is generally more acidic (pH 6.5 to 7.2), due to the increased glycolysis and plasma membrane proton-pump activity of tumor cells, which make them produce more lactic acid than normal cells and leach out the acid to the extracellular milieu (Swallow et al., 1990; Montcourrier et al., 1997). Normal tissue has a pH of around 7.4 (Qian et al., 2012). Certain nanocarriers will only release the drugs they contain in specific pH ranges. pH-responsive micelle conjugated with a novel moiety against overexpressed cell surface platelet derived growth factor receptor (PDGFR), loaded with TMZ, are able to target PDGFR on GBM cells. This results in pH-dependent release of TMZ preferably in tumor tissue, thereby reducing systemic toxicity. pH sensitive micelles exhibit specific uptake and increased cell killing in GBM cells and accumulated in brain tumor tissues (Miller at al., 2016).

The overproduction of enzymes such as the matrix metalloproteinases (MMPs) is also common in most tumors, because MMPs are important for angiogenesis, metastasis, and other extracellular signaling events involved in tumor propagation (Egeblad and Werb, 2002). Early expression of MMPs, either by the tumor cells themselves or by surrounding stromal cells, helps to remodel the Extra Cellular Matrix (ECM) and release ECM and/or membrane-bound growth factors, which provides a favorable microenvironment for the establishment of the primary tumor. As the tumor grows, an angiogenic switch occurs (possibly in part because of hypoxia) in which the balance of proangiogenic factors (*e.g.*, bFGF and VEGF) overcomes the expression of angiogenic inhibitors (*e.g.*, thrombospondins, angiostatin, and IFNs) (Hanahan and Folkman, 1996). Both MMP-2 and MMP-9 have been implicated in the induction of the angiogenic switch in different model systems (Egeblad and Werb, 2002). Further up-regulation of MMP expression, in particular the gelatinases, which can degrade basement membrane components, allows the tumor cells to invade into the adjacent stroma and to break down the basement membranes associated with capillaries and lymphatic vessels allowing tumor cells to enter the circulation (intravasation) (Chambers and Matrisian, 1997). MMPs are also involved in cell migration by removing sites of adhesion, exposing new binding sites, cleaving cell-cell or cell-matrix receptors, and releasing chemo-attractants from the ECM (McCawley and Matrisian, 2011). Similar to intravasation, MMPs are necessary for the circulating tumor cells to be able to exit the blood vessels (extravasation), although this step does not appear to be rate limiting for the establishment of metastases (Chambers and Matrisian, 1997). MMP overexpression has been explored as a way of "turning on" imaging agents and locating tumors or other lesions (Mok et a., 2009; Lee et al., 2008; Scherer et al., 2008; Wunder et al., 2004; Weissleder et al., 1999)

In GBM MMP2 expression correlates in GBM with high malignancy and poor prognosis (Ramachandran et al., 2017). MMP2 activatable nanocarriers have shown promising results *in vitro* and *in vivo* rat model of GBM (Gu et al., 2013). However, more detailed experiments and more precise *in vivo* model, such as Patient Derived Xenograft (PDX), are required to better understand the suitability of this system as drug delivery.

3.5 Nano-therapies for GBM treatment

In the last years many attempts have been done to develop NPs suitable for GBM, from drug delivery to diagnostic and imaging (Wiwatchaitawee et al., 2021). Nanodrugs investigated in GBM are platforms with different backbones, such as vesicles (liposome, micelles), linear polymers, metals (Au, Gd,), carbon dots, dendrimers (Prasad et al., 2018), and increasing complexity of functionalizations. Agents active against GBM such as immune entity, chemotherapeutic/anti-angiogenic drugs or sensitizers could be load inside the NV core while specific moieties able to target GBM cellular receptors/angiogenic blood vessels or to open the BBB are bind at its surface (Wadajkar et al., 2017). Two higher levels of complexity are i) the possibility to associate fluorescent/radioactive compounds to enable NVs localization in the organism (Gonawala and Ali, 2017) and ii) the possibility to activate NP on demand by an external source of energy such as X-rays, ultrasounds, or alternating magnetic field (Sneider et al., 2017) (**Fig 14**).

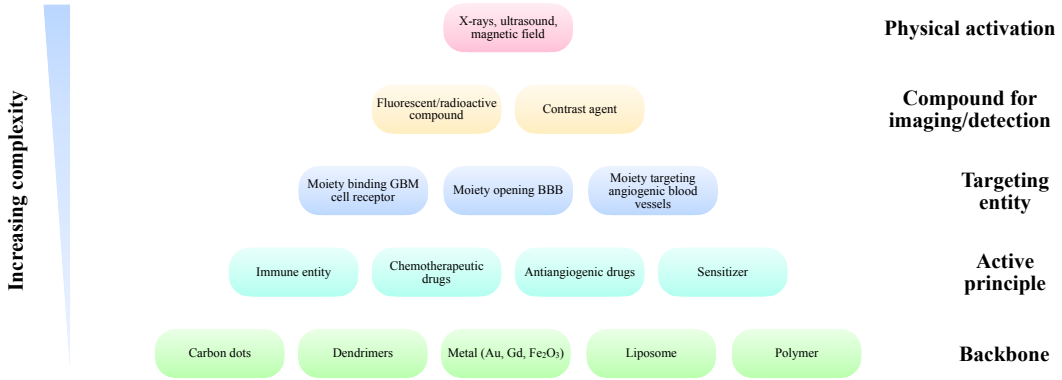

Fig. 14: Increasing complexity of NPs for GBM treatment. NPs development required extremely precise engineering starting from the material of the backbone (or core) of the NP. The complexity of the NPs can be increased by different functionalization such as the active principle we choose to give efficacy to the treatment and the targeting entity to give specificity to GBM cells. The system can be further complicated by the adding of compound useful for imaging or detection such as fluorescent molecules or contrast agent. The highest level of complexity for a NPs is the possibility to be activated on demand by external physical sources like radiation, ultrasound or magnetic field. Adapted from Alphandéry, 2020

In the last years many attempts have been done to combined NVs standard treatments, for example RT, in GBM treatment. It has been demonstrated that fractionated dose of 2Gy (to a maximum dose of 20-30 Gy) increases the BBB permeability (van Vulpen et al., 2002) (**Fig. 15**). Taking advantage from this, Tamborini et al., in 2016 demonstrated that a single

dose radiation is sufficient to improve the BBB crossing of nanoparticles in *in vivo* experiments (Tamborini et al., 2016).

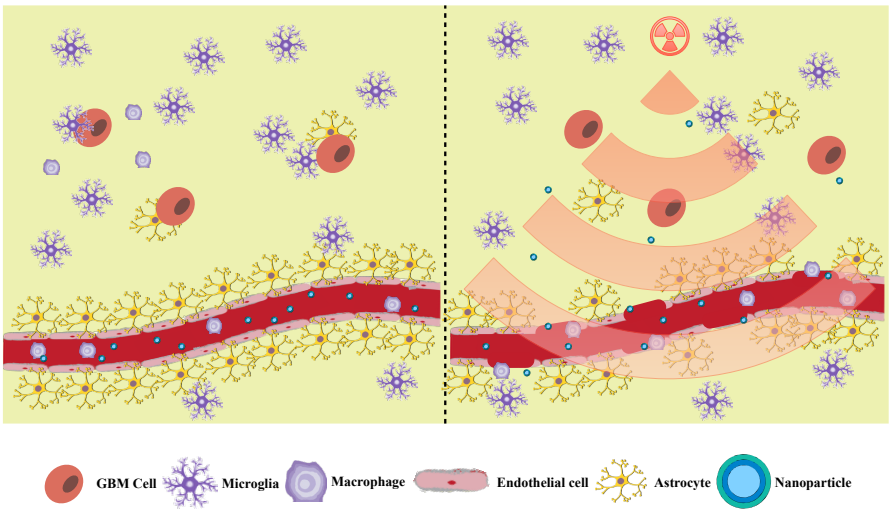

Fig. 15: BBB breakdown after irradiation. Sublethal dose radiation induce transient BBB breakdown and consequent enhance permeability. This represents a useful therapeutic mechanism to reach the single GBM cells disperse into the healthy parenchima., for example with nanoparticles as demonstrated by Tamborini et al., 2016.

Only a small number of all the NVs under investigation were studied in clinical trial. Indeed, only 6 NP based drugs have reached phase I or II clinical trials (**Fig. 16**). Despite NPs are well tolerated and did not exert severe side effects, non of these regimens do significantly improve patients' outcome in terms of progression free survival and overall survival (Hsu et al., 2021)

Name	Case number/patients	Formulation/composition	Main results
Nanothermotherapy Phase II	59 patients with recurrent GBM	Thermotherapy and Magnetic iron-oxide nanoparticles + reduced dose radiotherapy	This combination is safe and effective, leading to longer overall survival.
EDV-doxorubicin Phase I	14 patients with recurrent GBM expressing EGFR	EnGenelC delivery vehicle (EDV)-doxorubicin + radiation and oral TMZ	EDVDox was well tolerated, with no dose limiting toxicity and no withdrawals from the study due to adverse events.
Interleukin-12 Phase I, II	Adult patients with recurrent GBM	Semliki Forest virus vector carrying IL-12 gene encapsulated in cationic liposomes	Liposomally encapsulated virus can be efficiently delivered to GBM using the convection-enhanced delivery.
5-fluorouracil Phase II	95 GBM patients were randomized after surgery	5-fluorouracil-releasing microspheres followed by early radiotherapy	Only slightly increased overall survival in the study group when compared with those received radiotherapy alone.
Caelyx, PEG-Dox Phase I, II	63 patients with newly diagnosed GBM	Pegylated liposomal doxorubicin + prolonged TMZ and radiotherapy	The progression free survival after 12 months was 30.2%, and the median overall survival was 17.6 months. Neither the addition of PEG-Dox nor prolonged temozolomide resulted in a meaningful improvement.
PEG-Dox Phase II	40 patients with newly diagnosed GBM after surgery	TMZ and Pegylated liposomal doxorubicin after radiotherapy and surgery	The progression free survival after 6 months was 58%, and the median overall survival was 13.6 months. Combination of temozolomide and PEG-Dox does not add clinical benefit.

Fig. 16: Clinical trials using nanotechnology and nano carrier based delivery system for treating GBM. Adapted from Hsu et al., 2021.

The limited number of patients included in the trials and the lack of a specific targeting system that confer BBB crossing and GBM specificity could be the main reasons for the lack of significance.

Rationale of the study

The ultimate goal of the project is the synthesis of multi-task targeted, drug-loaded nanovectors able to penetrate GBM tumors and release chemotherapeutics for GBM treatment. To this end the research activity focused on three essential requisites to assure therapeutic efficacy to the drug delivery nanovectors:

1. BBB crossing aptitude
2. selectivity to GBM that includes GSCs and surrounding microenvironment
3. Reduced drug toxicity

Considering the crucial involvement of the LDL-receptor in the transport of macromolecules from the blood stream to the brain, the mApoE peptide known to confer BBB crossing capacity to nanovectors in the context of neurodegenerative diseases (Dehouck et al., 1997; F, Re et al., 2011; C. Balducci et al., 2014) was selected as BBB targeting moiety.

Two strategies were investigated to achieve specific GSCs targeting and commitment to cell death:

1. **The mApoE peptide** - Thanks to an extensively reprogrammed cellular metabolism, tumor cells survive and proliferate under nutrient and oxygen deprivation. In this context, GBM cells are highly dependent on cholesterol supply for survival and rely on exogenous cholesterol uptake, mediated by LDLR (Villa et al., 2016). Indeed, LDLR is expressed in GBM and its upregulation correlates with tumor progression and drug resistance (Geng et al., 2016; Guo et al., 2011; Maletinska et al., 2000). Moreover, LDLR is highly expressed at the BBB (Wagner et al., 2012) and is crucially involved in the transport of macromolecules from the blood stream to the brain, by RMT (Fung et al., 2018; Pulgar et al., 2018). LDLR binds and internalizes Apolipoprotein E (ApoE)-containing lipoproteins which mediate the brain metabolism of cholesterol (Pirmoradi et al., 2019). Therefore, a peptide derived from ApoE (mApoE) should assure to a

nanovector the two main issues of glioblastoma treatment: the BBB transcytosis and cancer cell specific targeting (**Fig. 8**).

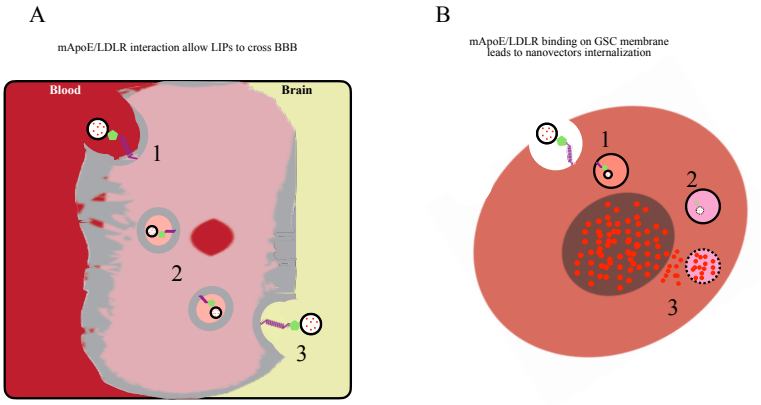

Fig 8: mApoE dual-targeting strategy simultaneously targeting BBB and GSCs. A) Schematic representation of mApoE-NV BBB crossing by RMT. Upon mApoE-LDLR interaction on the apical membrane of endothelial cells, mApoE-NVs are internalized (1). The endosome transports the complex to the basolateral membrane (2) where the mApoE-NVs are released into brain parenchyma. **B**) Schematic representation of mApoE-NV internalization into GSCs. After mApoE-LDLR mediated cell uptake and internalization (1), NVs inside endosome are degraded (2) and the DOXO released in the cytoplasm and penetrates into the nucleus.

2. **MMP-Activable Low Molecular Weight Protamines (LMWPs)** - Taking advantage of the remarkable upregulated expression of MMP-2 and -9 in the GBM tumors (Ramachandran et al., 2017), and in order to increase nanovector cellular uptake and GBM tumor specificity, a strategy based on the use of Cell Penetrating Peptides (CPP) coupled to an MMP2/9 activatable peptide sequence was investigated. Protamines are short peptides enriched in arginine that confers them high cell penetrating ability. As the non-selective mechanisms of cellular entrance, LMWPs generate important side effects when utilize to deliver drug-loaded NVs. The link of LMWP to a MMPs-sensitive sequence makes LMWP-NVs activable (ALMWP-NVs) in MMPs rich environments like the tumor microenvironment. When MMP2 cleave the cleavable PLGLAG sequence, polyanionic domain is separated by polycationic one, allowing LMWP-cell membrane interaction and LMWP uptake (**Fig. 9**). This would assure reduced unspecific interaction in tissue where MMPs are low or absent like brain healthy parenchyma and blood.

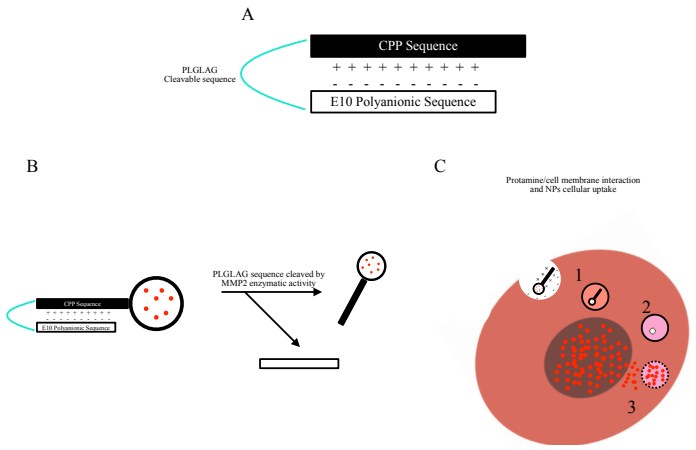

Fig 9: ALMWP assembly and mechanism of action. A) CPP sequence (Low Molecular Weight Protamine, LMWP) is linked to the E10 polyanionic sequence by a MMP2 cleavable sequence (PLGLAG). Negative charges on the E10 polianionic sequence counterbalance the positives on CPP inhibiting its interaction with the cell membrane. **B**) Schematic representation of mechanism of action of ALMWP functionalized NVs. When the ALMWP-NVs is in the MMP2 enriched tumor microenvironment, PLGLAG is cleaved by MMP2 enzymatic activity, CPP-NVs are separated from the E10 sequence and, consequently, LMWP positive charges can freely interact with the cell membrane, negatively charged (1), allowing NVs internalization in endosome (2). The NVs are subsequently degraded and the DOXO released in the cytoplasm where it penetrates into the nucleus and can intercalates the DNA (3).

The different types of targeted nanovectors were chosen to deliver the chemotherapeutic agent DOXO. It was chosen as incapsulated drugs as paradigm of anticancer drug effective against GMB cells *in vitro* but with poor efficacy *in vivo* due to extrusion by multidrug resistance-related proteins present both on BBB and GBM cells (Gomez-Zepeda et al., 2019). Furthermore, cancer cells exposed to DOXO elicit antitumor immunity by immunogenic cell death (ICD), a functionally unique form of cell death that occurs when apoptotic cells secrete distress signals called damage-associated molecular patterns (DAMPs) to trigger an antigen-specific immunity (Kroemer et al., 2013, Kawano et al., 2016). A critical step for ICD is the engulfment of dying cells by professional macrophages and the activation of a variety of cells of the innate immunity, essential for the priming of the adaptive immune response (Galluzzi et al., 2017; Rapoport et al., 2019). Finally, DOXO exhibit severe side effects when administered as free drug (Zhao and Zhang 2017): the encapsulation should reduce the insurgence of these side effect, in particular cardiotoxicity.

Results

1. Nanovector BBB crossing and GBM therapeutic opportunities

Different NPs based formulation have been tested for cancer treatment(Hsu et al., 2021). Among them DOXO-loaded liposomes (DOXO-LIPs), up to date, the only nanomedicines approved for solid tumor (Marchal et al., 2015; Wicki et al., 2015). Due to a significantly lower systemic toxicity, liposomal DOXO was the first FDA-approved nano-drug in 1995. In particular, liposomal-DOXO showed promising results as adjuvant agent in some solid tumor in particular breast cancer (Zhao et al., 2017; Li et al., 2019). Unfortunately, two different clinical studies conducted to assess the eligibility of liposomal-DOXO as GBM treatment did not reach significant prognosis and overall survival results, actually unaltered compared to standard protocol (Menei et al., 2005; Beier et al., 2009). The main cause of these failures was the inability of liposomal DOXO to cross BBB and, therefore, reach brain parenchyma and GBM (Ananda et al., 2011).

It appears clear that NPs would not be effective on GBM without a system able to specifically target the BBB triggering NPs translocation into the brain. Among the possible mechanisms that could lead to BBB crossing, RMT is one of particular interest because it takes advantage of receptors expressed on the membrane of the endothelial cells that composed brain capillaries.

In this prospective, the laboratory of the Nanomedicine Center (NANOMIB) of the University of Milano-Bicocca has developed a LIPs conjugated with a modify peptide derived from the protein component of the ApoE lipoprotein named mApoE-LIPs. In two different studies they demonstrated their ability to cross the BBB and be effective to remove β-amiloid (Aβ) plaques in Alzheimer Disease models (Re et al., 2011; Balducci et al., 2014). Taking advantage from their long and outstanding expertise on the use of mApoE-LIPs, we collaborated with them to translate the LIPs to GBM treatment. To this end, mApoE-LIPs were loaded with DOXO (mApoE-DOXO-LIPs) in order to have system able to both cross the BBB by RMT through the mApoE/LDLR interaction (Wagner et al.,

2012) and, moreover, possibly target GSCs in the brain parenchyma (Geng et al., 2016; Guo et al., 2011; Maletinska et al., 2000).

1.1 mApoE-LIPs and *in vitro* BBB crossing

LIPs were synthesized by extrusion procedure mixing Sphingomyelin (Sm), Cholesterol (Chol) and PE-PEG-mal (48.75:48.75:2.5 molar ratio). Successively, LIPs were incubated with DOXO to obtain DOXO-LIPs and, finally, they were functionalized to obtain mApoE-DOXO-LIPs (**Fig. 10 A**). The final preparations were formed by mono dispersed LIPs of a diameter ranging from 102 to 128 nm and negatively charged (**Fig. 10 B**). Drug release kinetic from mApoE-DOXO-LIP demonstrate that LIPs are extremely stable nanovectors, having a DOXO release rate of just 0.11%/hr at pH 5 and 0.05%/hr at pH 6.5 and 7.4 (**Fig. 10 C**).

A

B

NV formulation	Size ± SD (nm)	Z-Potential ± SD (mV)	Polydispersion Index
LIP	102 ± 5	-25.51 ± 0,82	0,077
DOXO-LIP	117 ± 12	-18.74 ± 1.25	0,106
mApoE-DOXO-LIP	128 ± 15	-12.48 ± 2.02	0,081

C

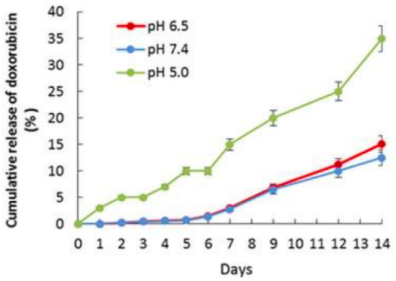

Fig. 10: characterization of mApoE-DOXO-LIPs. A) Schematic representation of Sphingomyelin (Sm)/Cholesterol (Chol) LIPs functionalized with mApoE peptide and embedding DOXO. **B**) cumulative DOXO release (%) over time from mApoE-DOXO-LIPs at pH 5.0, 6.5 of 7.4 at 37°C. The reported data are the mean of at least five different measurement ± SD. **C**) Physiochemical parameters of synthesized LIPs: mean diameter (size); polydispersion index (PDI) by dynamic light scattering (DLS); Zeta-poyrnyial (ζ-pot) by Zeta potential analyzer. All liposome preparations maintained a constant size and ζ-potential for up to 10 days within the experimental error (<2.6% of variation). The yield of DOXO encapsulation into LIP was 95±3% and the final preparation contained 220±12 µg of DOXO/µmol of lipids. The yield of LIP surface functionalization with mApoE peptide ranged between 55% and65% corresponding to 1.25% of total lipids. These data were kindly provided by Francesca Re (PhD) laboratory.

mApoE-DOXO-LIP ability to cross the BBB and target GBM cells was investigated *in vitro* using a transwell system integrated with a human brain capillary endothelial cell monolayer (hCMEC/D3), as a model of BBB (**Fig. 11 A**). A significant enhancement (approximately 5-fold) in DOXO permeation through the BBB was observed for mApoE-

DOXO-LIPs compared to DOXO-LIPs without affecting LIPs integrity (**Fig. 11 B, C**). Moreover, mApoE-DOXO-LIPs didn't alter BBB model transepithelial electrical resistance (TEER) and permeability compared to free DOXO, indicating that the drug incorporation into LIPs reduces its cytotoxicity on non-target cells (**Fig 11 D**).

In order to assess mApoE-DOXO-LIPs anti-tumor ability after BBB crossing, BBB model was integrated with GBM cells (U87MG and A172) in the lower chamber of the transwell (**Fig. 11 E**). Results in **Fig. 11 F** showed that the addiction in the upper chamber of mApoE-DOXO-LIPs, but not DOXO-lip, significantly reduced the viability of both U87MG and A172 cells by approximately 53% and 60% respectively after BBB crossing.

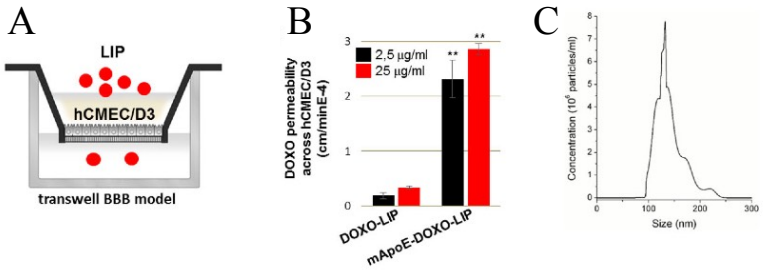

D

NV formulation	TEER (Ω cm²)	EP of Lucifer yellow (cm/min)
CTR	41.12 ± 7	1.87 ± 0.6*10^{-3}
DOXO-LIP	30.58 ± 9	1.48 ± 0.05*10^{-3}
mApoE-DOXO-LIP	33.30 ± 11	1.53 ± 0.08*10^{-3}
Free DOXO	21.58 ± 6	3.06 ± 0.2*10^{-3}

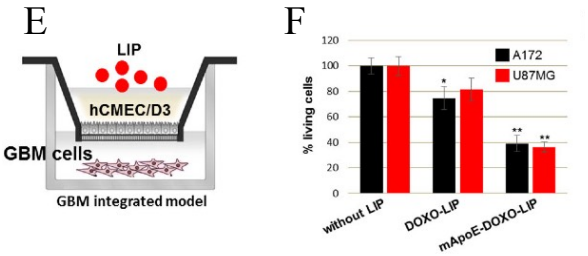

Fig. 11: ***In vitro*** **BBB crossing and GBM cell viability**. **A**) Schematic representation of the *in vitro* BBB model prepared using hCMEC/D3 cells seeded on the transwell filter. **B**) EP to embedded DOXO determined by adding samples in the apical compartment and monitoring DOXO fluorescence in the basolateral one after 3h incubation. **C**) mApoE-DOXO-LIP size after BBB crossing determined by nanoparticle tracking analysis of LIPs present in the basolateral compartment. **D**) TEER and EP to LY of endothelial monolayers after 3h incubation with DOXO (25µg/ml), free or embedded into LIPs. **E**) Schematic representation of the integrated transwell system prepared seeding adherent GBM cells in the basolateral compartment. **F**) hCMEC/D3 cells, in co-culture with U87MG or A172, were incubated with DOXO-LIPs or mApoE-DOXO-LIPs added in the apical compartment (DOXO 25 µg/ml). After 3h incubation, the transwell insert was removed and GBM cells viability was determined by MTT assay after additional 72h of culture. Pairwise comparison was performed by Student's *t*-test. **P*< 0.05, ***P*< 0.01, **** *P*<0.0001. Data kindly provided by Francesca Re's (PhD) laboratory.

To verify that LIPs needed an active mechanism of internalization, GBM cells were treated with mApoE-DOXO-LIPs and DOXO-LIPs and analyzed by confocal microscopy. Results indicated a 3- to 6-fold increase of nuclear DOXO triggered by mApoE surface LIP functionalization (**Fig. 12 A, B**), suggesting the inability of LIPs to be internalized without a functionalization. Moreover, to confirm the receptor mediated and not unspecific internalization, cells were treated with the clathrin-mediated endocytosis inhibitor chlorpromazine (CPZ) and with the endocytosis inhibitor dynasore (DYN). mApoE-DOXO-LIPs internalization was significantly inhibited in the presence of both the inhibitor, confirming that mApoE-DOXO-LIPs needed a receptor to be internalized by transcytosis (**Fig. 12 C, D**).

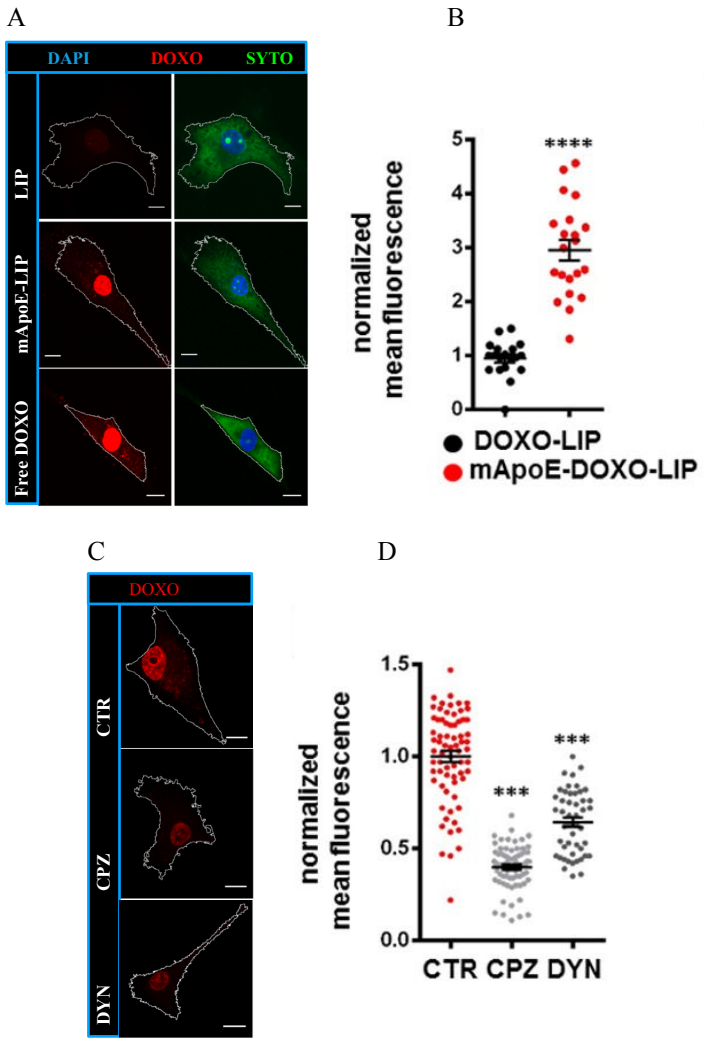

Fig. 12: LIP internalization in GBM cells. A) Maximum projections of DOXO and Syto/DAPI merged signals acquired by means of confocal microscopy in U87MG cells incubated with liposomes (DOXO-LIP or mApoE-DOXO-LIP) or free-DOXO. **B**) Nuclear DOXO quantification in U87MG cells incubated with the indicated LIPs. **C**) Maximum projections of DOXO signals in U87MG cells incubated with mApoE-DOXO-LIP alone (CTRL) or in the presence of the endocytosis inhibitors chlorpromazine (CPZ) and dynasore (DYN). **D**) with mApoE-DOXO-LIPs alone (CTRL) or in the presence of CPZ and DYN. All data are reported as the mean of at least three independent experiments ± SD.Pairwise comparison was performed by Student's *t*-test. ***P<0.001, ****P<0.0001

1.2 LIPs cellular uptake and cytotoxicity in patient-derived GSCs

One of the main causes of GBM recurrence is the presence of the GSCs able to invade brain parenchyma and resist to standard treatment (Singh et al., 2004; Bao et al., 2006; Chen et al., 2012; Bao et al., 2006; Chen et al., 2012; Cheng et al., 2011). Therefore, to investigate whether mApoE-LIPs could be exploited to target the tumor stem cell subpopulation, three GSC lines established from patient surgical samples named BG003, BG005 and GBM3 were treated with DOXO-LIPs and mApoE-DOXO-LIPs.

GSCs were first tested *in vitro* for their ability to internalize functionalized LIPs. mApoE-DOXO-LIP intracellular uptake was evaluated through nuclear DOXO fluorescence quantification. DOXO-LIP conjugation with mApoE significantly favored nuclear DOXO accumulation in all three GSC cultures (**Fig. 13 A, B**). Dose-dependent inhibition of cell viability was observed when GSCs were exposed to mApoE-targeted LIPs indicating that embedded DOXO was functional and effective. Conversely, non-targeted DOXO-LIPs did not affect GSC viability, even at the highest DOXO dosage, thus excluding cellular adverse responses to endotoxin contaminants possibly present in the LIP preparations (**Fig. 13 C**).

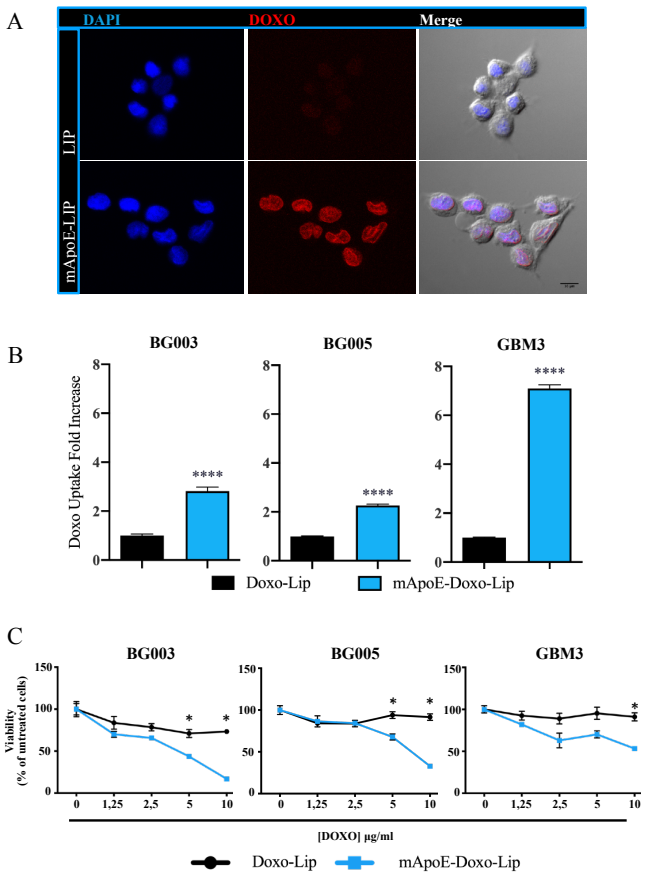

Fig. 13: LIP internalization and cytotoxicity in patient-derived GSC lines. A) Representative images of DOXO, DAPI and bright-field differential interference contrast merged signals in GCS3 cells incubated with mApoE-DOXO-LIP or DOXO-LIP. **B**) Nuclear DOXO quantification expressed as mean fluorescence intensity (MFI) ± SE normalized to 16 MFI detected in cells incubated with DOXO-LIPs (4h, DOXO 4mg/ml). **C**) Cell viability after 48h incubation with LIPs at the indicated increasing DOXO concentrations. Values are expressed as mean percentage survival (six replicates ± SE) normalized to corresponding untreated. Pairwise comparison was performed by Student's *t*-test.**P*<0.05, *****P*<0.0001.

Considering that GBM standard treatment involve radiotherapy (RT) and that RT could alter protein expression (Wahaba et al., 2017), LDLR expression was measured in GSCs before and after a sub-lethal dose radiation of 2Gy, corresponding to the daily dose administered to the patients in a fractionated radiation protocol. BG003 and BG005 cells exhibited an approximate 2-fold and 4-fold increase of LDLR expression respectively while no LDLR modulation was observed in GBM3 cell cultures (**Fig. 14 B**). As a consequence, the radiation-induced LDLR expression was paralleled by higher levels of mApoE-DOXO-LIP uptake by BG003 and BG005 cells. Consistently with lack of LDLR induction, no difference in mApoE-DOXO-LIP uptake was observed in irradiated GBM3 cells (**Fig. 14 C**).

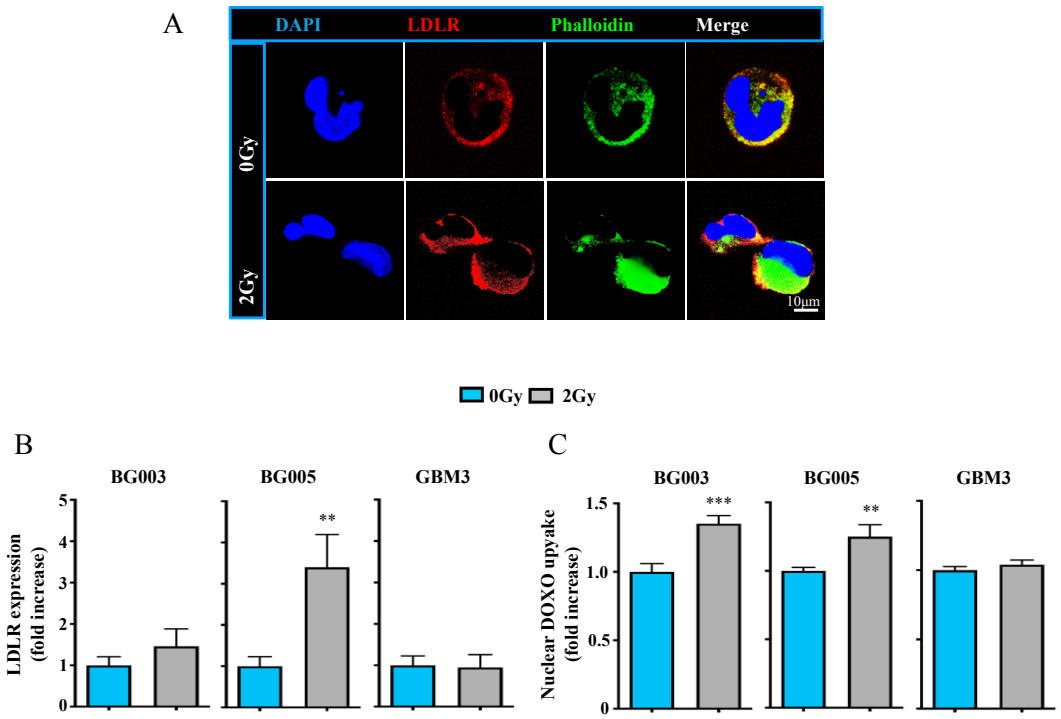

Fig. 14: effect of radiations on LDL-R expression and BBB permeability. A) Representative confocal images of irradiated (2Gy) and non-irradiated (0Gy) BG005 cells immunostained for human LDLR (red). In blue is the nuclear staining (DAPI). The cell bodies were defined by Phalloidin staining (green). **B**) LDLR level of expression in non-irradiated (0Gy) and irradiated (2Gy) GSCs. The results are expressed as mean LDLR fluorescent area respect to non-irradiated samples ± SE. **C**) Intracellular DOXO quantification in non-irradiated and irradiated GSCs incubated with mApoE-DOXO-LIPs. Results are expressed as MFI normalized to MFI of non-irradiated cells ± SE. Pairwise comparison was performed by Student's *t*-test.**P* < 0.05, ***P*<0.01.

Alteration in GSC protein expression after radiation could reflect on the surrounding microenvironment. A pivotal point could be the effect of this modified microenvironment on BBB protein expression and permeability. Hence, conditioned medium (CM) obtained culturing irradiated (2Gy) GSCs were added to the transwell BBB models in order to recapitulate irradiated microenvironment and compared to non-irradiated (0Gy) CM. Both the conditioned medium induced an upregulation of LDLR on hCMEC/d3 cells but only CM from irradiated GSCs caused a stable drop of TEER, indicating an increased BBB permeability (**Fig 15 A, B**).

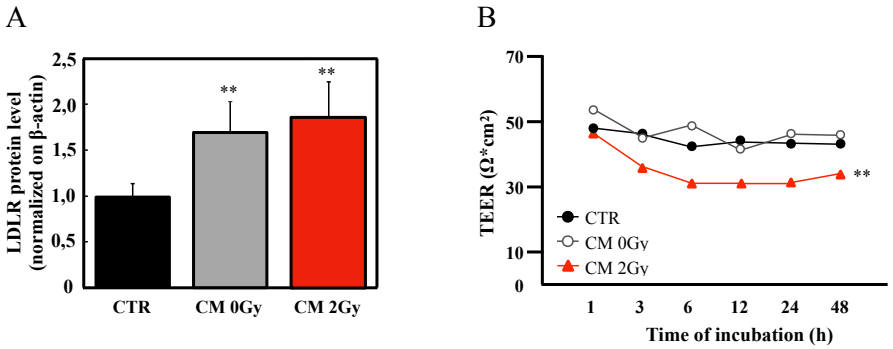

Fig. 15: effect of irradiated GSC conditioned medium on BBB. A) TEER values of BBB transwell model untreated (CTR) or incubated with GSC conditioned media (CM) before (0Gy) and after radiation (2Gy). **B**) LDLR protein level in hCMEC/D3 cells before (CTR) and after 12h-incubation with CM from non-irradiated and irradiated GSCs. Pairwise comparison was performed by Student's *t*-test.*$P < 0.05$, **$P<0.01$.

Overall, these results demonstrate the ability of mApoE-DOXO-LIPs to target *in vitro* different patient-derived GSCs biding LDLR. Moreover, the enhanced expression of LDLR on GSC cells after irradiation and the overexpression of the receptor on endothelial cell induced by GSC CM suggested that mApoE-DOXO-LIPs and radiotherapy could be efficiently combined to develop an *in vivo* protocol.

1.3 mApoE-DOXO-LIP antitumor activity in orthotopic GSC-PDXs

The *in vitro* results strongly suggested that RT may facilitate LIP brain delivery and uptake by tumoral cells. Therefore, mApoE-DOXO-LIPs were delivered either as single treatment or in combination with radiations to BG003-PDX obtained by orthotopic injection of luciferase-transfected BG003 (BG003luc). Injection of human cells in mouse represents a great issue since host immune system immediately recognizes tumor cells as non-self and

rejects the graft. To overcome tumor cells rejection, BG003luc cells were implanted in NOD/SCID mice that have impaired T and B cell lymphocyte development and lack in natural killer (NK) cell function. Tumor growth in this model is quite slow. Indeed, it took 60 days after BG003luc intracranial injection (D60) to detect a visible tumor mass (**Fig 16 B**). Starting from D60 mice were treated with mApoE-functionalized LIPs as single agent (mApoE-DOXO-LIP) or in combination with radiation (2Gy/mApoE-DOXO-LIP) according to the schedule reported in (**Fig 16 A**). Untreated mice (CTR), and mice treated with untargeted LIPs (DOXO-LIP) or radiation only (2Gy) were included as controls.

BLI performed during (D67) and at the end (D75) of the treatment (**Fig. 16 B**) indicated an overall low tumor growth rate that underwent a considerable boost in the subsequent ten days (D85) reaching an 8.4±5.3 and 12.0±8.2-fold increase, in untreated and DOXO-LIP controls, respectively. Treatment with mApoE-DOXO-LIP slowed tumor expansion to a 6.3±2.7 fold increase (**Fig. 16 C, D**). Importantly, the highest and significant level of tumor growth inhibition, -6.4±4.7 times, was observed in mice receiving radiation together with mApoE-DOXO-LIPs (2Gy/mApoE-DOXO-LIP) (**Fig. 16 B, D**). Accordingly, overall survival equaled tumor expansion/inhibition, with 2Gy/mApoE-DOXO-LIP treatment resulting in increased survival compared to any other treatments (**Fig. 16 E**).

Morton and Griffith's parameters of animal condition (body weight, physical appearance, measurable clinical signs, unprovoked behavior and response to external stimuli) (Morton and Griffith, 1985) were monitored periodically until the end of the experiment. Body weight monitoring indicated a loss of weight, approximately 12%, in all mice receiving LIPs. Weight loss stopped in concomitance with the end of the treatment (D75) and since then mice started gaining weight regardless tumor volume and death event (**Fig. 16 F**) suggesting a sensible, yet compatible with life, LIP systemic toxicity.

mApoE-DOXO-LIP biodistribution performed after a single injection in healthy mice with radio labelled DOXO and LIPs showed LIPs prolonged DOXO circulation half-life and reduced DOXO accumulation in liver, kidney, lungs and hearth (**Fig. 16 G, H**). Nonetheless, the liver remains the main organ where approximately 40-50% of the injected LIPs accumulate, probably inducing the systemic suffering and weight loss observed.

A progressive increase of DOXO accumulation was detected upon mApoE-DOXO-LIP delivery in brain. Results indicated that 24h after injection the amount of free DOXO in the brain was reduced by 2.7-fold whereas it was 4.4-fold higher after the administration of mApoE-DOXO-LIP (**Fig. 16 G**). However, low levels of signal were detected in the brain suggesting a limited amount of mApoE-DOXO-LIP could cross intact BBB.

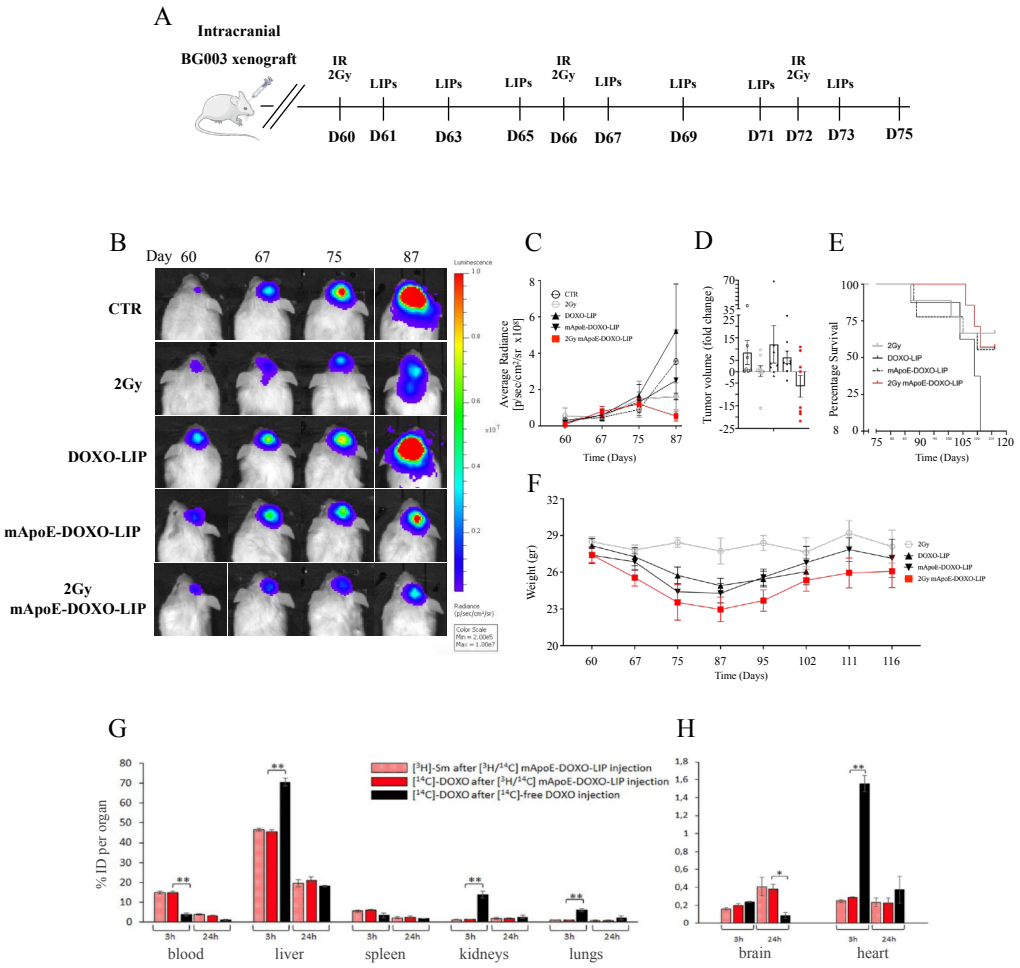

Fig. 16: ***in vivo*** **efficacy of mApoE-DOXO-LIPs in the GSC-PDX model. A**) Treatments started sixty days (D60) after intracranial injection of BG003luc cells and were administered according to the indicated schedule. BG003luc bearing mice (n=9 mice/group) received 35 µg/dose of encapsulated DOXO intraperitoneally. Irradiation (2Gy) was administered as whole-brain treatment. **B**) Representative BLI imagines of tumor-bearing mice untreated (CTR), and treated with untargeted DOXO-LIPs (DOXO-LIP), mApoE-functionalized LIPs as single agent (mApoE-DOXO-LIP) or concomitant with radiation (2Gy/mApoE-DOXO-LIP). **C**) Time course quantification of tumor BLI signals. Results are expressed as mean of radiance values ± SE detected at the indicated time points. P-values are calculated using two-way ANOVA and Tukey's multiple comparisons test (**P < 0.01). **D**) Tumor growth/inhibition at D85 (12 days after treatment end). Data are expressed as relative BLI radiance mean values ± SE normalized to BLI values at D75. **E**) Kaplan–Meier survival curve. P-log = 0.0863. **F**) Body weights of the alive animals at the indicated time points. Data are presented as the mean values ± SE. **G**) mApoE-DOXO-LIP distribution in peripheral organs and across intact BBB. Dually radiolabeled mApoE-DOXO-LIP ([3H]-Sm/[14C]-DOXO) or free-[14C]-DOXO were intravenously injected in healthy mice. Mice were sacrificed 3h or 24h after the injection. Radioactivity in peripheral organs was measured by liquid scintillation counting. The amount of [3H]-Sm or [14C]-DOXO is expressed as percentage of injected dose (ID) ± SD. Pairwise comparison was performed by Student's t-test. *P< 0.05, **P< 0.01.

To examine in depth the tumor growth inhibition in mApoE-DOXO-LIP-treated mice, BLI experiments were corroborated by histological analyses. A new group of mice were injected with BG003-luc and treated as in the previous experiment (**Fig. 16 A**). At the end of the treatment (D75), brains were collected from sacrificed mice and three section of each brain were analyzed (**Fig. 17 A**). Results confirmed that BG003 cells maintained their stemness demonstrated by the expression of the stem markers Nestin and SOX2 (**Fig 17 B**). BG003 detected by Human Nuclei (HU) immunohistochemistry in GSC xenograft confirmed tumor shrinkage in mice receiving radiation and mApoE-DOXO-LIPs (**Fig. 17 C**). In order to obtain an index of tumor growth and progression, BG003 cells were counted in the contralateral, not-injected hemisphere. BG003 quantification revealed a reduction of tumor cell spreading along commissural fibers upon treatment with radiation either alone (2Gy) or in combination with mApoE-LIPs (2Gy/mApoE-DOXO-LIP) as indicated by the significant lower number of DAPI/HU-positive cells in the contralateral hemisphere (**Fig 17 C, D**).

Apoptosis analysis (TUNEL assay) indicated a co-localization between TUNEL and HU staining (**Fig. 17 C**). Notably, apoptotic BG003 cells were observed exclusively in the xenografts of mice receiving mApoE-DOXO-LIPs, both as single agent (0Gy/mApoE-DOXO-LIP) or concomitant with radiation (2Gy/mApoE-DOXO-LIP). No/low TUNEL staining was observed in mice treated with radiation alone (2Gy) and in HU-negative nuclei (murine cells) (**Fig. 17 E**).

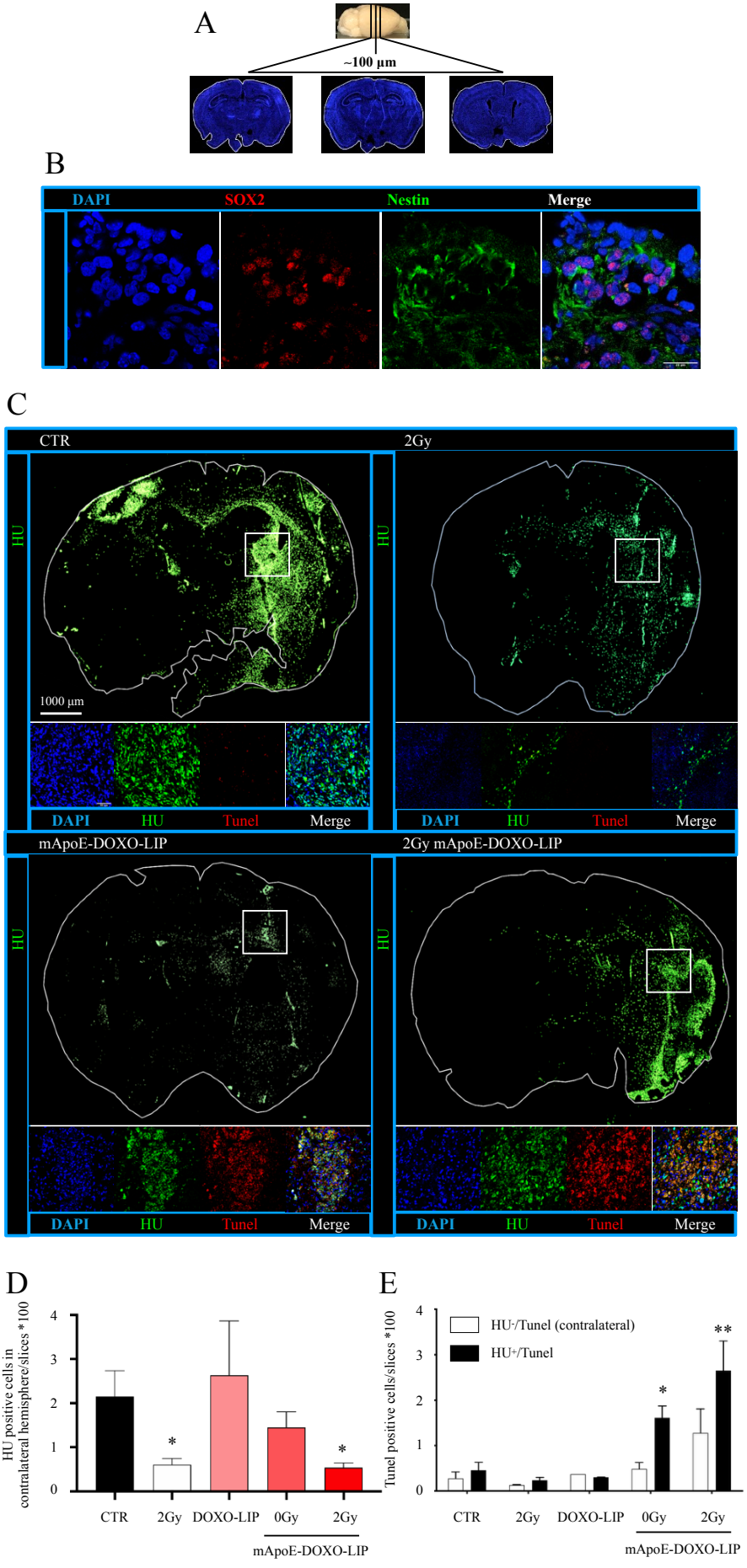
A
~100 µm
B
DAPI
SOX2
Nestin
Merge
C
CTR
2Gy
mApoE-DOXO-LIP
2Gy mApoE-DOXO-LIP
HU
1000 µm
DAPI
HU
Tunel
Merge
D
HU positive cells in contralateral hemisphere/slices *100
CTR
2Gy
DOXO-LIP
0Gy
2Gy
mApoE-DOXO-LIP
E
Tunel positive cells/slices *100
HU-/Tunel (contralateral)
HU+/Tunel

Fig. 17: tumor growth and apoptosis in mApoE-DOXO-LIP treated GSC-PDX. Mice (*n*=4 mice/group) treated as previously described (Fig.4A) were sacrificed at D75 and brains collected for histological analyses. **A**) Three coronal brain cryosection (10 µm) were analyzed for each treated and untreated mouse. Cryosection at the intersection of the tumor injection site and serial anterior posterior sections (50 mm distance) were considered. Coronal images were acquired using a DMi8 fluorescent microscope and a Leica Application Suite X (LASX) imaging system (Leica Microsystems). DAPI signal (blue) for nuclei detection was used to delimitate brain section contour (white line). **B**) Representative image of staminal markers nestin (green) and sox2 (red) expression in BG003 xenografts 80 days after intracranial injection. In blue is the DAPI signal for nucleus detection. **C**) Representative coronal sections from untreated (CTR) and 2Gy/mApoE-DOXO-LIP treated mice. BG003 cells were detected by anti-human nuclei (HU) immunofluorescence. Apoptotic cells were detected by TUNEL staining on the same brain sections. **D**) Quantification of BG003 cells in contralateral, not-injected hemisphere calculated as number of HU+/DAPI+ nuclei with a fixed area range of 12-50 mm2. Imaging analysis was carried out using the FIJI software. Results are expressed as mean of HU+/DAPI+ nuclei ± SE. **E**) Quantification of apoptotic cells defined by nuclear HU, DAPI and TUNEL co-localization. Results are expressed as mean values ± SE of HU-positive (human, black bars) and HU-negative (murine, white bars) cells. Only murine cells in the contralateral hemisphere were considered. Imaging analysis was carried out as in panel B. One-way ANOVA and Bonferroni *post hoc* testing were used to assess differences between treatments, $*P < 0.05$; $**P < 0.01$.

These data confirmed tumor reduction in mApoE-DOXO-LIPs treated mice and the adjuvant effect that targeted LIPs have in combined therapy with radiation. Moreover, DOXO encapsulation suggested reduced side toxicity on non-humoral cells.

ICD induced by DOXO on tumor cells should induce the removal of death cells by scavenger cells (Werfel and Cook, 2018). In the context of GBM these cells are represented by Glioma-Associated Microglia/Macrophages (GAMMs) (Gieryng et al., 2017). GAMM infiltration was evaluated in the BG003-xenographt by means of Iba1 immunostaining. No relevant differences were detected in the extent of GAMM infiltration among the treatments (**Fig. 18 A, B**). Conversely, a conspicuous difference in the morphology of Iba1-positive cells was observed (**Fig 18 B**). In untreated tumors, infiltrating GAMMs displayed a ramified, highly branched shape disclosing a resting status. In contrast, in mApoE-DOXO-LIP treated tumors GAMMs had an amoeboid morphology revealing a phagocytic/activated phenotype (**Fig. 18 B**). Moreover, HU-positive fragments were visible inside GAMMs of mApoE-DOXO-LIP-treated mice (**Fig. 18 C**).

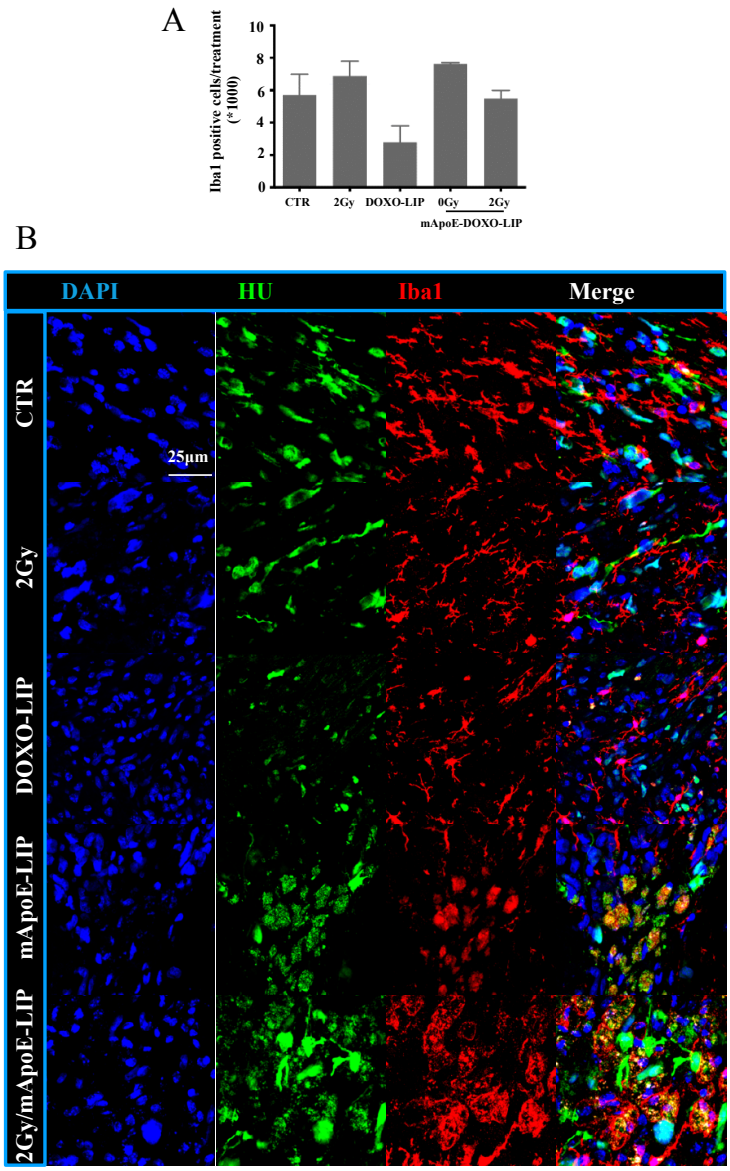

Fig. 18: Iba1 cells infiltration in xenograpgt and morphology. **A**) Quantification of microglia macrophages in brain cryosections by Iba1 and DAPI staining detected using a DMi8 fluorescent microscope (Leica Micro systems). Iba1/ DAPI-positive cells present in the tumor-injected hemisphere were counted in three serial section for each brain (Fig. 11 A). Quantification was carried out by imaging analysis (FIJI software). Results are expressed as mean values±SE of at least nine sections of the indicated treatment group. **B**) Representative images of cryosectons in the tumoral area from untreated mice (CTR) and animals treated with radiation (2Gy), DOXO-LIPs or mApoE-DOXO-LIPs alone (0Gy)or incombination withradiation (2Gy).

Of note, GAMM amoeboid morphology and HU-positive fragments co-localized with TUNEL staining (**Fig. 19 B**), indicating GAMM-mediated phagocytosis of cellular/nuclear debris released by apoptotic BG003 cells. As a further support, Iba1-positive cells associated to vital TUNEL-negative BG003 cells had a branched morphology and an intact nucleus (**Fig. 19 B**).

To further demonstrate that LIP-encapsulated DOXO can trigger ICD, CD11 expression was analyzed as marker of antigen presentation (Hume, 2008) in GAMM of BG003-xenographt. No CD11c induction was detected in resting microglia/macrophages from both untreated and irradiated mApoE-DOXO-LIP-treated mice, whereas CD11c was upregulated in activated GAMM upon mApoE-DOXO-LIP/radiation combined treatment (**Fig. 19 C**).

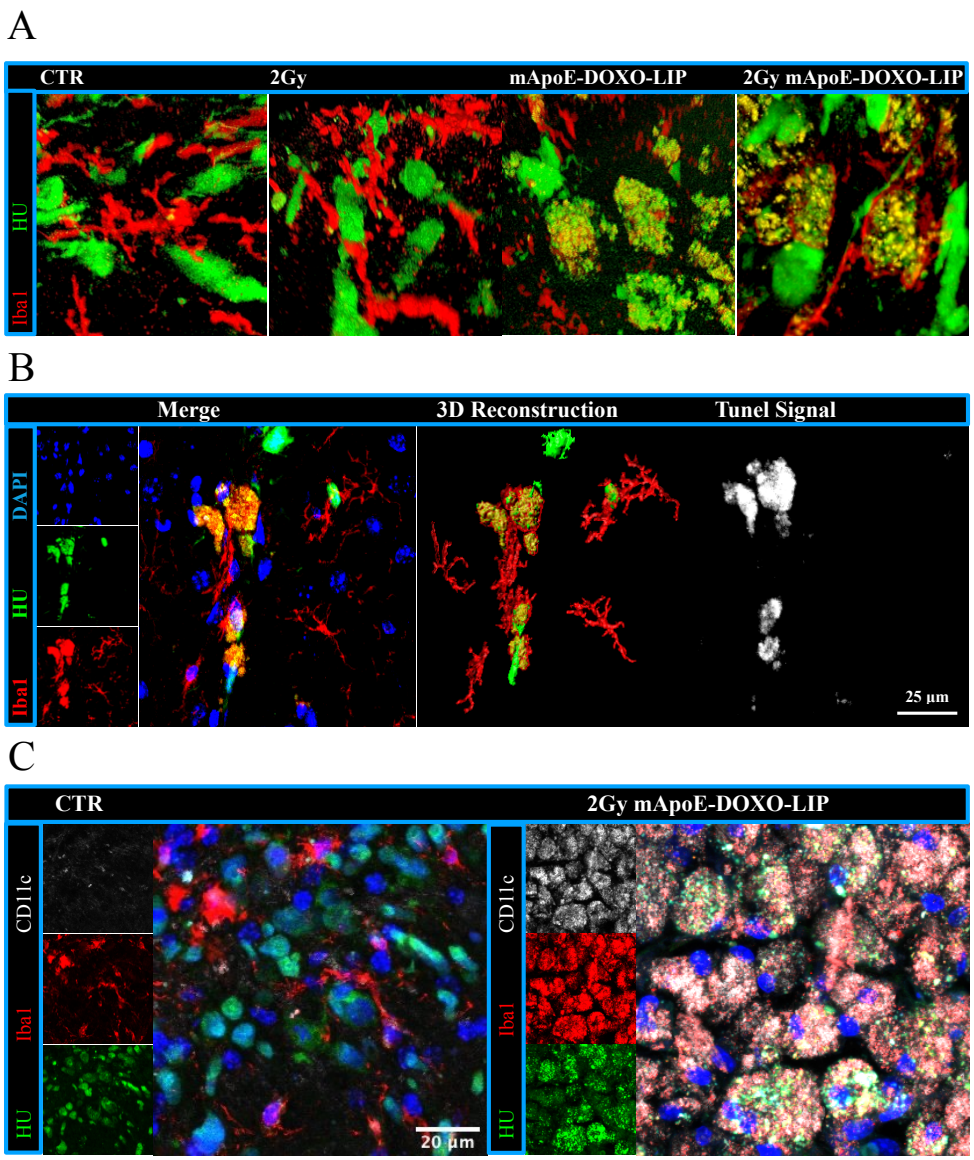

Fig. 19: immune activation in GSC xenografts. **A**) Representative 3D images of Iba-positive, tumor infiltrating microglia/macrophage in untreated (CTR), irradiated (2Gy) and mApoE-DOXO-LIP, without (0Gy) and with (2Gy) radiation, treated mice. Yellow staining indicates HU and Iba1 co-localization. **B**) *In situ* TUNEL detection within Iba1-positive cells at tumor border. **C**) Representative confocal images of CD11c (white) immunohistochemical detection in Iba1-positive (red) cells in untreated and 2Gy/mApoE-DOXO-LIPs treated mice.

These *in vivo* results demonstrate the ability of the mApoE peptide to efficiently target both the BBB and the GSCs leading to a reduced tumor growth and cellular dissemination in the healthy parenchyma. Reduced tumor growth and cellular dissemination could be the cause of the prolonged overall survival shown in the mice group treated with the combined treatment 2Gy + mApoE-DOXO-LIPs. Notably, this treatment seems to activate the immune system through the ICD induced on the tumor cells, suggesting a possible enhancement of the response against the tumor in an immune competent organism.

However, a considerable treatment toxicity was observed. LIPs treated mice experienced a body weight loss of approximately 12%. Since the observed systemic toxicity could endanger the feasible use of LIPs as nano-carrier for GBM treatments, a more specific and less toxic system need to be tested in order to achieve the **reduction of the treatment toxicity** prefixed in the rationale of this thesis.

2. MMP2-activatable polymeric nanovectors to reduce toxicity

Despite the positive results, mApoE-targeted, DOXO-loaded LIPs were able to fulfill only the following prefixed features:

1. BBB crossing aptitude
2. selectivity to GSCs
3. Activation of surrounding microenvironment

However, the excessive weight loss shown in the *in vivo* experiments suggests a systemic toxicity also due to the scaffold since the weight loss was registered in all the group treated with the LIPs, both conjugated or not. Therefore, in order to reduce the treatment toxicity, a different delivery system based on polymer technology was investigated.

Polymer are FDA approved materials used in nanoparticle synthesis.. Polymeric NPs are considered less toxic compared to LIPs (Sharma et al., 2012) and, moreover, polymers are a more versatile material (Rideau et al., 2018). These two aspect make polymeric NPs an optimal biocompatible scaffold in order to create efficient and safe targeted nanosystems. Different type of polymer used to create NPs including poly(lactic-co-glycol acid) (PLGA), poly(ε-caprolactone) (PCL) the most used and characterized polymer to synthesized NVs.

As mApoE exerts no/limited activity on the cells present in the surrounding tumor microenvironment, in order to increase GBM specificity, NP functionalization was implemented I with a MMP2/9 activatable strategy. Indeed, the activatable system was created by fusing a Low Molecular Weight Ptoramine (ALMWP) with an inhibitory sequence spaced by a MMP2/9 sensitive peptide (see Fig. 9). The presence of high level of MMP2/9 in the GBM microenvironment should assure the correct activation of the NPs only near the tumor, reducing the uptake by other cells in particular scavenger one.

The polymer chosen to create the implemented system was PLGA, a well characterized and known materials (Sharma et al., 2012; Rideau et al., 2018) and was conjugated with the MMP-activatable sequence. The synthesis and characterization of the NPs was

conducted in prof Cellesi's lab at the department of Chemistry, Materials and Chemical Engineering "Giulio Natta" (CMIC), Politecnico of Milan.

2.1 Characterization and selection of MMP-expressing GSC lines

GSCs with similar sensitivity to DOXO and different MMP2 enzymatic activity were designated as suitable cellular model for the development of GBM specific activatable nanovectors. Patient-derived GSC primary lines present in the laboratory's collection (see methods section) were tested for MMP2 expression and activity by real-time PCR, western blot and zymography. Among the cell lines available ICH001, ICH003 and ICH013 GSC lines were selected. The selected cell lines displayed similar cellular response to DOXO (**Fig 20 A**) and equivalent amount of MMP2 mRNA (**Fig. 20 B**). Interestingly, while ICH013 GSCs showed the lowest amount of MMP2 protein level, a higher enzymatic activity was observed in ICH013 supernatant compared to ICH001 and ICH003 ones (**Fig. 20 C, D**).

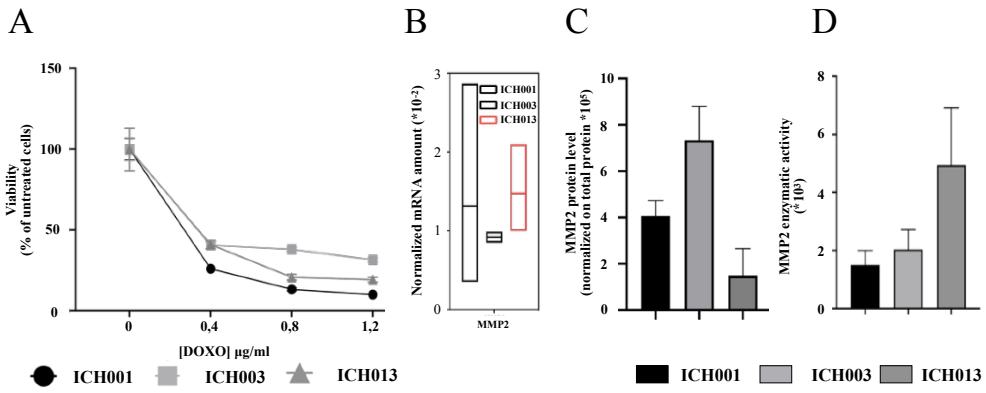

Fig. 20: GSCs drug sensitivity and MMP2 activity. A) Free DOXO responsiveness of ICH001, ICH003 and ICH013 determined by MTT viability assay after 48h incubation at increasing drug concentration. Values are expressed as percentage of untreated cells. **B**) MMP2 mRNA levels determined by real time PCR. Values are expressed as the mean of at least 4 technical replicates normalized on GAPDH mRNA expression. **C**) MMP2 protein amount determined by western-blot. **D**) MMP2 enzymatic activity detected in 24h cell culture supernatant and assay by zymography. Values are expressed as the mean ± SE of three independent experiments.

2.2 PLGA / poly(ethylene glycol) (PEG) copolymer

Due to their high biocompatibility PLGA and PEG are polymers approved by Food and Drug Administration (FDA) and European Medicines Agency (EMA) and therefore employed in various drug delivery systems (Rideau et al., 2018). DOXO-loaded, MPP-Activable PLGA-PEG NVs were synthesized by carbodiimide chemistry from commercial

PLGA and amino-PEG-acid. The resulting copolymer was further functionalized with a maleimide group, to obtain the PLGA-PEG-MALE polymer. The PLGA-PEG-MALE was conjugated with a cysteine-terminated LMWP or ALMWP peptide through a Micheal-type-addition. Finally, DOXO was encapsulated by standard nanoprecipitation (**Fig. 21 A**).

NVs size distribution was evaluated before and after DOXO encapsulation by nanoparticle tracking analysis (**Fig. 21 B**) using a NS300 NanoSight (Malvern Panalytical, Malvern, UK), showed NVs uniform diameter size of about 130 nm, negative Z-potential and Polydispersity Index (PDI) lower than 1 (**Fig. 21 B, C**).

To demonstrate that the observed cytotoxic effect was due to embedded DOXO and not to nanovector polymeric core itself, a viability assay was carried out with unloaded, non-encapsulated DOXO, empty nanovectors (**Fig. 21 D**). As expected, the results showed no inhibition of GSC viability caused by polymeric scaffold. Differently, an increasing dose-dependent toxicity, up to 60% reduction of cell viability, was observed upon GSCs incubation with LMWP and ALMWP decorated empty nanovectors. Nevertheless, these values were never used in the experiments.

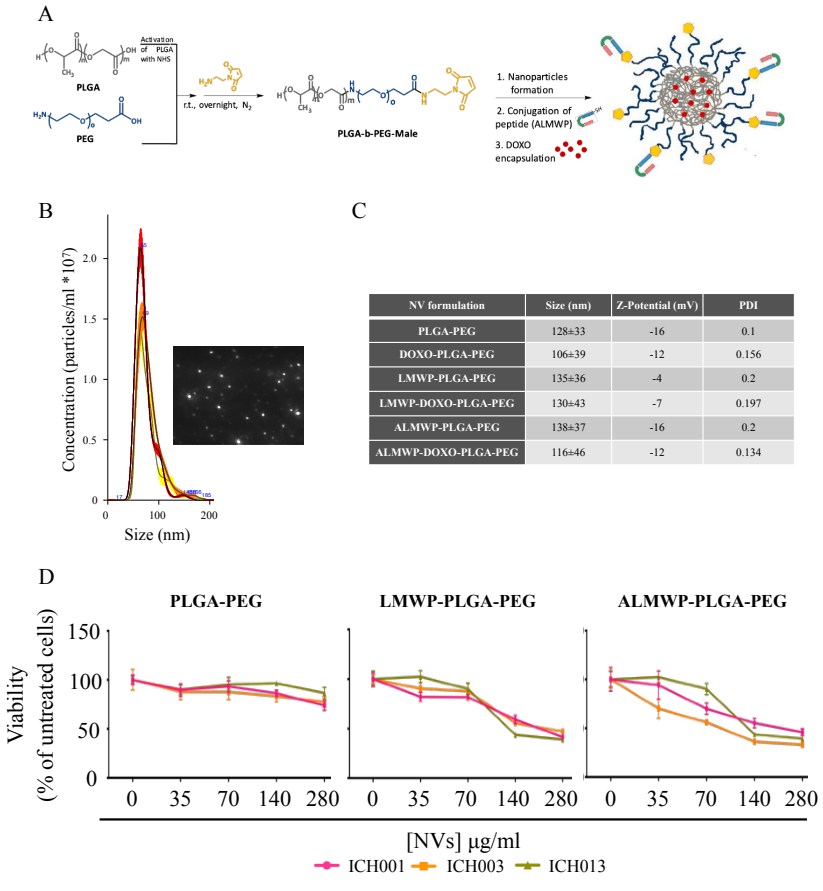

NV formulation	Size (nm)	Z-Potential (mV)	PDI
PLGA-PEG	128±33	-16	0.1
DOXO-PLGA-PEG	106±39	-12	0.156
LMWP-PLGA-PEG	135±36	-4	0.2
LMWP-DOXO-PLGA-PEG	130±43	-7	0.197
ALMWP-PLGA-PEG	138±37	-16	0.2
ALMWP-DOXO-PLGA-PEG	116±46	-12	0.134

Fig. 21: ALMWP-DOXO-PLGA-PEG synthesis and characterization. A) PLGA-PEG nanovectors synthesis and DOXO encapsulation. **B**) Representative nanovectors signal obtained by light scattering at NanoSight NS300 and representative NVs size distribution determined by NTA analysis. **C**) Mean size ± SD, Z-potential and PDI of empty and DOXO loaded PLGA-PEG nanovectors. Parameters were obtained after 3 repetition in ultra pure water. Data kindly provided by prof Cellesi's lab **D**) Cell viability assayed by MTT test after 48 h incubation with unloaded, not encapsulating DOXO empty nanovectors. Values are expressed as mean percentage survival of 4 technical replicates ± SE normalized to the corresponding values of untreated GSC cultured without nanovectors.

As MMP production in and NV activation are time-dependent and connected events, real-time cellular uptake/internalization driven by ALMWP cleavage was investigated in ICH001, ICH003 and ICH013 GSC lines by cell microscopy and imaging (DMi8 microscope and LAS-X software, Leica) (**Fig. 22**).

Three different NVs formulation were tested:

1) DOXO-PLGA-PEG without any external decoration but encapsulating DOXO;
2) LMWP-DOXO-PLGA-PEG nanovectors functionalized with active CPP peptide;
3) ALMWP-DOXO-PLGA-PEG nanovectors funtionalized with MMP2-activatable CPP peptide.

Nuclear DOXO quantification showed no difference in the uptake rate of ALMWP-DOXO-PLGA and LMWP-DOXO-PLGA that is consistently higher than not-functionalized nanovectors.

Overall, nuclear DOXO quantification showed a time dependent cellular uptake and internalization rate more manifest when GSCs were incubated with CPP-functionalized (LMWP-DOXO) and MMP2-activatable (ALMWP-DOXO) nanovectors (**Fig. 22 B**). Both LMWP-DOXO and ALMWP-DOXO-PLGA nanovectors displayed a similar degree of internalization that was mostly higher compared to non-decorated control nanovector. No consistent differences were observed between GSCs with low (ICH001, ICH003) and high (ICH013) MMP2 activity (**Fig 20 D, Fig 22 B**). Therefore, despite these results suggest that the ALMWP-peptide can efficiently work in the presence of GSCs, an MMP dependent activation was not indicated.

More importantly, after a 10 hour incubation with DOXO-PLGA-PEG nanovectors, cell nuclei were visibly engulfed by DOXO (**Fig 22 A**) and no significant difference in nuclear DOXO accumulation were detected (**Fig. 22 B**), suggestive of a passive and uncontrol DOXO internalization due to nanovector drug release. A fast (starting from 4-5 hours of incubation) drug release is reminiscent of a probable non-specific, off-target cytotoxic effect that would restrain the advantages of a targeted delivery system. Indeed, cell viability assay performed at 24 and 48 h incubation in the presence of increasing concentration of nanovectors/DOXO indicated the lack of significant differences in cell death among nanovectors, including the untargeted DOXO-PLGA negative control (**Fig. 23**).

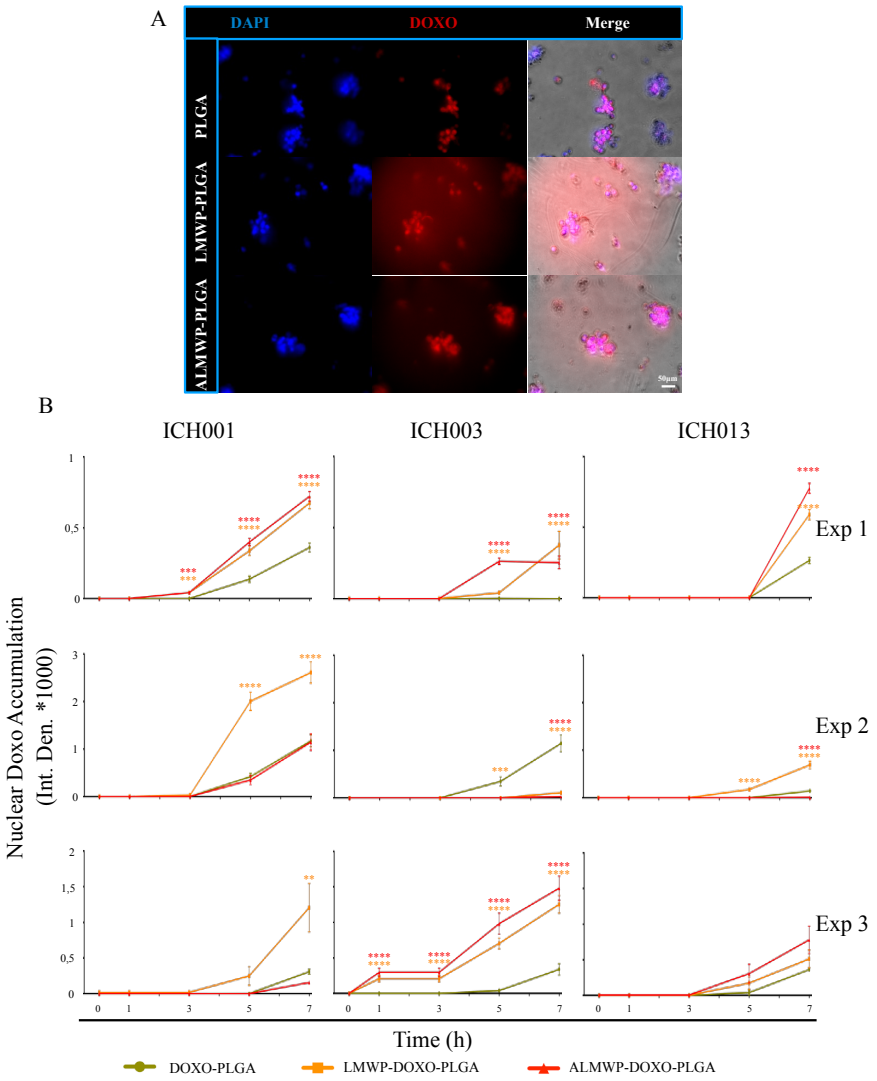

Fig. 22: DOXO-PLGA nanovectors live imaging uptake. GSCs were incubated with nanovectors at a [DOXO] of 4µg/ml. One images per hours was capture by *r*eal-time microscopy. **A**) Representative images of ICH001 cells incubated with the indicated nanovectors showing DOXO (red) inside the cells. DAPI was used for nuclear staining. The right panel shows te bright-field differential interference contrast merged signals. **B**) Real-time nuclear DOXO quantification expressed as Integrated Density (Int. Den) ± SE in ICH001, ICH003 and ICH013 GSC patient-derived cell lines incubated with the indicated PLGA-PEG-DOXO nanovectors (0-10 h, [DOXO] 4 µg/ml) in 3 independent experiments. At least 100 cells per hour was analyzed. Pairwise comparison was performed by Student's *t*-test. **P<0.01, ***P<0.001, ****P<0.0001.

After 24h incubation, both decorated and undecorated nanovectors induced the same cell viability reduction (**Fig 23**). Unfortunately, also the negative control reaches the same % of cell viability, except on the ICH001. After 48h all nanovectors were able to kill more than 50% of cells at the lower concentration of encapsulated DOXO (1,25 µg/ml) considered (**Fig. 23**). Interestingly, these results are comparable to those obtained by incubating the GSCs with the same quantity of free DOXO supporting that embedded DOXO released by nanovectors enter the GSC and acts as free DOXO (**Fig. 19 A**).

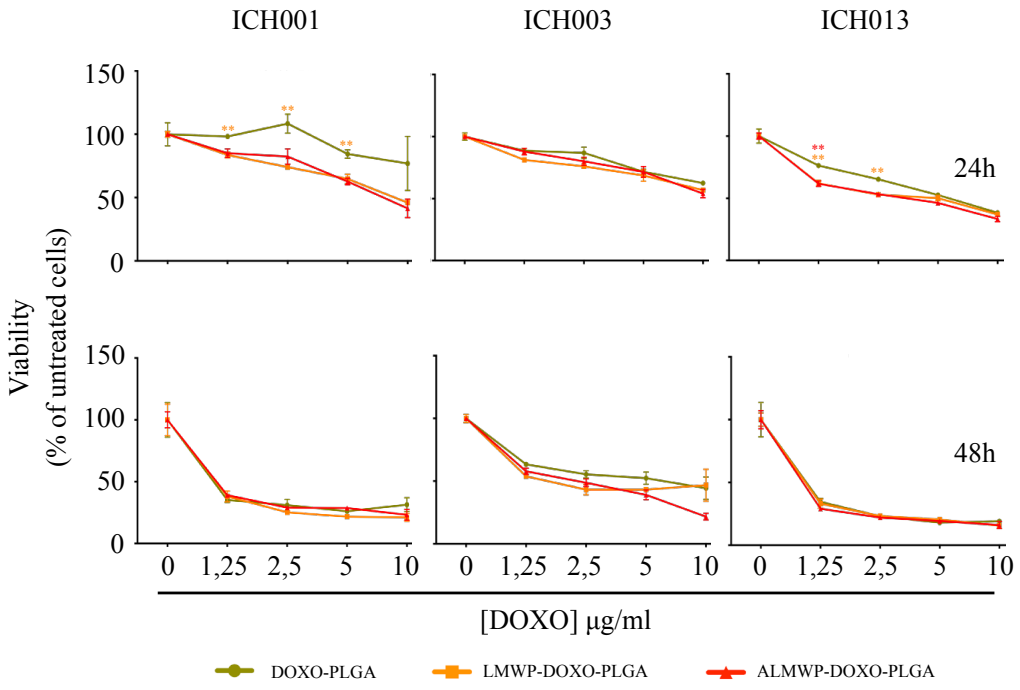

Fig. 23: viability assay on GSCs treated with DOXO-PLGA nanovectors. Cell viability assayed by MTT test after 24 and 48h incubation with the indicated nanovectors and [DOXO]. Values are expressed as mean percentage survival of 4 technical replicates ± SE normalized to the corresponding values of untreated GSC cultured without nanovectors.

Overall, these results are consistent with an overtime DOXO release from the PLGA-PEG polymeric core. In a recent publication, Malinovskaya et al. reported that PLGA-based nanovectors passively released nearly 50% of the encapsulated DOXO after 6 hours at pH 7.4 (Malinovskaya et al., 2017). Uncontrolled release of DOXO represents a great concern and setback to the translation of DOXO-loaded PLGA-based nanovectors in the clinic.

Therefore, due to the failure of drug retention and the consequent toxicity, in accordance with the engineers, we decided improve the material and polymer structure for the nanovectors formulation, in order to obtain a functional drug delivery system.

2.3 Star-shaped PCL-PEG based nanovector

As the attempts to ameliorate DOXO-entrapping into PLGA did not produce suitable results, PLGA-PEG nanovectors were substituted with novel nanovectors obtained by self-assembly of an alternative star-shape PCL based macromolecules. PCL was selected to enhance the hydrophobicity of the nanovectors core, aiming to improve stability and drug retention (Kommareddy et al., 2005). The star-shaped PCL-PEG brush architecture was designed for a better control of nanoparticle self-assembly and functionality in term of peptide grafting and presentation.

As PCL could better retain DOXO inside the PCL core, the uptake analysis should better discriminate the nuclear DOXO amount of NVs decorated with CPP compared to PCL-PEG-DOXO. Moreover, the star-shape and the multi-functionalized brushes should reduce the time that NVs needs to interact with the cells.

Star-shaped multifunctional PCL-PEG copolymers were synthesized through controlled polymerization of PCL- and PEG- based macromonomers, using 4-arm PCL-based macroinitiators. The copolymers were further acrylated and functionalized via Michael type addition with the active peptides (LMWP, ALMWP). DOXO was finally encapsulated by a standard nanoprecipitation method (**Fig 24 A**).

Nanovectors size distribution was evaluated before and after DOXO encapsulation. NTA showed a uniform diameter size of about 90-100 nm. DOXO encapsulation didn't significantly changed the size of the nanovectors (**Fig. 24 B, C**). Functionalized nanovectors showed a negative Z-potential while untargeted, both loaded and unloaded, has positive Z-potential (**Fig 24 C**). PDI was always lower than 1 (**Fig 24 C**).

Viability assay performed with empty nanovectors showed a 40% viability reduction in GSCs treated with undecorated and LMWP decorated nanovecrtors. Differently, ALMWP decorated nanovector was the most safe formulation with a 10-15% viability reduction depending on GSCs (**Fig. 24 D**).

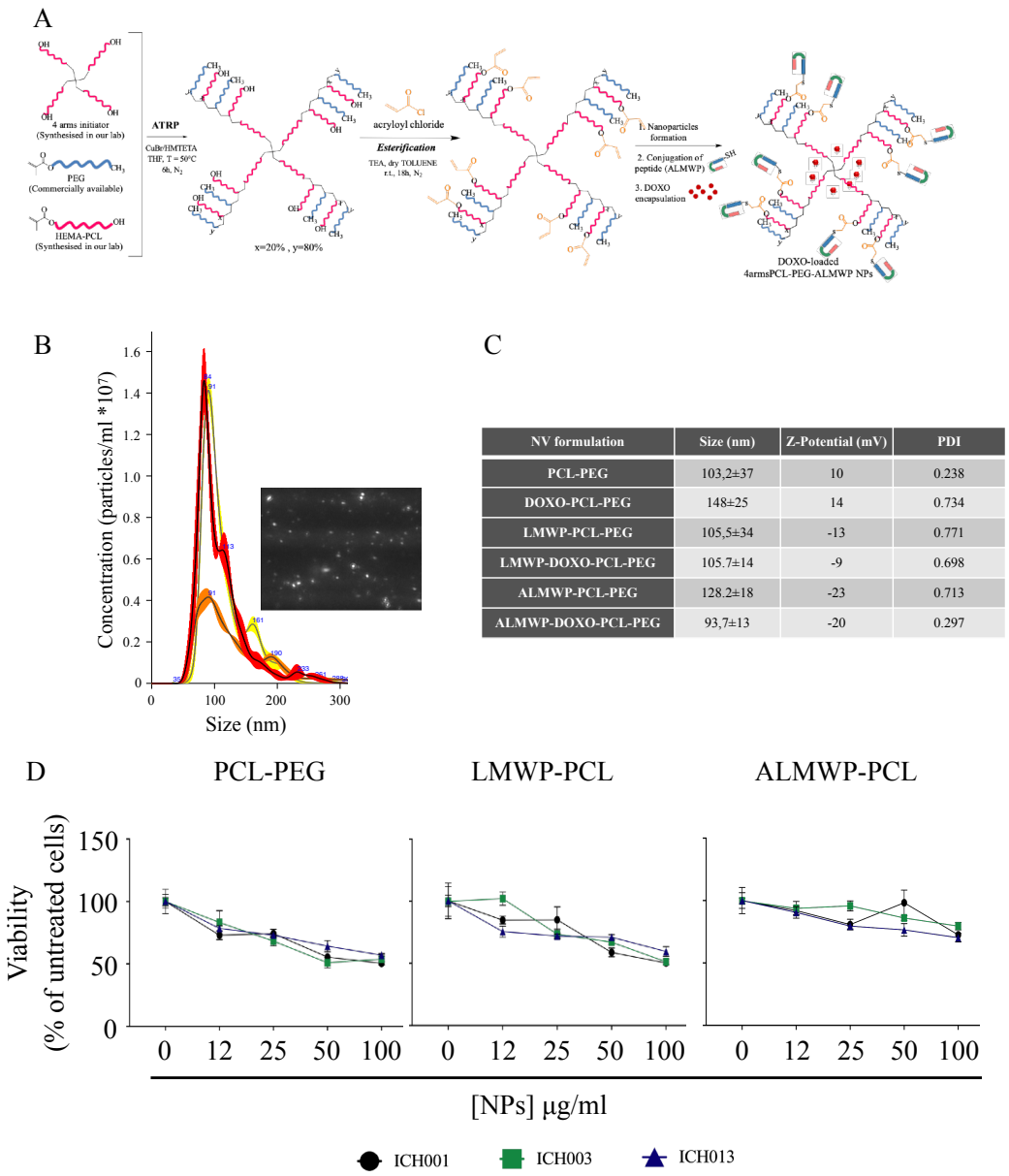

Fig. 24: synthesis and characterization loaded PCL-PEG based nanovectors . A) Schematic representation of PCL-PEG nanovector synthesis, peptide functionalizastion and DOXO encapsulation. **B**) Representative image of nanovectors light scattering obtained by NanoSight (Malvern Panalytical). **C**) Representative NVs size distribution and concentration obtain by NTA. Data kindly provided by prof Cellesi's lab **D**) Mean size and Z-potential of each different PLGA-PEG NVs, both empty and DOXO loaded. Parameters were obtained in ultra-pure water. **E**) Cell viability assayed by MTT test after 48 h incubation with unloaded, not encapsulating DOXO empty nanovectors. Values are expressed as mean percentage survival of 4 technical replicates ± SE normalized to the corresponding values of untreated GSC cultured without nanovectors.

Three different PCL-PEG nanovectors formulation were investigated:

1) DOXO-PLGA without any external decoration but encapsulating DOXO;
2) LMWP-DOXO-PLGA nanovectors functionalized with active CPP peptide;
3) ALMWP-DOXO-PLGA nanovectors funtionalized with MMP2-activatable CPP peptide

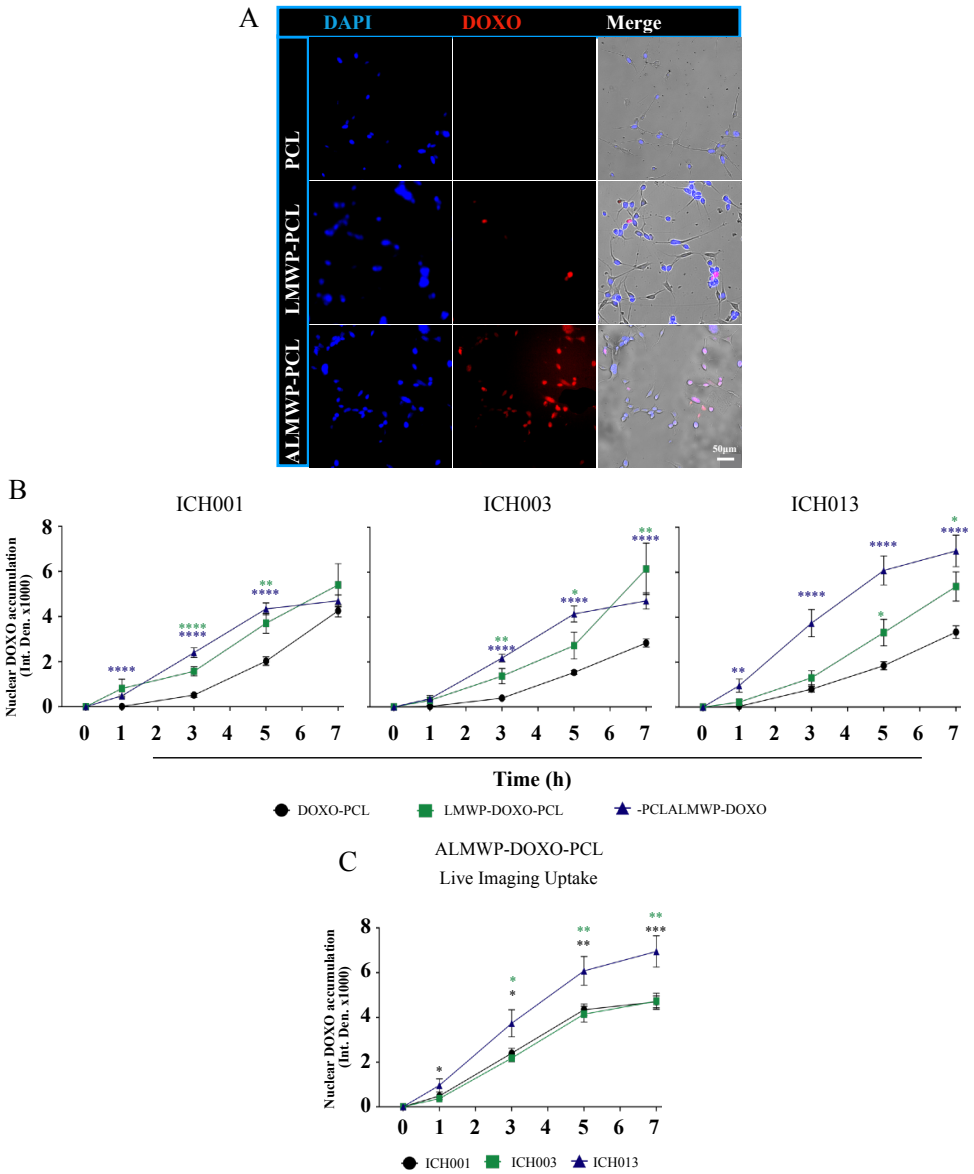

Fig. 25: PCL-PEG NVs live imaging uptake. GSCs were plated and treated with NVs at a [DOXO] of 1,2µg/ml. One images per hours was capture for each well by DMi8 microscope (Leica). **A)** Representative live microscopy images of ICH013 cells incubated with the indicated nanovectors for 7h showing DOXO (in red) inside the cells. DAPI was used for nuclear staining. The right panel shows three bright-field differential interference contrast merged signals. **B)** Real-time nuclear DOXO quantification expressed as Integrated Density (Int. Den) ± SE in ICH001, ICH003 and ICH013 GSC patient-derived cell lines incubated with the indicated PCL-DOXO nanovectors (1-5h, [DOXO] 1,2 µg/ml). Images were analyzed by LAS-X software (Leica). Nuclear DOXO amount was quantify in 90-100 cells per time point in one experiment. **C)** Comparison of ALMWP-DOXO-PCL uptake between the three GSC lines analyzed in panel B. Pairwise comparison was performed by Student's *t*-test. *P<0.05, **P<0.01, ***P<0.001, ****P<0.0001.

Likewise PLGA-PEG nanovectors, incubation with DOXO-loaded PCL-PEG nanovectors triggered a time-dependent nuclear DOXO accumulation in all three GSC lines considered. However, differently from PLGA-PEG nanovectors, significant DOXO accumulation was promptly observed with MMP-activatable (ALMWP-DOXO-PCL) and CPP-decorated (LMWP-DOXO-PCL) compared to non.functionalized (DOXO-PCL)

nanovectors starting from one hour incubation and at a lower DOXO concentration (1,2 *vs* 4 μg/ml) (**Fig. 25 A, B**).

A different magnitude of nuclear DOXO level was observed among the GSCs after ALMWP-DOXO-PCL- incubation with ICH013 showing the highest level of DOXO accumulation (**Fig. 25 C**). Importantly, ICH013 highest level of DOXO accumulation correspond to their highest MMP2 activity (**Fig. 20 D**) suggesting a positive correlation between ALMWP nanovectors activation and level of MMP2.

These results suggested that the star-shaped PCL-PEG scaffolds could effectively better retain DOXO into the nanovector core compared to PLGA-PEG one and that the activatable peptide could be cleaved by GSC MMPs exposing the CPP allowing targeted DOXO-PCL nanovector enter the cells. Moreover, the corresponding level of MMP2 activity and ALMWP-DOXO-PCL cellular uptake supported the crucial involvement of the MMP2 enzymatic activity in the activation of the ALMWP nanovector.

Viability assay enforced these observations showing significant differences among decorated and undecorated nanovectors. ALMWP-DOXO-PCL significantly reduced viability compared to DOXO-PCL in ICH001 and ICH003, 40% and 45% respectively, comparable to LMWP-DOXO-PCL positive control. ICH013 seemed to be more sensible to both undecorated and decorated nanovectors. Nevertheless, ALMWP-DOXO-PCL showed a 50% viability reduction compared to both DOXO-PCL negative control and LMWP-DOXO-PCL positive control, suggesting that the ALMWP nanovectos higher uptake observed (**Fig. 25 A, B**) effectively reflected a higher toxicity (**Fig 26**).

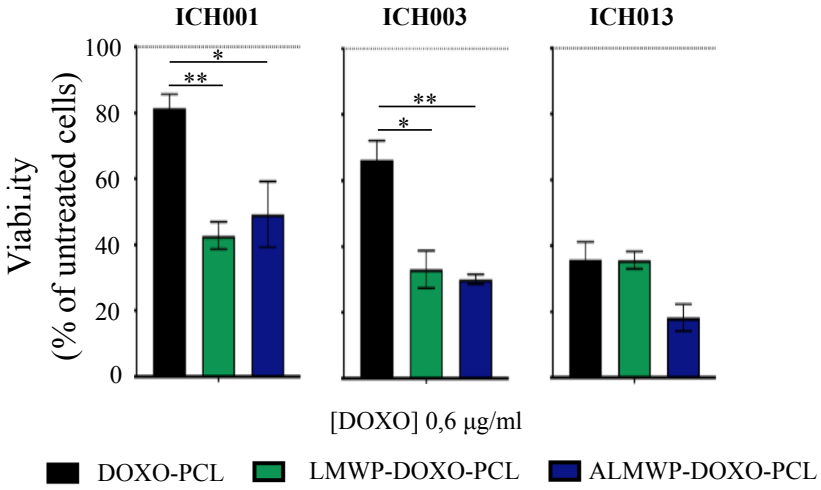

Fig. 26: viability assay. Cell viability assayed by MTT test on ICH001, ICH003 and ICH013 with the indicated nanovectors at [DOXO] of 0,6 µg/ml. Values are expressed as mean percentage survival of 4 replicates ± SE normalized to corresponding untreated cells. Pairwise comparison was performed by Student's *t*-test. *P<0.05,**P<0.01.

To better characterize ALMWP-DOXO-PCL, its toxicity was assayed at different concentration (0,6 *vs* 1,2 µg/ml) and time point (48 *vs* 72h). In all the GSCs, ALMWP-DOXO-PCL induced a significant dose response halving cell viability (**Fig. 27**). Moreover, in ICH003 and ICH013 ALMWP nanovector significantly induced a time dependent viability reduction (**Fig. 27**). No time dependent viability reduction was observed in ICH001.

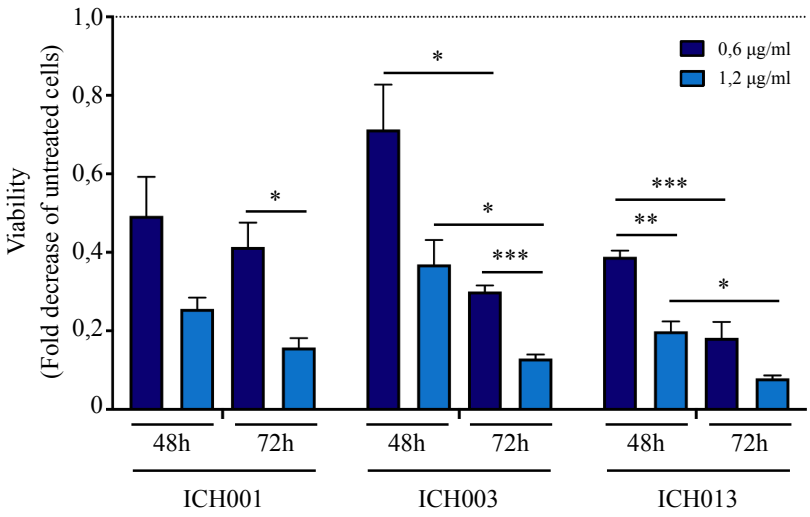

Fig. 27: ALMWP-DOXO-PCL dose response/time dependent viability assay. A) Cell viability assayed by MTT test after 48 and 72h incubation with ALMWP-DOXO-PCL at [DOXO] of 0,6 or 1,2 µg/ml. Values are expressed as mean percentage survival of 4 repetitions ± SE normalized to corresponding untreated cells cultured without nanovectors. Pairwise comparison was performed by Student's *t*-test. *P<0.05,**P<0.01, ***P<0.001

To further demonstrate that the cell entry to the activatable nanovectors was due to MMPs and, at the same time, that nanovectors were non-toxic to non-tumoral cells, ALMWP-

DOXO-PCL uptake was investigated in hCMEC/d3 human endothelial cell line that does not express MMP2 (**Fig. 28 A**).

As expected, results clearly showed that, opposite to GSC lines, endothelial cells displayed the highest DOXO uptake upon exposure to the LMWP-DOXO-PCL (CPP-targeted positive control) and the lowest one upon MMP2-acyivatable ALMWP-DOXO-PCL nanovectors. ALMWP-DOXO-PCL did not enter hCMEC/d3 cells and nuclear DOXO signal was comparable to the one of the cells incubated with untargeted DOXO-PCL (negative control) (**Fig. 28 B, C**).

Consequently, as only the active CPP peptide could interact directly with the hCMEC/d3 cell membrane, LMWP-DOXO-PCL resulted the most toxic nanovectors while ALMWP-DOXO-PCL treated cells showed a significant 70-80% survival rate equivalent to untargeted DOXO-PCL (**Fig. 28 D**)

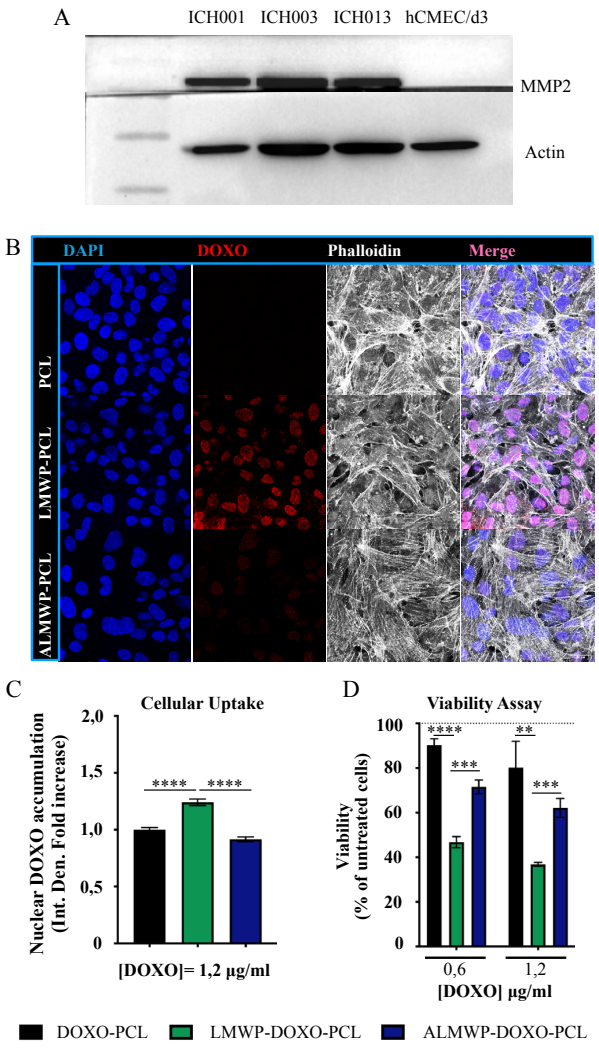

Fig. 28: uptake and viability assay on hCMEC/d3 to verify MMP2 involvement in NVs internalization and toxic effect. A) Representative image of MMP2 protein amount in endothelial cells compared to GSCs. Image acquired by ChemiDock (BioRad). **B**) Representative confocal images of human endothelial cells (hCMEC/d3) after 5-hour incubation with indicated PCL-DOXO nanovecors, [DOXO] 1,2 μg/ml. In blue is the Hoechst signal for nucleus detection and in white is Phalloidin for cell body detection. **C**) Nuclear DOXO quantification expressed as Integrated Density (Int. Den) ± SE in cells incubated with PCL-DOXO nanovectors as indicated (6h, [DOXO] 1,2 μg/ml). At least 300 cells per condition were analyzed. **D**) Cell viability detected by MTT assay after 24h incubation with the indicated nanovectors at [DOXO] 0,6 μg/ml. Values are expressed as mean percentage survival (for replicates ± SE) normalized to corresponding untreated. Pairwise comparison was performed by Student's *t*-test. **P<0.01***P<0.001, ****P<0.0001.

Taken together these results confirm that ALMWP-DOXO-PCL nanovectors efficiently targets GSCs, due to their high MMP2 expression and release in the surrounding microenvironment. The specificity of the MMP2 dependent activation has been demonstrated by the inability of the endothelial cells that do not express MMP2 and, consequently, did not activate the nanovector. Moreover, the reduction of encapsulated DOXO amount (from 10 μg/ml to 1,2 μg/ml) to efficiently affect GSCs viability represents a further step forward to the possibility to reduce the treatment related toxicity. Indeed, not only the PCL is considered a less toxic scaffold respect the LIPs (Sharma et al., 2012) but, moreover, they display higher efficiency compared LIPs to vehicle encapsulated DOXO into GSCs allowing to reduce the amount of the administered drug.

3. mApoE-DOXO-PCL *vs* mApoE-DOXO-LIP

To confirm the observation that star-shaped PCL nanovectors are more efficient in drug delivery compared to LIPs, a direct comparison of the two system was investigated.

To uniform the DOXO-loaded PCL and LIP platforms, the mApoE peptide, crucially required for BBB crossing but never investigated on PCL-based nanovectors, was chosen as surface functionalization.

The nuclear DOXO uptake determined by live imaging confirmed the higher efficacy of mApoE-PCL to be internalized into the cell (ICH001) within 3h incubation, while mApoE-LIP was even undetectable (**Fig. 29 A, B**). Consequently, after 72h incubation mApoE-PCL significantly induced viability reduction on ICH001 compared to mApoE-DOXO-PCL (**Fig. 29 C**). Moreover, mApoE-DOXO-PCL seemed to induce a dose response as DOXO dosage increase (**Fig. 29 C**).

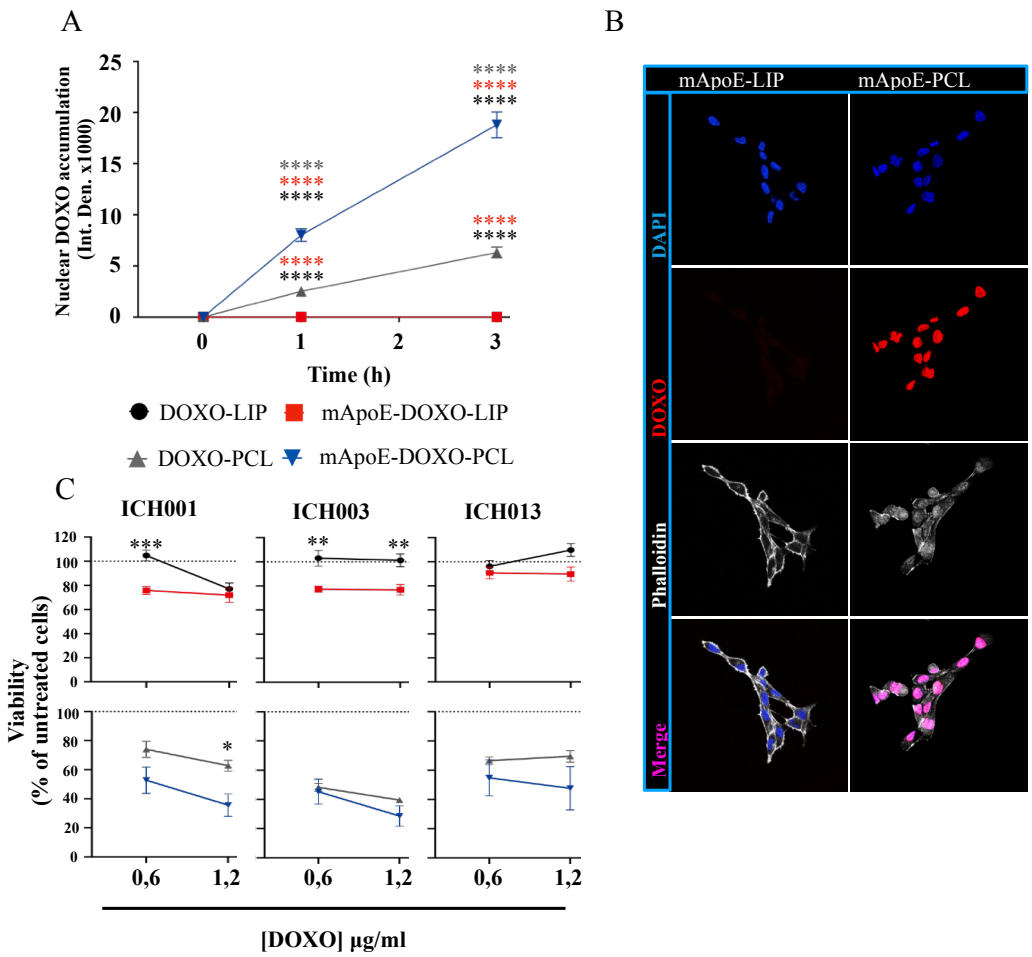

Fig. 29: mApoE-DOXO-PCL *vs* mApoE-DOXO-LIP uptake and viability assay on GSC. A) Real-time nuclear DOXO quantification expressed as Integrated Density (Int. Den) ± SE in ICH001 cells incubated with the indicated nanovectors (1-3h, [DOXO] 1,2 µg/ml). Images were analyzed by LAS-X software (Leica). Nuclear DOXO amount was quantify in 90-100 cells per time point. **B**) Representative confocal images of ICH001 cells after 5-hour incubation with indicated nanovecors, [DOXO] 1,2 µg/ml. In blue is the DAPI signal for nucleus detection and in white is Phalloidin for cell body detection. **C**) Cell viability detected by MTT assay after 72h incubation with the indicated nanovectors at [DOXO] of 0,6 and 1,2 µg/ml. Values are expressed as mean percentage survival (for replicates ± SE) normalized to corresponding untreated. Pairwise comparison was performed by Student's *t*-test. *P<0.05, **P<0.01,***P<0.001, ****P<0.0001.

This preliminary experiment strongly suggests that PCL nanovectors independently from GSCs targeting functionalization are more efficient in GSCs targeting since they can work at a lower DOXO concentration compared to LIPs.

The goal of this thesis was to generate a drug delivery system able to reach three crucial points of GBM treatment development:

1. BBB crossing aptitude
2. selectivity to GBM that includes GSCs and surrounding microenvironment
3. Reduced drug toxicity

The first attempt to satisfy these points was the mApoE-DOXO-LIPs synthesized by NANOMIB at the University of Milano-Bicocca. Results indicated a crucial role of mApoE not only to deliver drug-loaded nanovectors across BBB but, importantly, also to GSCs. DOXO nuclear accumulation occurred only in the presence of mApoE-functionalized LIPs and was significantly inhibited by the incubation with endocytosis inhibitors, thus indicating a receptor-mediated targeted delivery. In irradiated (2Gy) GSCs the higher level of LDLR expression was associated with an increased cellular internalization of mApoE/DOXO/LIPs further supporting an mApoE/LDLR specific mechanism of cell entry associated to mApoE-functionalized nanovectors.

The *in vivo* experiments performed in GSC-PDX demonstrated that despite mApoE-DOXO-LIPs cross the BBB and target GSCs yet their accumulation and diffusion into the brain parenchyma did not reach an adequate tissue concentration to cause a satisfactory therapeutic effect. Highest and significant level of tumor growth inhibition associated with increased overall survival was observed only in mice receiving radiation together with mApoE-DOXO-LIPs (2Gy/mApoE-DOXO-LIP). A dose as low as 2Gy is sufficient to modulate LDLR expression and BBB permeability allowing effective liposomal DOXO delivery and GSC cell death commitment by apoptosis. Importantly, GSCs death by apoptosis seems to activate the ICD and the consequent recruitment of the resident immune cell. The over expression of CD11c suggests that the $Iba1^{+}$ cells (macrophages and microglia) could act as presenting cell after ICD activation

Moreover, in vivo biodistribution indicated that healthy BBB allowed a modest accumulation of mApoE-DOXO-LIPs. A low crossing rate through intact BBB combined to a higher delivery rate in the irradiated field, would confer tumor tissue selectivity to

mApoE-conjugated and drug loaded nanovectors protecting healthy brain parenchyma from off-target effects.

In the last years some LIPs have been approved for clinical applications in oncology (Marchal et al., 2015; Wicki et al., 2015). Among them, liposomal DOXO (i.e. Caelyx® or Doxil®) is currently used in different protocol of tumor treatment (Zhao et al., 2017). However, it failed to be effective against GBM because it can't cross the BBB (Menei et al., 2005; Beier et al., 2009; Ananda et al., 2011). The results of this thesis have demonstrated that the mApoE conjugation can overcome the limitation of the older formulation of liposomal DOXO conferring two fundamental aptitudes:

1. BBB crossing aptitude
2. selectivity to GBM that includes GSCs and surrounding microenvironment

These improvements are essential to create a more safe and precise system to target and finally treat GBM. Nevertheless, the protocol used in *in vivo* experiments underlines the presence of a pitfall in this system: all mice receiving DOXO-loaded LIPs experienced a loss of weight of approximately 12% of the body mass. Weight loss stopped following the end of the treatment. Thereafter, mice gained weight regardless tumor volume and death event suggesting a sensible DOXO-LIP systemic toxicity. mApoE-DOXO-LIP biodistribution indicated that, despite encapsulation significantly reduced DOXO accumulation in the principal peripheral organs (liver, kidney, lung, heart), the liver remains the main organ where approximately 40-50% of the injected LIPs accumulate. Therefore, despite the good results obtained with mApoE-DOXO-LIPs, a more efficient systems was needed to reduce treatment toxicity.

The advantages of using MMP-activatable CPP-functionalized nanocarriers to tackle GBM stay in the possibility to improve simultaneously tumor specificity and cell penetrance, thus limiting off-target effects. MMP overexpression is a key feature of the tumor environment (Egeblad and Werb, 2002) and, moreover, the occasional occurrence of the activating conditions in normal tissues supports the applicability of MMP-activatable strategies. The multiple and non-selective mechanisms of cellular entrance engaged by CPPs to drive the cargo inside the cells make them a powerful and efficient tool to target

not only tumoral cells but also the surrounding microenvironment. Moreover, weight loss observed also in mice treated with untargeted DOXO-LIPs indicated a systemic toxicity caused by the liposome scaffold itself. Hence, to ameliorate both drug pharmacokinetic and pharmacodynamic, it appeared necessary to investigate alternative nanovector formulations based on biocompatible nanomaterial, such as polymers, combined to a more tumor specific functionalization.

The first attempt with ALMWP-DOXO-PLGA failed to achieve the expected results. The extremely fast DOXO release from the core avoid the possibility to have a target and incapsulated system, making the treatment a free DOXO administration. Therefore, a different and innovative star-shaped ALMWP-DOXO-PCL was selected for the *in vitro* characterization.

A different magnitude of nuclear DOXO accumulation was observed after GSC incubation with activable ALMWP-DOXO-PCL nanovectors. Consistent with the higher MMP2 activity, ICH013 cells displayed highest and faster nanovector internalization and higher cell viability inhibition upon incubation with activable ALMWP-DOXO-PCL compared to active penetrating LMWP-DOXO-PCL nanovector. A dose- and time-dependent DOXO cytotoxicity and inhibition of cell viability was observed by culturing GSCs in the presence of the activable ALMWP-DOXO-PCL nanovector at increasing dose of DOXO and/or time of incubation. Conversely, and as expected, at the same DOXO concentration, no/low DOXO internalization and cytotoxic effect was observed in hCMEC/d3 non-tumoral endothelial cells not expressing MMP2 confirming the requirement of MMP2 enzymatic activity for ALMWP nanovector activation. As MPP activity level determines the success of the activatable nanocarrier, this result indicates that the link of a low molecular weight protamine with cell penetrating properties to a MMPs-sensitive sequence is a feasible tumor-targeting strategy for GBM.

The star-shaped PCL-PEG brush architecture was designed for a better control of nanovector self-assembly and functionality including peptide grafting. Notably, equivalent viability impairment was achieved incubating GSC with ALMWP-DOXO-PCL nanovectors at approximately 10 times lower concentration of embedded DOXO compared

to mApoE-DOXO-LIPs, 1,2 *vs* 10 μg/ml respectively. This is possible because the 4-arms with terminal "brushes" of star-shaped nanovectors allow a larger number of functionalizations per chain as compared to the linear and spheric structures, and, consequently, a higher frequency of CPP/cell membrane interactions.

These results were confirmed by the direct comparison of LIP and PCL nanovectors both functionalized with mApoE. mApoE-DOXO-PCL effectively increase the efficacy of DOXO delivery respect mApoE-DOXO-LIP at very low DOXO concentration, enforcing the hypothesis that 4-arms polymeric core is a more efficient drug delivery system respect liposome. Nevertheless, viability reduction induced by mApoE-DOXO-PCL was lower respect ALMWP-DOXO-PCL, suggesting that the activatable CPP is actually a better targeting functionalization.

Taken together, the results clearly answer to the aims of the thesis since they demonstrate that:

1. Functionalized NVs are able to deliver drugs that normally don't cross the BBB to brain parenchyma
2. mApoE and MMP2-activable NVs could efficiently target different GSCs
3. Different formulation could reduce NVs side toxicity

Discussion

Current standard of care is not successful in delivering effective and persistent treatments to GBM. Several elements contribute to therapy failure, including the high amount of chemo-, radio-resistant tumor-initiating GSCs and the presence of intact BBB in the peripheral niches (Geraldo et al., 2019). An effective help can be given by nano medicine. By combining passive and active targeting strategies, nano-based drug delivery systems can provide better penetration of therapeutics within the cancerous tissue in comparison to conventional cancer therapies while avoiding toxicity in healthy cells. Thus, nanocarriers can be used for strategic development of novel drug delivery systems and reformulating existing drugs to enhance effectiveness. Several drug delivery nanosystems, in particular nanoparticles, are currently undergoing advanced clinical trials or, as in the case of liposomes (LIPs), have been approved for clinical applications in oncology (Marchal et al., 2015; Wicki et al., 2015). However, the current approved untargeted liposomal formulation failed to be effective against GBM due to the presence of the BBB and for the lack of specificity for GBM cells, in particular the infiltrating GSCs (Lathia et al., 2015).

To cope with the limited and inefficient delivery of chemotherapeutic to the brain, LIPs surface-functionalization with the mApoE peptide were investigated as NVs to deliver DOXO to the brain and target GSCs. The results obtained demonstrate that the mApoE functionalization confer to LIPs the ability to efficiently cross the BBB and target GSCs in PDX mice. In particular, mApoE-DOXO-LIPs were able to reduce the migration of GBM cells in the contralateral hemisphere and enhance the apoptosis of the tumor cells compared to DOXO-LIPs.

A key point was the cotreatment of GSC-PDX with radiation together with mApoE-DOXO-LIPs. The ability of radiation to temporarily open the BBB (Tamborini et al., 2016) proved a key factor in order to achieve mApoE-DOXO-LIP therapeutic accumulation and diffusion within the GBM tumor area, in particular in the peritumoral border where BBB maintain almost an intact structure and where the unresected GSCs lead to recurrence. Indeed, the highest efficacy on tumor regression and overall survival was obtained with

2Gy/mApoE-DOXO-LIPs cotreatment, suggesting the possibility to use mApoE-functionalized LIPs as adjuvantof RT in GBM patients.

An intriguing observation is the activation of the Iba1^{+} GAMM after the phagocytosis of tumor debris. Knowing that DOXO is a drug able to induce ICD in tumor cells (Kroemer et al., 2013, Kawano et al., 2016), GAMM change in morphology and consequently CD11c overexpression suggest that mApoE-DOXO-LIPs can induce ICD activation in GSCs that in turn activate GAMM as Antigen Presenting Cells (APC). The confirmation of this activation could represent a pivotal step further in immune system activation against GBM in a sort of *in situ* activation. However, the *in vivo* experiments conducted on GSCs transplanted in NOD/SCID mice represents a limitation in ICD activation by mApoE-DOXO-LIPs. In particular, the absence of T cells forbid to verify the effective ability of GAMM to activate adaptive immune response. Therefore, it is essential to verify this mechanism in an immune fully competent *in vivo* model such as intracranial injection of mouse-derived glioma GL261 cell line in a synergic mouse. This would allow to follow not only the ICD activation in tumor cells but also to monitor the activation of the presenting cells and, finally, the activation of infiltrating T cells by antigen presentation. The proof of T cell activation by apoptotic GBM cells would represent a step forward to a possible mApoE-DOXO-LIPs translation to the clinic. Indeed, considering that all the components of this nanocarrier are already approved by FDA, the approval to the clinical use could be shorter than a new drug, giving a new possible therapeutic option as GBM immune therapy.

Importantly, the use of DOXO as incapsulated drug represents an important achievement. DOXO is one of the most commonly used chemotherapeutic agent. It is known to display excellent antineoplastic activity in GBM cells *in vitro* but poor efficacy *in vivo* due to extrusion by multidrug resistance-related proteins present on both BBB and GBM cells (Haar et al., 2012). The conjugation of the mApoE peptide on liposomal DOXO formulations could efficiently overcome the impediments handed by the BBB, including drug resistance by molecular extrusion. Interestingly, mApoE confer a dual targeting system: on BBB and on GSCs. This aspect is essential to reduce the modification needed and enhance the efficacy.

Although significant tumor inhibition and increase overall survival, mApoE-DOXO-LIPs displayed a moderate, despite transient, systemic toxicity possible due to the tendency of nanovectors, mApoE-DOXO-LIPs included, to accumulate into the liver. Indeed, almost 40% of the injected LIPs were found in the liver.

This can constrain and make difficult the translation of mApoE-LIPs to the clinic. Therefore, different formulations were considered in order to obtain a drug delivery system more GBM-specific, efficient and safe. Different scaffold and functionalization were studied. LIPs were substitute with polymeric cores while mApoE targeting was replaced with a MMP2 activatable penetrating peptide.

The polymeric NVs functionalized with MMP2 sensible CPP (ALMWP-DOXO-PCL) demonstrated to be extremely efficient to target GSCs derived from different GBM patients. Thanks to the high MMP2 synthesis by the GSCs, the ALMWP confer high specificity to tumor microenvironment without affecting healthy cells viability. ALMWP-DOXO-PCL incubation with the endothelial cell line hCMEC/d3 demonstrated that in the proximity of a microenvironment with poor MMP2 activity the NVs remain inactivated and, consequently, it cannot target surrounding cells.

Due to the presence of multi-functionalized terminal brushes, the star-shape architecture of the PCL NVs increase the possibility of interactions between targeting moiety/cell membrane and, consequently, NVs cellular internalization. Indeed, our results indicated ALMWP-DOXO-PCL are a more efficient GSC targeting NVs compared to mApoE-DOXO-LIPs. The increased target efficacy is reflected by a higher cytotoxic effect. Indeed, ALMWP-DOXO-PCL exerted extremely GSC cytotoxicity at a DOXO concentration about ten-time lower compared to mApoE-DOXO-LIPs.

This is a pivotal point of this thesis because the reduced DOXO amount required to obtain significant reduction of GSCs viability suggests the possibility that ALMWP-PCL could limit the undesired systemic side effect observed in LIPs. However, a more deep characterization is needed.

A more detailed direct comparison between liposome and PCL NVs is needed to definitively confirm that PCL NVs are more efficient as drug delivery compared to LIPs. Both uptake and cytotoxicity need to be confirmed in GSC derived from different patients. In particular, different DOXO concentration need to be tested to determine the exact minimal effective dose of both LIP and PCL. Moreover, the PCL NVs tested so far lack a functionalization that confer the BBB crossing ability. Therefore, a PCL NVs complete of activatable CPP and a functionalization that confers the BBB crossing ability, such as mApoE peptide already tested on LIPs, need to be tested both *in vitro* and *in vivo*.

Conclusion

In the last 15 years many attempts have been done to develop new drugs or to use molecules effective in other cancer treatment to treat GBM but all of them have failed. In this context, nanomedicine could have a pivotal role in GBM treatment efficacy, specifically targeting tumor cells and allowing drugs accumulation at the tumor site. The work of this thesis represents a step forward to demonstrate that drug-loaded targeted nanovectors can function as a delivery strategy to specifically and effectively drive chemotherapeutics into GBM tumor microenvironment and cells.

mApoE-DOXO-LIPs demonstrated to be effective against GBM cells *in vivo* when coupled with RT, prolonging the mice overall survival, demonstrating that the encapsulation of a drug inside a NVs can enhance its efficacy against GBM thanks to the specific targeting of the tumor. Moreover, this data confirmed that chemotherapy need to be coupled with RT to be effective, working as an adjuvant agent likewise TMZ. In this way mApoE-DOXO-LIPs could be proposed as alternative adjuvant chemotherapy in a treatment protocol.

Another important aspect is the use of DOXO as incapsulated drug against GBM. In a kind of drug repurposing, DOXO could be an “old-new” drug that could help to prolong GBM patient survival. In particular, DOXO ability to induce ICD activation after tumor cell death could be the cornerstone to elicit a stronger response against GBM guided by the immune system. This thesis demonstrated that nanomedicine could effectively play this role in drugs repurposing, giving new life to DOXO in GBM treatment. Finally, ICD

activation confirms we need to improve our understanding in GBM microenvironment and how we can take advantage of it to obtain a stronger response against GBM and, why not, defeat it.

In my opinion, the next years research in GBM treatment should focus on the development of more and more smart drug delivery systems able to cross the BBB and accumulate in the microenvironment of the GBM where directly target the tumor cells, especially the single GSCs disseminated at the tumor border, and able to remodulate the microenvironment component, specially the immune cells. In particular, this system should be able to induce a systemic response against the tumor to enhance the efficacy of the drugs and overcome the resistance mechanisms of the tumor cells.

Methods

1. Synthesis and characterization of mApoE-DOXO-LIPs

LIP composed of Sm/Chol/PE-PEG-mal (48.75:48.75:2.5 molar ratio) in ammonium sulphate (500 mM, pH 5.5) were prepared by extrusion procedure. LIPs (5 µmolstotal lipids) were incubated with 1 mg/ml DOXO for 1 h at 65°C to obtain DOXO-LIP. DOXO-LIPs were then functionalized with mApoE (CWGLRKLRKRLLR-NH_2, DBA Segrate, Italy) as described previously (Bana et a., 2014) to obtain mApoE-DOXO-LIPs. LIPs were purified by gel filtration (Sephadex G-25 fine resin). DOXO loading was quantified by measuring the DOXO fluorescence (λex = 495 nm; λem =592 nm) after liposomes disruption with 0.1% Triton X-100. Phospholipids content was quantified by Stewart Assay. The amount of mApoE attached on LIP surface was determined by measuring the shift of tryptophan fluorescence intensity (λex = 280 nm). Non-functionalized LIP and DOXO-LIP were used as controls. Stability was measured in PBS by following size and polydispersity index (PDI) by DLS for 10 days. The reported data are the mean of at least five different measurements. For transmission electron microscopic (TEM) evaluation, mApoE-DOXO-LIP were deposited on formvar and carbon coated 300 mesh copper grids (EMS, Hatfield—PA) and negatively stained with a solution of 2% Uranyl Acetate. After drying, the grids were examined under a Philips CM10 TEM (FEI, Eindhoven, NL) with an accelerating voltage of 80 kV and images were acquired with a Morada camera and iTEM software (Olympus, Tokyo, JP). Release of DOXO from loaded LIP was monitored at 37°C in phosphate buffered saline (PBS) at pH 7.4, 6.5 or 5.0. At various time points up to 14 days, an aliquot was withdrawn from LIP suspension and filtered using a 10 kDaMWCO spin filter, at 4000 rpm. The filtrate, which contained DOXO released from the LIP, was analyzed for DOXO content as described above by spectrofluorimetry. DOX release was calculated using Eq. (1):

DOXO release (%) = ([DOXO] filtrate / [DOXO] initial sample) * 100

2. Synthesis and characterization of DOXO-loaded PLGA based nanovectors

PLGA NVs. A solution of 19 mg of polymers (16.59 mg of PLGA-PEG and 2.41 mg of PLGA-PEG-Male, to obtain 10% of NPs surface with maleimide group) and 1 mL of acetone was dropwise into 1 mL of PBS (10mM pH 7.4) and stirred for 5 minutes (the solution became opaque). Then acetone was removed under reduced pressure (from 600 mbar to 100 mbar in 30 minutes and then 1 hour at 100 mbar, at 37°C), obtaining 1 mL of PLGA-PEG-Male NPs suspension in PBS.

The peptides (LMWP, CVSRRRRRRGGRRRR; ALMWP, EEEEEEEEEEPLGLAGVSRRRRRRGGRRRRC (CASLO APS, Kongens Lyngby, Denmark) in PBS (0.1 eq. for each maleimide group, 290 µL for LMWP and 567 µL for ALMWP; from a 1 mg/mL stock solution) and tris(2-carboxyethyl)phosphine hydrochloride (TCEP) in PBS (0.5 eq. for each maleimide group; from a 6.58 mg/mL stock solution) were mixed in a vial for 5 minutes, then added dropwise in 1 mL of PLGA-PEG-Male NPs suspension in PBS (19 mg/mL, 1 eq. of maleimide group). The reaction continued overnight under not vigorous stirring at room temperature. To remove TCEP, the solution was purified by ultrafiltration with Centrifugal Filters (MWCO 100 kDa, Amicon®) at 1500 rcf for 10 minutes, washing with 1 mL of PBS for 4 times to obtain 1 mL of suspended NPs.

Finally, 1.5 mg of Doxorubicin hydrochloride (DOXO-HCl) were dissolved in 1 mL of acetone with 0.71 µL of TEA. This solution was then added dropwise to the PLGA-PEG-peptide NPs suspension (19 mg/mL) and stirred for 10 minutes. Acetone was then removed under reduced pressure (under controlled pressure gradient: from 600 mbar to 100 mbar in 30 minutes and 1 hour at 100 mbar) at 32 °C. The free doxorubicin was removed by ultrafiltration with Centrifugal Filters (MWCO 100 kDa, Amicon®) at 1500 rcf for 10 minutes, washing with 1 mL of PBS for 4 times, obtaining 1 mL of final NPs suspension (PLGA-PEG-**LMWP** DOXO-loaded NPs; PLGA-PEG-**ALMWP** DOXO-loaded NPs).

3. Synthesis and characterization of star shaped, four arms PCL based nanovectors

A solution of 19 mg of $A_4CL_{10}PEG_{16}$-co-PCL_4Acr dissolved in 1 mL of acetone were added dropwise into 1 mL of stirred PBS (10mM pH 7.4). After 5 minutes, acetone was removed under reduced pressure (under controlled gradient of pressure: from 600 mbar to

100 mbar in 30 minutes and then 1 hour at 100 mbar) at 32 °C, obtaining 1 mL of NPs suspension in PBS.

The peptides in PBS (0.1 eq. for each acrylate group: 891 µL for LMWP, 1.74 mL for ALMWP, 782 µL for mApoE; from a 1 mg/mL stock solution) and Tris(2-carboxyethyl)phosphine hydrochloride (TCEP) in PBS (0.5 eq. for each acrylate group; from a 8.9 mg/mL stock solution) were mixed in a vial for 5 minutes, then added dropwise in 1 mL of $A_4CL_{10}PEG_{16}$-co-PCL_4Acrilated NPs suspension in PBS (19 mg/mL, 11.85 eq. of acrylate group). The reaction continued overnight under not vigorous stirring at room temperature. To remove TCEP, the solution was purified by ultrafiltration with Centrifugal Filters (MWCO 10 kDa, Amicon®) at 1500-2000 rcf for 10 minutes, washing with 1 mL of PBS for 4 times to obtain 1 mL of suspended NPs.

Finally, 1.5 mg of Doxorubicin hydrochloride (DOXO-HCl) were dissolved in 1 mL of acetone with 0.71 µL of TEA. This solution was then added dropwise to the NPs suspension (19 mg/mL) and stirred for 10 minutes. Acetone was then removed under reduced pressure (under controlled gradient of pressure: from 600 mbar to 100 mbar in 30 minutes and 1 hour at 100 mbar) at 32 °C. The free doxorubicin was removed by ultrafiltration with Centrifugal Filters (MWCO 10 kDa, Amicon®) at 1500-2000 rcf for 10 minutes, washing with 1 mL of PBS for 4 times to obtain 1 mL of final NPs suspended ($A_4CL_{10}PEG_{16}$-co-PCL_4-**LMWP** DOXO-loaded NPs; $A_4CL_{10}PEG_{16}$-co-PCL_4-**ALMWP** DOXO-loaded NPs; $A_4CL_{10}PEG_{16}$-co-PCL_4-**mApoE** DOXO-loaded NPs).

4. Patient-derived GSC primary cell culture establishment

Patient-derived Glioma stem cell (GSC) primary cultures were obtained from GBM surgical samples of patients undergoing surgery for brain tumor removal. Surgical specimens were collected from consenting patients in the Department of Neurosurgery at Humanitas Research Hospital (Rozzano, Italy) and Neurological Institute "C. Besta" (Milan, Italy) under "Humanitas" and "C. Besta" research ethics committee approval. Tumor samples were processed as by Gritti et al. (Gritti et al., 1996). Briefly, resection specimens received from neurosurgical unit of Humanitas Hospital were quickly dissected with scalpels and incubated with collagenase and DNAse. After 20 min incubation at 37°C, cell suspension were centrifuged and the pellet incubated with dH_2O in order to eliminate erythrocytes. Finally, after dH_2O rebalance with 10X PBS, cell suspension was filtered

through a 40µm strainer and incubated in fresh medium. Brain tumor-derived neurospheres were evident as early as 1 week after plating (**Fig. 30 A**). Spheres were grown for at least 3 weeks or until they reached a size adequate for plating and passaging (~200 µm).

Six different GSC lines were used in this project. All GSCs were tested for stemness by Extreme Limiting Dilution Analysis (ELDA) as described by Hu and Smyth (Hu, Y, and Smyth, GK, 2009). GSCs were plated at a concentration of 1, 2, 5, 10 or 40 cells per well in a 96 wells plate. The frequency of cells able to renew tumor spheres was determined after two weeks of culture by counting the number of spheres generated per single well. All the GSCs demonstrated a high renewing capacity: in ICH001 renewed 1 cell every 1,4; in ICH003 1 every 2,32; in ICH013 1 every 2,90; in BG003 1 every 3,74; in BG005 1 every 5,22; in GBM3 1 every 4,22.

The expression of the "stemness" markers CD133 and SOX2 were evaluated by real-time PCR in the GSC cultures and the differentiated human astrocyte (SVG cell line) (**Fig. 30 B**).

Pro-neural (PN) and Mesenchymal (MES) GSCs subtype (Bath et al., 2013; Halliday et al., 2014; Moreno et al., 2017; Rooj et al., 2017; Minata et al., 2019) were determined by gene profiling using the selected PN genes CD133, SOX2, SOX9, OLIG2, ADGRG1, and MES genes CD44, CTGF, FN1, CHI3L1, ALDH1A3. BG003 and BG005 displayed a PN profile. ICH001, ICH003 and GBM3 had a mixed PN/MES phenotype and could be classified as "classical" GSC lines. ICH013 showed a MES profile (**Fig. 30 C**).

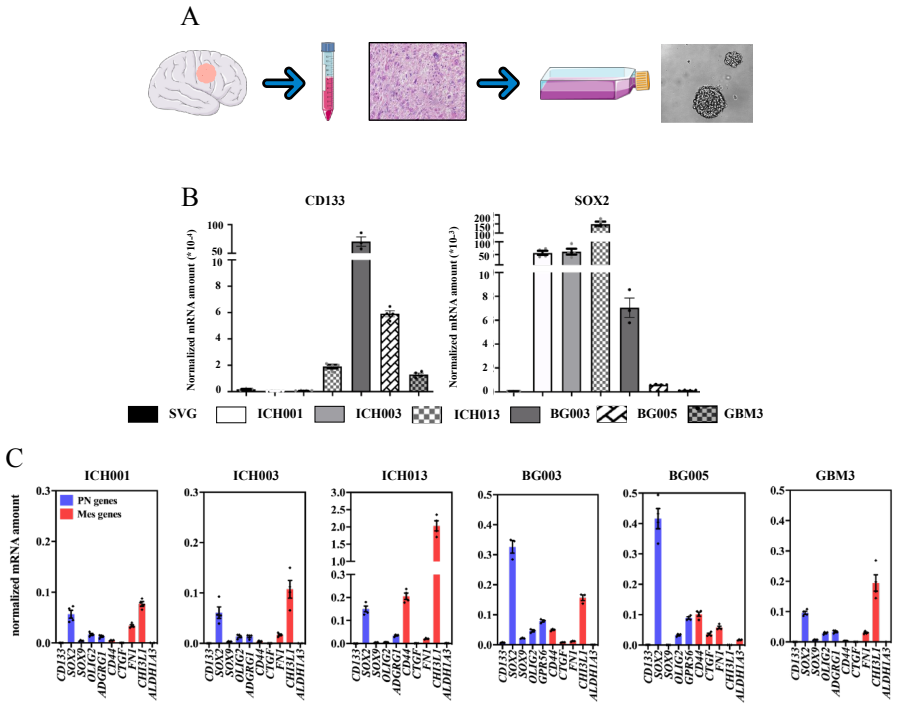

Fig. 30: patient-derived GSC primary culture establishment and characterization. A) Schematic representation of patient derived GSCs line preparation. After surgical resection, GBM tissue is mechanically dissected into tiny pieces that undergo enzymatic digestion to obtain single cells suspension. This suspension is then plated in culture medium until cell line is stabilized and ready to be used. **B**) Gene expression analysis of the stem marker CD133 and SOX2 in the indicated GSCs and in the differentiated human glial cells (SVG cell lines). **C**) PN/MES gene profiling by real-time PCR. Pairwise comparison was performed by Student's *t*-test: *p < 0.05.

5. In vitro transwell BBB model

hCMEC/D3 cells (7×104 cells/cm2, passages 25-35) were seeded on 12-well transwell inserts coated with type I collagen and cultured with 0.5 ml or 1 ml of culture medium in the upper and in the lower chamber. hCMEC/D3 monolayers integrity was verified by measuring the endothelial permeability (EP) of [14C]-sucrose and [3H]-propranolol and the transendothelial electrical resistance (TEER) (measured by EVOMX meter, STX2 electrode; World Precision Instruments). For permeability experiments, after 3 h of incubation with 2.5 or 25 µg/ml of DOXO, free or embedded into LIPs, the amount of DOXO in the basolateral compartment was measured by fluorescence and the EP to DOXO calculated as described (Ceccherelli et al., 1999). LIP integrity after BBB crossing was evaluated by Nanoparticle Tracking Analysis (NanoSight NS300, Malvern Panalytical). Impact of free-DOXO or DOXO-LIPs on cell monolayers was checked by measuring TEER and EP of Lucifer Yellow (50 µM) after hCMEC/D3 incubation. For cytotoxicity experiments, hCMEC/D3 were co-culture with U87-MG, A172 cells (5.4x104 cells/well) adherent to the bottom of the basolateral compartment. 25 µg/ml of DOXO, free or embedded in LIP, were added to apical compartment and incubated for 3h. Then, upper inserts were removed and GBM cells cultured for additional 48h in the lower chambers. Viability was evaluated by MTT assay.

6. In vitro viability assay

GSCs (10^4 cells/well) or endothelial hCMEC/D3 cells (5 10^3 cells/well) were plated in 96-well plates in a final volume of 200 µl of medium in the absence/presence of increasing doses of different NVs at the indicated doses of DOXO. Only in the experiments using the GBM integrated BBB model, LIPs were removed 3h after treatment. 24-48-72h after treatment depending on experimental design, the mitochondrial enzymatic activity, index an indicator of cell viability, was assessed by MTT assay. Briefly, 4h before the end of the treatment, 20 µl of MTT were added directly in each well to a final concentration of 0,5

mg/ml. At the finish of the treatment, plate were centrifuged at 1500 rpm for 15 min to pellet down the cells. Surnatnat was removed and 100 µl of DMSO were added in each well to solubilized the formazan salt crystals. After 15 min shaking at room temperature, absorbance was red at 570 and 630 nm. Final absorbance values were determined subtracting 630 nm value to the corresponding 570 nm.

7. Nuclear DOXO quantification by confocal microscopy

GBM cells (U87-MG, A172 and T98G), GSCs and hCMEC/d3 endothelial cells were seeded on glass coverslips at a concentration of 3500 cell/cm^2. The day after the cells were incubated at different condition: free DOXO, DOXO-LIP or mApoE-DOXO-LIP at [DOXO] of 4 µg/ml for 4h; DOXO-PCL, LMWP-DOXO-PCL or ALMWP-DOXO-PCL [DOXO] of 1,2 µg/ml for 6h. In the experiments with the endocytosis inhibitors, Chlorpromazine (10 µM) or Dynasore (80 µM) were added to the cell medium one hour before the cell incubation with the liposomes. The inhibitors were kept into the cell medium during the whole experiment (5 hours' incubation). Irradiated GSCs were incubated with LIPs 20h after radiation treatment. Cells were irradiated with a single dose of 2 Gy using an X-ray biological irradiator operating at 12 mA/190kV (RADGIL, Gilardoni, Lecco, Italy) at a dose rate of 0.65 Gy/min. Cells were fixed in PFA 4% in PBS for 15 min, DAPI (Sigma-Aldrich) stained (10 µg/ml in PBS, 30 min) and mounted in 90% glycerol in PBS. The Z-stack series of the cells in different experimental conditions were acquired by means of a confocal microscope (TCS SP5, Leica Microsystems GmbH) with the HCX PL APO 63x/1.4 OIL objective. The DAPI (Ex/Em: 405/415-450 nm), Syto45 (Ex/Em: 458/470-500 nm) and DOXO autofluorescence (488/570-700) signals were acquired sequentially at high scan rate. Images were processed using Fiji (Schindelin et al., 2012) using the DAPI signal to segment the nucleus. The DOXO fluorescence was quantified in the nuclei as mean grey values in the optical section were the nucleus area were maximized.

8. Nuclear DOXO quantification by live imaging microscopy

GSCs were seeded in a 96 well "flat bottom" pre-coated (5µg/ml collagene, 1µg/ml fibronectin) plate at a concentration of 15625 cells/cm^2. After 24h, cell's were treated with

PLGA-PEG NVs (PLGA-PEG-DOXO, PLGA-PEG-LMWP-DOXO or PLGA-PEG-ALMWP-DOXO, [DOXO] 4 μg/ml in every condition) or PCL-PEG NVs (PCL-PEG-DOXO, PCL-PEG-LMWP-DOXO or PCL-PEG-ALMWP-DOXO, [DOXO] 1,2 μg/ml in every condition) up to 10 h. Nuclear DOXO accumulation was monitored once per hour in each well (4 repetition per each treatments per GSCs) by DMi8 fluorescent microscopy and LasX software (Leica Microsystems GmbH). The DAPI (Ex/Em: 405/415-450 nm) and DOXO autofluorescence (488/570-700) signals were acquired sequentially at 20X magnification. Images were processed using Fiji using the DAPI signal to determinate nucleus area. The DOXO fluorescence was quantified as mean grey values in the nucleus area.

9. Immunocytochemistry

LDLR level of expression in GSC cultures was detected by immunostaining incubating the cells ($5x10^4$ cells on 18mm coverslips) with primary antibody against human LDLR (1:100, Sigma-Aldrich) over night at 4°C. After primary antibody, samples were incubated with anti-mouse secondary antibody conjugated with Alexa Fluor® 488 (1:200, Thermo Fisher, Waltham, Mas) and anti-Phalloidin conjugated with Alexa Fluor® 647 (1:200, Thermo Fisher, Waltham, Mas) for 1h at room temperature. Glasses were mounted with a PBS/glycerol mixture (1:1) with DAPI (1:40.000) (Sigma-Aldrich, St. Louis, MO). LDLR level of expression was quantified by confocal images processed using Fiji software and the "Analyze Particles" tool. The central, upper, and lower sections of 1μm z-stack were analyzed for each image and the LDLR threshold, determined on the negative control, was kept constant in each of the experimental conditions. LDLR level was calculated as LDLR-positive fluorescent area normalized to the cellular cytoplasmatic area demarcated by the Phalloidin staining.

10. MMP2 protein level and enzymatic activity

MMP2 protein level was determined by Western Blot analysis on $4*10^6$ GSC cells incubated 24h in 4 ml of fresh complete culture medium. 1:1000 ab α-MMP2 (Sigma-

Aldrich, St. Louis, Mis) was incubated overnight at 4°C. 1:5000 secondary ab (Thermo Fisher, Waltham, Mas) was incubated 1h at room temperature. The signal intensity was determined by ChemiDoc Imaging System (BioRad, Hercules, CA) and analyzed by Image Lab software (BioRad, Hercules, CA). Samples were normalized on protein total amount. MMP2 activity was determined by zymography as described in Frankowski et al. (Frankowski et al., 2012). Briefly, 5µl of medium conditioned by cells employed for Western Blot were mixed with 15 µl of Zymogram Sample Buffer (BioRad, Hercules, CA) and loaded in a 8% polyacrylamide gel supplemented with 0,1% gelatin B (MMP2 substrate). After 2h running at 90 V voltage for 2h, gel was washed 3 times with Zymogram Renaturation Buffer (BioRad, Hercules, CA). Then, gel was incubated with Zymogram Development Buffer (BioRad, Hercules, CA) for 1h at room temperature. After changing Development buffer with fresh one, gel was incubated at 37°C for at least 12h. Finally, gel was incubated with Safe Comassie (BioRad, Hercules, CA) for 2h and destained in dH_2O until the desired blue coloring. The digestion intensity was determined by ChemiDoc Imaging System (BioRad, Hercules, CA) and analyzed by Image Lab software (BioRad, Hercules, CA).

11. mApoE-DOXO-LIP biodistribution

All procedures involving animals were conducted according to Italian laws and the Animal Utilization Protocols approved by the Italian Ministry of Health. 6–8 weeks old male Balb/c mice (3 mice/group; Charles-River Laboratories) were injected via the tail vein with 100 µL of radiolabelled mApoE-DOXO-LIP (10mM total lipids, 5 mg/kg DOXO, 0.5 µCi/mouse [3H]-Sm, 0.3 µCi/mouse [14C]-DOXO) or free DOXO (5 mg/kg, 0.3 µCi/mouse [14C]-DOXO) in PBS. After mice were sacrificed a total of 0.1 g of each tissue or 100 µl of blood, in triplicate, were solubilized at 55◦C for 2h and cooled to room temperature. Radioactivity was measured by liquid scintillation counting. Data were expressed as percentage of injected dose on total organ weight/volume ± SD. The possible radioactivity derived from the blood was subtracted from the radioactivity values measured in the brain (-5% of measured radioactivity).

12. GSC orthotopic xenografts and treatments

To study mApoE-DOXO-LIP antitumor activity, luciferase transfected GSC1luc cells (4 × 104) were stereotactically injected into the right striatum of 4-week-old male NOD/SCID mice (NOD.CB-17-Prkdcscid/J, Charles-River). Luciferase stable expression was obtained using the pRRL.sin.PPT.CMV.Luciferase.iresEMCVwt.eGFP.pre lentiviral vector engineered by Dr E.Vigna and kindly provided by Dr. C.Boccaccio (Candiolo Cancer Institute, Candiolo, Torino, Italy) (De Bacco et al., 2016). From 6 weeks after intracranial inoculation, tumors were monitored by BLI imaging (IVIS® II Imaging, Caliper Life Sciences-PerkinElmer) once a week. Treatments started at 8 weeks after tumor injection (D60) when tumors were detectable by BLI. In order to obtain comparable results, animals were randomized according to BLI imagines into groups homogeneous for tumor dimension. All treated mice received 35 μg/dose/mouse of DOXO delivered by DOXO-LIPs or mApoE-DOXO-LIPs administered intraperitoneal. Whole-brain radiation (2Gy) was performed using an X-ray irradiator operating at 12 mA/190kV (RADGIL, Gilardoni). mApoE-DOXO-LIPs were administered 16-18h after radiation.

13. Histopathology analysis and TUNEL assay

Animals were euthanized with intracardiac perfusion of saline solution, followed by 4% paraformaldehyde fixation. Harvested brains were frozen, and serial cryosections (10m thick) were prepared and stored at -80C°. Three coronal sections (one at the intersection of the tumor injection site plus one anterior and one posterior sections at 50 m distance, were analyzed for each single treated and untreated mouse.

Frozen brain sections were immunostained with mouse anti-Human Nuclei (clone 235-1, Sigma), rabbit anti-Iba1 (Wako) primary antibodies followed by anti-mouse Alexa Fluor 488 and anti-rabbit Alexa Fluor 555 secondary antibodies (Thermo Fisher, Waltham, Mas). The Click-iT Plus Alexa Fluor 647 TUNEL Assay (Thermo Fisher, Waltham, Mas) was used to detect in situ apoptosis and DAPI for nuclei staining. Coronal images were acquired using a DMi8 fluorescent microscope and Leica Application Suite X (LAS X) imaging system (Leica Microsystems). Confocal microscopy was performed using a Leica TCS SP8 confocal microscope. Maximum projections were obtained from 29-35 Z-stacks. Image analysis was carried out by FIJI or Imaris (Bitplane, Zurich, Switzerland) for 3D rendering.

14. Statistical analysis

In vitro data are expressed as mean values ± standard deviation (SD) or standard error (SE) of at least three independent experiments performed in replicates. Student's t-test was used for pairwise comparison. Significance was defined at $P < 0.05$. *In vivo* statistical significance among treatments was evaluated by ANOVA using correction post hoc tests (Bonferroni or Turkey's multiple comparisons as indicated). Statistical analyses were performed using Prism 8 (GraphPad Software).

List of abbreviations

ABC Adenosine Triphosphate Binding Cassette
ALMWP Activatable Low Molecular Weight Protamine
ApoE Apolipoprotein E
BBB Blood Brain Barrier
BBTB Blood-Brain Tumor Barrier
BCSFB Blood-Cerebrospinal Fluid Barrier
BER Base Excision Repair
cIMPACT-NOW Consortium to Inform Molecular and Practical Approaches to CNS Tumor Taxonomy
cRGD Arg-Gly-Asp
CAR himeric Antigen Receptor
CBC complete blood counts
Chol Cholesterol
CNS Central Nervous System
CPP Cell Penetrating Peptide
CPZ Chlorpromazine
CTLA-4 Cytotoxic T-Lymphocyte Antigen 4
DAMP Damage-Associated Molecular Pattern
DYN Dynasore
ECM Extra Cellular Matrix
EGFR Epidermal Growth Factor Receptor
EPR Enhanced Permeability and Retention effect
FDA Food and Drug Administration
FUS Focus Ultrasound
GAMM Glioma-Associated Microglia/Macrophages
GBM Glioblastona
GL261 Glioma 261
GSC Glioblastoma Stem-like cells
DOXO Doxorubicin
HSP Heat Shock Protein
HU Human Nuclei
ICD Immune Cell Death
IDH1 Isocotrate Dehydrogenase 1
IL-1β Interleukin 1β
IL13Rα2 Interleukin-13 Receptor Alpha 2
ISF Interstitial Fluid
HBsAg Hepatitis B Surface Antigen

LDLR Low Density Lipoprotein Receptor

LIP Liposome

LRP Lipoprotein Receptor-related Protein

mABS Monoclonal Antibodies

MDM2 Mouse Double Minute 2

MDR1 Multi Drug Resistance gene 1

MES Mesenchymal

MGMT O−6−Methylguanine−DNA Methyltransferase promoter methylation

MMP Matrix Metalloproteinases

mTOR mammalian Target of Rapamicine

NP Nanoparticle

NV Nanovector

NVU Neurovascular Unit

NF-κB Nuclear Factor kappa-light-chain-enhancer of activated B cells

NK Natural Killer

PCL poly(ε-caprolactone)

PD-1 Programmed cell Death 1

PD-1 L Programmed cell Death 1 Ligand

PDGFA Platelet Derived Growth Factor a

PDGFRα Platelet Derived Growth Factor Receptor alpha

PEG Polyethilen Glicol

P-gp P-glycoprotein

PDI Polydispersity Index

PLGA Poly(lactic-co-glycol acid)

PMT Proneural to Mesenchymal transition

PN Proneural

PTEN Phosphatase and Tensing homologue

RB Retinoblastoma

RMT Receptor Mediated Transcytosis

RN Radiation Necrosis

RT Radiotherapy

SLC Solute Carrier

Sm Sphingomyelin

TAA Tumor Associated Antigen

Tf Transferrin

TJ Tight Junction

TMZ Temozolomide

TNFα Tumor Necrosis Factor α

VEGF Vascular Epithelial Growth Factor

WHO World Health Organization

wt wild-type

List of publications

Radiation and Adjuvant Drug-Loaded Liposomes target Glioblastoma Stem Cells and Trigger In-situ Immune Response

Marco Pizzocri, Beatrice Formicola, Elisabetta Stanzani, Matteo Tamborini, Eliana Lauranzano, Federica Ungaro, Simona Rodighiero, Maura Francolini, Maria Gregori, Alessandro Perin, Francesco DiMeco, Massimo Masserini, Francesca Re, Michela Matteoli, Lorena Passoni

A Microfluidic Human Model of Blood–Brain Barrier Employing Primary Human Astrocytes

Eliana Lauranzano, Elena Campo, Marco Rasile, Raffaella Molteni, Marco Pizzocri, Lorena Passoni, Lorenzo Bello, Davide Pozzi, Ruggero Pardi, Michela Matteoli, and Ana Ruiz-Moreno

Bibliography

- Abbott NJ, Patabendige AA, Dolman DE, Yusof SR, Begley DJ. **Structure and function of the blood-brain barrier.** Neurobiol Dis. 2010 Jan;37(1):13-25. doi: 10.1016/j.nbd.2009.07.030. Epub 2009 Aug 5. PMID: 19664713.

- Adhikari A, Mondal S, Darbar S, Kumar Pal S. **Role of Nanomedicine in Redox Mediated Healing at Molecular Level.** Biomol Concepts. 2019 Oct 29;10(1):160-174. doi: 10.1515/bmc-2019-0019. PMID: 31661433.

- Agnihotri S, Burrell KE, Wolf A, Jalali S, Hawkins C, Rutka JT, Zadeh G. **Glioblastoma, a brief review of history, molecular genetics, animal models and novel therapeutic strategies**. Arch Immunol Ther Exp (Warsz). 2013 Feb;61(1):25-41. doi: 10.1007/s00005-012-0203-0. Epub 2012 Dec 7. PMID: 23224339.

- Alexander BM, Cloughesy TF. **Adult Glioblastoma.** J Clin Oncol. 2017 Jul 20;35(21):2402-2409. doi: 10.1200/JCO.2017.73.0119. Epub 2017 Jun 22. PMID: 28640706.

- Alphandéry E. **Nano-Therapies for Glioblastoma Treatment.** Cancers (Basel). 2020 Jan 19;12(1):242. doi: 10.3390/cancers12010242. PMID: 31963825; PMCID: PMC7017259.

- Ananda S, Nowak AK, Cher L, Dowling A, Brown C, Simes J, Rosenthal MA; Cooperative Trials Group for Neuro-Oncology (COGNO). **Phase 2 trial of temozolomide and pegylated liposomal doxorubicin in the treatment of patients with glioblastoma multiforme following concurrent radiotherapy and chemotherapy.** J Clin Neurosci. 2011 Nov;18(11):1444-8. doi: 10.1016/j.jocn.2011.02.026. Epub 2011 Aug 2. PMID: 21813279.

- Arvanitis CD, Ferraro GB, Jain RK. **The blood-brain barrier and blood-tumour barrier in brain tumours and metastases.** Nat Rev Cancer. 2020 Jan;20(1):26-41. doi: 10.1038/s41568-019-0205-x. Epub 2019 Oct 10. PMID: 31601988.

- Ayloo S, Gu C. **Transcytosis at the blood-brain barrier.** Curr Opin Neurobiol. 2019 Aug;57:32-38. doi: 10.1016/j.conb.2018.12.014. Epub 2019 Jan 30. PMID: 30708291; PMCID: PMC6629499.

- Balducci C, Mancini S, Minniti S, La Vitola P, Zotti M, Sancini G, Mauri M, Cagnotto A, Colombo L, Fiordaliso F, Grigoli E, Salmona M, Snellman A, Haaparanta-Solin M, Forloni G, Masserini M, Re F. **Multifunctional liposomes reduce brain β-amyloid burden and ameliorate memory impairment in Alzheimer's disease mouse models**. J Neurosci. 2014 Oct 15;34(42):14022-31. doi: 10.1523/JNEUROSCI.0284-14.2014. PMID: 25319699; PMCID: PMC4198543.

- Bana L, Minniti S, Salvati E, Sesana S, Zambelli V, Cagnotto A, Orlando A, Cazzaniga E, Zwart R, Scheper W, Masserini M, Re F. **Liposomes bi-functionalized with phosphatidic acid and an ApoE-derived peptide affect Aβ aggregation features and cross the blood-brain-barrier: implications for therapy of Alzheimer disease.** Nanomedicine. 2014 Oct;10(7):1583-90. doi: 10.1016/j.nano.2013.12.001. Epub 2013 Dec 10. PMID: 24333591.

- Banelli B, Carra E, Barbieri F, Würth R, Parodi F, Pattarozzi A, Carosio R, Forlani A, Allemanni G, Marubbi D, Florio T, Daga A, Romani M. **The histone demethylase KDM5A is a key factor for the resistance to temozolomide in glioblastoma.** Cell Cycle. 2015;14(21):3418-29. doi: 10.1080/15384101.2015.1090063. PMID: 26566863; PMCID: PMC4825557.

- Banerji CR, Miranda-Saavedra D, Severini S, Widschwendter M, Enver T, Zhou JX, Teschendorff AE. **Cellular network entropy as the energy potential in Waddington's differentiation landscape**. Sci Rep. 2013 Oct 24;3:3039. doi: 10.1038/srep03039. PMID: 24154593; PMCID: PMC3807110.

- Bao S, Wu Q, McLendon RE, Hao Y, Shi Q, Hjelmeland AB, Dewhirst MW, Bigner DD, Rich JN. **Glioma stem cells promote radioresistance by preferential activation of the DNA damage response.** Nature. 2006 Dec 7;444(7120):756-60. doi: 10.1038/nature05236. Epub 2006 Oct 18. PMID: 17051156.

- Beier CP, Schmid C, Gorlia T, Kleinletzenberger C, Beier D, Grauer O, Steinbrecher A, Hirschmann B, Brawanski A, Dietmaier C, Jauch-Worley T, Kölbl O, Pietsch T, Proescholdt M, Rümmele P, Muigg A, Stockhammer G, Hegi M, Bogdahn U, Hau P. **RNOP-09: pegylated liposomal doxorubicine and prolonged temozolomide in addition to radiotherapy in newly diagnosed glioblastoma--a phase II study.** BMC Cancer. 2009 Sep 2;9:308. doi: 10.1186/1471-2407-9-308. PMID: 19725960; PMCID: PMC2749868.

- Bhaduri A, Di Lullo E, Jung D, Müller S, Crouch EE, Espinosa CS, Ozawa T, Alvarado B, Spatazza J, Cadwell CR, Wilkins G, Velmeshev D, Liu SJ, Malatesta M, Andrews MG, Mostajo-Radji MA, Huang EJ, Nowakowski TJ, Lim DA, Diaz A, Raleigh DR, Kriegstein AR. **Outer Radial Glia-like Cancer Stem Cells Contribute to Heterogeneity of Glioblastoma.** Cell Stem Cell. 2020 Jan 2;26(1):48-63.e6. doi: 10.1016/j.stem.2019.11.015. PMID: 31901251; PMCID: PMC7029801.

- Bhat KPL, Balasubramaniyan V, Vaillant B, Ezhilarasan R, Hummelink K, Hollingsworth F, Wani K, Heathcock L, James JD, Goodman LD, Conroy S, Long L, Lelic N, Wang S, Gumin J, Raj D, Kodama Y, Raghunathan A, Olar A, Joshi K, Pelloski CE, Heimberger A, Kim SH, Cahill DP, Rao G, Den Dunnen WFA, Boddeke HWGM, Phillips HS, Nakano I, Lang FF, Colman H, Sulman EP, Aldape K. **Mesenchymal differentiation mediated by NF-κB promotes radiation resistance in glioblastoma.** Cancer Cell. 2013 Sep 9;24(3):331-46. doi: 10.1016/j.ccr.2013.08.001. Epub 2013 Aug 29. PMID: 23993863; PMCID: PMC3817560.

- Binabaj MM, Bahrami A, ShahidSales S, Joodi M, Joudi Mashhad M, Hassanian SM, Anvari K, Avan A. **The prognostic value of MGMT promoter methylation in glioblastoma: A meta-analysis of clinical trials.** J Cell Physiol. 2018 Jan;233(1):378-386. doi: 10.1002/jcp.25896. Epub 2017 May 16. PMID: 28266716.

- Blaes J, Thomé CM, Pfenning PN, Rübmann P, Sahm F, Wick A, Bunse T, Schmenger T, Sykora J, von Deimling A, Wiestler B, Merz C, Jugold M, Haberkorn U, Abdollahi A, Debus J, Gieffers C, Kunz C, Bendszus M, Kluge M, Platten M, Fricke H, Wick W, Lemke D. **Inhibition of CD95/CD95L (FAS/FASLG) Signaling with APG101 Prevents Invasion and Enhances Radiation Therapy for Glioblastoma.** Mol Cancer Res. 2018 May;16(5):767-776. doi: 10.1158/1541-7786.MCR-17-0563. Epub 2018 Feb 16. PMID: 29453321.

- Brahm CG, van Linde ME, Enting RH, Schuur M, Otten RHJ, Heymans MW, Verheul HMW, Walenkamp AME. **The Current Status of Immune Checkpoint Inhibitors in Neuro-Oncology: A Systematic Review.** Cancers (Basel). 2020 Mar 4;12(3):586. doi: 10.3390/cancers12030586. PMID: 32143288; PMCID: PMC7139638.

- Brennan CW, Verhaak RG, McKenna A, Campos B, Noushmehr H, Salama SR, Zheng S, Chakravarty D, Sanborn JZ, Berman SH, Beroukhim R, Bernard B, Wu CJ, Genovese G, Shmulevich I, Barnholtz-Sloan J, Zou L, Vegesna R, Shukla SA, Ciriello G, Yung WK, Zhang W, Sougnez C, Mikkelsen T, Aldape K, Bigner DD, Van Meir EG, Prados M, Sloan A, Black KL, Eschbacher J, Finocchiaro G, Friedman W, Andrews DW, Guha A, Iacocca M, O'Neill BP, Foltz G, Myers J, Weisenberger DJ, Penny R, Kucherlapati R, Perou CM, Hayes DN, Gibbs R, Marra M, Mills GB, Lander E, Spellman P, Wilson R, Sander C, Weinstein J, Meyerson M, Gabriel S, Laird PW, Haussler D, Getz G, Chin L; TCGA Research Network. **The somatic genomic landscape of glioblastoma.** Cell. 2013 Oct 10;155(2):462-77. doi: 10.1016/j.cell.2013.09.034. Erratum in: Cell. 2014 Apr 24;157(3):753. PMID: 24120142; PMCID: PMC3910500.

- Buzea C, Pacheco II, Robbie K. **Nanomaterials and nanoparticles: sources and toxicity.** Biointerphases. 2007 Dec;2(4):MR17-71. doi: 10.1116/1.2815690. PMID: 20419892.

- Caccese M, Indraccolo S, Zagonel V, Lombardi G. **PD-1/PD-L1 immune-checkpoint inhibitors in glioblastoma: A concise review**. Crit Rev Oncol Hematol. 2019 Mar;135:128-134. doi: 10.1016/j.critrevonc.2018.12.002. Epub 2019 Feb 1. PMID: 30819441.

- Cecchelli R, Dehouck B, Descamps L, Fenart L, Buée-Scherrer V V, Duhem C, Lundquist S, Rentfel M, Torpier G, Dehouck MP. **In vitro model for evaluating drug transport across the blood-brain barrier.** Adv Drug Deliv Rev. 1999 Apr 5;36(2-3):165-178. doi: 10.1016/s0169-409x(98)00083-0. PMID: 10837714.

- Chambers AF, Matrisian LM. **Changing views of the role of matrix metalloproteinases in metastasis.** J Natl Cancer Inst. 1997 Sep 3;89(17):1260-70. doi: 10.1093/jnci/89.17.1260. PMID: 9293916.

- Chang HH, Hemberg M, Barahona M, Ingber DE, Huang S. **Transcriptome-wide noise controls lineage choice in mammalian progenitor cells.** Nature. 2008 May 22;453(7194):544-7. doi: 10.1038/nature06965. PMID: 18497826; PMCID: PMC5546414.

- Chang JE, Khuntia D, Robins HI, Mehta MP. **Radiotherapy and radiosensitizers in the treatment of glioblastoma multiforme**. Clin Adv Hematol Oncol. 2007 Nov;5(11):894-902, 907-15. PMID: 18185489.

- Chen J, Li Y, Yu TS, McKay RM, Burns DK, Kernie SG, Parada LF. **A restricted cell population propagates glioblastoma growth after chemotherapy**. Nature. 2012 Aug 23;488(7412):522-6. doi: 10.1038/nature11287. PMID: 22854781; PMCID: PMC3427400.

- Chen NG, Szalay AA, Buller RM, Lauer UM. **Oncolytic viruses**. Adv Virol. 2012;2012:320206. doi: 10.1155/2012/320206. Epub 2012 Jun 6. PMID: 22754567; PMCID: PMC3384932.

- Cheng L, Wu Q, Guryanova OA, Huang Z, Huang Q, Rich JN, Bao S. **Elevated invasive potential of glioblastoma stem cells.** Biochem Biophys Res Commun. 2011 Mar 25;406(4):643-8. doi: 10.1016/j.bbrc.2011.02.123. Epub 2011 Mar 1. PMID: 21371437; PMCID: PMC3065536.

- Cloughesy TF, Cavenee WK, Mischel PS. **Glioblastoma: from molecular pathology to targeted treatment**. Annu Rev Pathol. 2014;9:1-25. doi: 10.1146/annurev-pathol-011110-130324. Epub 2013 Aug 5. PMID: 23937436.

- Cortés-Funes H, Coronado C. **Role of anthracyclines in the era of targeted therapy.** Cardiovasc Toxicol. 2007;7(2):56-60. doi: 10.1007/s12012-007-0015-3. PMID: 17652804.

- Cuccurullo V, Di Stasio GD, Cascini GL, Gatta G, Bianco C. **The Molecular Effects of Ionizing Radiations on Brain Cells: Radiation Necrosis vs. Tumor Recurrence.** Diagnostics (Basel). 2019 Sep 24;9(4):127. doi: 10.3390/diagnostics9040127. PMID: 31554255; PMCID: PMC6963489.

- Dal Magro R, Ornaghi F, Cambianica I, Beretta S, Re F, Musicanti C, Rigolio R, Donzelli E, Canta A, Ballarini E, Cavaletti G, Gasco P, Sancini G. **ApoE-modified solid lipid nanoparticles: A feasible strategy to cross the blood-brain barrier.** J Control Release. 2017 Mar 10;249:103-110. doi: 10.1016/j.jconrel.2017.01.039. Epub 2017 Jan 31. PMID: 28153761.

- Darmanis S, Sloan SA, Croote D, Mignardi M, Chernikova S, Samghababi P, Zhang Y, Neff N, Kowarsky M, Caneda C, Li G, Chang SD, Connolly ID, Li Y, Barres BA, Gephart MH, Quake SR. Single-Cell RNA-Seq **Analysis of Infiltrating Neoplastic Cells at the Migrating Front of Human Glioblastoma.** Cell Rep. 2017 Oct 31;21(5):1399-1410. doi: 10.1016/j.celrep.2017.10.030. PMID: 29091775; PMCID: PMC5810554.

- Davis ME. **Glioblastoma: Overview of Disease and Treatment.** Clin J Oncol Nurs. 2016 Oct 1;20(5 Suppl):S2-8. doi: 10.1188/16.CJON.S1.2-8. PMID: 27668386; PMCID: PMC5123811.

- De Bacco F, D'Ambrosio A, Casanova E, Orzan F, Neggia R, Albano R, Verginelli F, Cominelli M, Poliani PL, Luraghi P, Reato G, Pellegatta S, Finocchiaro G, Perera T, Garibaldi E, Gabriele P, Comoglio PM, Boccaccio C. **MET inhibition overcomes radiation resistance of glioblastoma stem-like cells.** EMBO Mol Med. 2016 May 2;8(5):550-68. doi: 10.15252/emmm.201505890. PMID: 27138567; PMCID: PMC5130292.

- Dehouck B, Fenart L, Dehouck MP, Pierce A, Torpier G, Cecchelli R. **A new function for the LDL receptor: transcytosis of LDL across the blood-brain barrier.** J Cell Biol. 1997 Aug 25;138(4):877-89. doi: 10.1083/jcb.138.4.877. PMID: 9265653; PMCID: PMC2138047.

- Deng Z, Sheng Z, Yan F. **Ultrasound-Induced Blood-Brain-Barrier Opening Enhances Anticancer Efficacy in the Treatment of Glioblastoma: Current Status and Future Prospects.** J Oncol. 2019 Nov 3;2019:2345203. doi: 10.1155/2019/2345203. PMID: 31781213; PMCID: PMC6875288.

- Dhermain F. **Radiotherapy of high-grade gliomas: current standards and new concepts, innovations in imaging and radiotherapy, and new therapeutic approaches.** Chin J Cancer. 2014 Jan;33(1):16-24. doi: 10.5732/cjc.013.10217. PMID: 24384237; PMCID: PMC3905086.

- Dirkse A, Golebiewska A, Buder T, Nazarov PV, Muller A, Poovathingal S, Brons NHC, Leite S, Sauvageot N, Sarkisjan D, Seyfrid M, Fritah S, Stieber D, Michelucci A, Hertel F, Herold-Mende C, Azuaje F, Skupin A, Bjerkvig R, Deutsch A, Voss-Böhme A, Niclou SP. **Stem cell-associated heterogeneity in Glioblastoma results from intrinsic tumor plasticity shaped by the microenvironment.** Nat Commun. 2019 Apr 16;10(1):1787. doi: 10.1038/s41467-019-09853-z. PMID: 30992437; PMCID: PMC6467886.

- Dropcho EJ. **Central nervous system injury by therapeutic irradiation**. Neurol Clin. 1991 Nov;9(4):969-88. PMID: 1758435.

- Duerinck J, Du Four S, Sander W, Van Binst AM, Everaert H, Michotte A, Hau P, Neyns B. **Sunitinib Malate plus Lomustine for Patients with Temozolomide-refractory Recurrent Anaplastic or Low-grade Glioma.** Anticancer Res. 2015 Oct;35(10):5551-7. PMID: 26408725.

- Egeblad M, Werb Z. **New functions for the matrix metalloproteinases in cancer progression.** Nat Rev Cancer. 2002 Mar;2(3):161-74. doi: 10.1038/nrc745. PMID: 11990853.

- Fang J, Nakamura H, Maeda H. **The EPR effect: Unique features of tumor blood vessels for drug delivery, factors involved, and limitations and augmentation of the effect.** Adv Drug Deliv Rev. 2011 Mar 18;63(3):136-51. doi: 10.1016/j.addr.2010.04.009. Epub 2010 May 2. PMID: 20441782.

- Fedele M, Cerchia L, Pegoraro S, Sgarra R, Manfioletti G. **Proneural-Mesenchymal Transition: Phenotypic Plasticity to Acquire Multitherapy Resistance in Glioblastoma**. Int J Mol Sci. 2019 Jun 4;20(11):2746. doi: 10.3390/ijms20112746. PMID: 31167470; PMCID: PMC6600373.

- Fisher DG, Price RJ. **Recent Advances in the Use of Focused Ultrasound for Magnetic Resonance Image-Guided Therapeutic Nanoparticle Delivery to the Central Nervous System.** Front Pharmacol. 2019 Nov 13;10:1348. doi: 10.3389/fphar.2019.01348. PMID: 31798453; PMCID: PMC6864822.

- Frankowski H, Gu YH, Heo JH, Milner R, Del Zoppo GJ. **Use of gel zymography to examine matrix metalloproteinase (gelatinase) expression in brain tissue or in primary glial cultures.** Methods Mol Biol. 2012;814:221-33. doi: 10.1007/978-1-61779-452-0_15. PMID: 22144310; PMCID: PMC3670093.

- Friedman AD, Claypool SE, Liu R. **The smart targeting of nanoparticles.** Curr Pharm Des. 2013;19(35):6315-29. doi: 10.2174/13816128113199990375. PMID: 23470005; PMCID: PMC4016770.

- Fung KYY, Fairn GD, Lee WL. **Transcellular vesicular transport in epithelial and endothelial cells: Challenges and opportunities.** Traffic. 2018 Jan;19(1):5-18. doi: 10.1111/tra.12533. Epub 2017 Nov 21. PMID: 28985008.

- Furusawa C, Kaneko K. **Chaotic expression dynamics implies pluripotency: when theory and experiment meet.** Biol Direct. 2009 May 15;4:17. doi: 10.1186/1745-6150-4-17. PMID: 19445676; PMCID: PMC2690595.

- Galluzzi L, Buqué A, Kepp O, Zitvogel L, Kroemer G. **Immunogenic cell death in cancer and infectious disease.** Nat Rev Immunol. 2017 Feb;17(2):97-111. doi: 10.1038/nri.2016.107. Epub 2016 Oct 17. PMID: 27748397.

- Geng F, Cheng X, Wu X, Yoo JY, Cheng C, Guo JY, Mo X, Ru P, Hurwitz B, Kim SH, Otero J, Puduvalli V, Lefai E, Ma J, Nakano I, Horbinski C, Kaur B, Chakravarti A, Guo D. **Inhibition of SOAT1 Suppresses Glioblastoma Growth via Blocking SREBP-1-Mediated Lipogenesis.** Clin Cancer Res. 2016 Nov 1;22(21):5337-5348. doi: 10.1158/1078-0432.CCR-15-2973. Epub 2016 Jun 8. Erratum in: Clin Cancer Res. 2017 Apr 15;23 (8):2127. PMID: 27281560; PMCID: PMC5093025.

- Gerweck LE, Seetharaman K. **Cellular pH gradient in tumor versus normal tissue: potential exploitation for the treatment of cancer.** Cancer Res. 1996 Mar 15;56(6):1194-8. PMID: 8640796.

- Gieryng A, Pszczolkowska D, Walentynowicz KA, Rajan WD, Kaminska B. **Immune microenvironment of gliomas.** Lab Invest. 2017 May;97(5):498-518. doi: 10.1038/labinvest.2017.19. Epub 2017 Mar 13. PMID: 28287634.

- Gomez-Zepeda D, Taghi M, Scherrmann JM, Decleves X, Menet MC. **ABC Transporters at the Blood-Brain Interfaces, Their Study Models, and Drug Delivery Implications in Gliomas.** Pharmaceutics. 2019 Dec 23;12(1):20. doi: 10.3390/pharmaceutics12010020. PMID: 31878061; PMCID: PMC7022905.

- Gonawala S, Ali MM. **Application of Dendrimer-based Nanoparticles in Glioma Imaging.** J Nanomed Nanotechnol. 2017 Jun;8(3):444. doi: 10.4172/2157-7439.1000444. Epub 2017 Jun 14. PMID: 28856067; PMCID: PMC5573247.

- Gritti A, Parati EA, Cova L, Frolichsthal P, Galli R, Wanke E, Faravelli L, Morassutti DJ, Roisen F, Nickel DD, Vescovi AL. **Multipotential stem cells from the adult mouse brain proliferate and self-renew in response to basic fibroblast growth factor.** J Neurosci. 1996 Feb 1;16(3):1091-100. doi: 10.1523/JNEUROSCI.16-03-01091.1996. PMID: 8558238; PMCID: PMC6578802.

- Grossman SA, Ye X, Lesser G, Sloan A, Carraway H, Desideri S, Piantadosi S; NABTT CNS Consortium. **Immunosuppression in patients with high-grade gliomas treated with radiation and temozolomide.** Clin Cancer Res. 2011 Aug 15;17(16):5473-80. doi: 10.1158/1078-0432.CCR-11-0774. Epub 2011 Jul 7. PMID: 21737504; PMCID: PMC3156964.

- Grunert M, Kassubek R, Danz B, Klemenz B, Hasslacher S, Stroh S, Schneele L, Langhans J, Ströbele S, Barry SE, Zhou S, Debatin KM, Westhoff MA. **Radiation and Brain Tumors: An Overview**. Crit Rev Oncog. 2018;23(1-2):119-138. doi: 10.1615/CritRevOncog.2018025927. PMID: 29953371.

- Gu G, Xia H, Hu Q, Liu Z, Jiang M, Kang T, Miao D, Tu Y, Pang Z, Song Q, Yao L, Chen H, Gao X, Chen J. **PEG-co-PCL nanoparticles modified with MMP-2/9 activatable low molecular weight protamine for enhanced targeted glioblastoma therapy.** Biomaterials. 2013 Jan;34(1):196-208. doi: 10.1016/j.biomaterials.2012.09.044. Epub 2012 Oct 12. PMID: 23069707.

- Gullotti E, Yeo Y. **Extracellularly activated nanocarriers: a new paradigm of tumor targeted drug delivery.** Mol Pharm. 2009 Jul-Aug;6(4):1041-51. doi: 10.1021/mp900090z. PMID: 19366234; PMCID: PMC2743941.

- Guo D, Reinitz F, Youssef M, Hong C, Nathanson D, Akhavan D, Kuga D, Amzajerdi AN, Soto H, Zhu S, Babic I, Tanaka K, Dang J, Iwanami A, Gini B, Dejesus J, Lisiero DD, Huang TT, Prins RM, Wen PY, Robins HI, Prados MD, Deangelis LM, Mellinghoff IK, Mehta MP, James CD, Chakravarti A, Cloughesy TF, Tontonoz P, Mischel PS. **An LXR agonist promotes glioblastoma cell death through inhibition of an EGFR/AKT/SREBP-1/LDLR-dependent pathway.** Cancer Discov. 2011 Oct;1(5):442-56. doi: 10.1158/2159-8290.CD-11-0102. Epub 2011 Sep 15. Erratum in: Cancer Discov. 2012 Feb;2(2):290-1. PMID: 22059152; PMCID: PMC3207317.

- Gutmann DH, Maher EA, Van Dyke T. **Mouse Models of Human Cancers Consortium Workshop on Nervous System Tumors**. Cancer Res. 2006 Jan 1;66(1):10-3. doi: 10.1158/0008-5472.CAN-05-3180. PMID: 16397207.

- Haar CP, Hebbar P, Wallace GC 4th, Das A, Vandergrift WA 3rd, Smith JA, Giglio P, Patel SJ, Ray SK, Banik NL. **Drug resistance in glioblastoma: a mini review.** Neurochem Res. 2012 Jun;37(6):1192-200. doi: 10.1007/s11064-011-0701-1. Epub 2012 Jan 10. PMID: 22228201; PMCID: PMC4518733.

- Halliday J, Helmy K, Pattwell SS, Pitter KL, LaPlant Q, Ozawa T, Holland EC. **In vivo radiation response of proneural glioma characterized by protective p53 transcriptional program and proneural-mesenchymal shift.** Proc Natl Acad Sci U S A. 2014 Apr 8;111(14):5248-53. doi: 10.1073/pnas.1321014111. Epub 2014 Mar 24. PMID: 24706837; PMCID: PMC3986190.

- Hambardzumyan D, Bergers G. **Glioblastoma: Defining Tumor Niches.** Trends Cancer. 2015 Dec;1(4):252-265. doi: 10.1016/j.trecan.2015.10.009. PMID: 27088132; PMCID: PMC4831073.

- Hanahan D, Folkman J. **Patterns and emerging mechanisms of the angiogenic switch during tumorigenesis.** Cell. 1996 Aug 9;86(3):353-64. doi: 10.1016/s0092-8674(00)80108-7. PMID: 8756718.

- Hanif F, Muzaffar K, Perveen K, Malhi SM, Simjee ShU. **Glioblastoma Multiforme: A Review of its Epidemiology and Pathogenesis through Clinical Presentation and Treatment.** Asian Pac J Cancer Prev. 2017 Jan 1;18(1):3-9. doi: 10.22034/APJCP.2017.18.1.3. PMID: 28239999; PMCID: PMC5563115.

- Hartmann C, Hentschel B, Wick W, Capper D, Felsberg J, Simon M, Westphal M, Schackert G, Meyermann R, Pietsch T, Reifenberger G, Weller M, Loeffler M, von Deimling A. **Patients with IDH1 wild type anaplastic astrocytomas exhibit worse prognosis than IDH1-mutated glioblastomas, and IDH1 mutation status accounts for the unfavorable prognostic effect of higher age: implications for classification of gliomas.** Acta Neuropathol. 2010 Dec;120(6):707-18. doi: 10.1007/s00401-010-0781-z. Epub 2010 Nov 19. PMID: 21088844.

- Hegi ME, Diserens AC, Gorlia T, Hamou MF, de Tribolet N, Weller M, Kros JM, Hainfellner JA, Mason W, Mariani L, Bromberg JE, Hau P, Mirimanoff RO, Cairncross JG, Janzer RC, Stupp R. **MGMT gene silencing and benefit from temozolomide in glioblastoma**. N Engl J Med. 2005 Mar 10;352(10):997-1003. doi: 10.1056/NEJMoa043331. PMID: 15758010.

- Hill MM, Bastiani M, Luetterforst R, Kirkham M, Kirkham A, Nixon SJ, Walser P, Abankwa D, Oorschot VM, Martin S, Hancock JF, Parton RG. **PTRF-Cavin, a conserved cytoplasmic protein required for caveola formation and function.** Cell. 2008 Jan 11;132(1):113-24. doi: 10.1016/j.cell.2007.11.042. PMID: 18191225; PMCID: PMC2265257.

- Hsu JF, Chu SM, Liao CC, Wang CJ, Wang YS, Lai MY, Wang HC, Huang HR, Tsai MH. **Nanotechnology and Nanocarrier-Based Drug Delivery as the Potential Therapeutic Strategy for Glioblastoma Multiforme: An Update.** Cancers (Basel). 2021 Jan 7;13(2):195. doi: 10.3390/cancers13020195. PMID: 33430494; PMCID: PMC7827410.

- Hu Y, Smyth GK. **ELDA: extreme limiting dilution analysis for comparing depleted and enriched populations in stem cell and other assays.** J Immunol Methods. 2009 Aug 15;347(1-2):70-8. doi: 10.1016/j.jim.2009.06.008. Epub 2009 Jun 28. PMID: 19567251.

- Hume DA. **Macrophages as APC and the dendritic cell myth.** J Immunol. 2008 Nov 1;181(9):5829-35. doi: 10.4049/jimmunol.181.9.5829. PMID: 18941170.

- Iacob G, Dinca EB. **Current data and strategy in glioblastoma multiforme.** J Med Life. 2009 Oct-Dec;2(4):386-93. PMID: 20108752; PMCID: PMC3019011.

- Jain AK, Thareja S. **In vitro and in vivo characterization of pharmaceutical nanocarriers used for drug delivery**. Artif Cells Nanomed Biotechnol. 2019 Dec;47(1):524-539. doi: 10.1080/21691401.2018.1561457. PMID: 30784319.

- Jeon HM, Sohn YW, Oh SY, Kim SH, Beck S, Kim S, Kim H. **ID4 imparts chemoresistance and cancer stemness to glioma cells by derepressing miR-9*-mediated suppression of SOX2.** Cancer Res. 2011 May 1;71(9):3410-21. doi: 10.1158/0008-5472.CAN-10-3340. Erratum in: Cancer Res. 2011 Jun 15;71(12):4325. Erratum in: Cancer Res. 2011 Sep 15;71(18):6085. Oh, Se-Young [corrected to Oh, Se-Yeong]. PMID: 21531766.

- Johnson DR, Guerin JB, Giannini C, Morris JM, Eckel LJ, Kaufmann TJ. **2016 Updates to the WHO Brain Tumor Classification System: What the Radiologist Needs to Know.** Radiographics. 2017 Nov-Dec;37(7):2164-2180. doi: 10.1148/rg.2017170037. Epub 2017 Oct 13. PMID: 29028423.

- Jones AR, Shusta EV. **Blood-brain barrier transport of therapeutics via receptor-mediation.** Pharm Res. 2007 Sep;24(9):1759-71. doi: 10.1007/s11095-007-9379-0. Epub 2007 Jul 10. PMID: 17619996; PMCID: PMC2685177.

- Kadry H, Noorani B, Cucullo L. **A blood-brain barrier overview on structure, function, impairment, and biomarkers of integrity.** Fluids Barriers CNS. 2020 Nov 18;17(1):69. doi: 10.1186/s12987-020-00230-3. PMID: 33208141; PMCID: PMC7672931.

- Kam WW, Banati RB. **Effects of ionizing radiation on mitochondria.** Free Radic Biol Med. 2013 Dec;65:607-619. doi: 10.1016/j.freeradbiomed.2013.07.024. Epub 2013 Jul 26. PMID: 23892359.

- Khan M, Sherwani S, Khan S, Alouffi S, Alam M, Al-Motair K, Khan S. **Insights into Multifunctional Nanoparticle-Based Drug Delivery Systems for Glioblastoma Treatment.** Molecules. 2021 Apr 14;26(8):2262. doi: 10.3390/molecules26082262. PMID: 33919694; PMCID: PMC8069805.

- Kawano M, Tanaka K, Itonaga I, Iwasaki T, Miyazaki M, Ikeda S, Tsumura H. **Dendritic cells combined with doxorubicin induces immunogenic cell death and exhibits antitumor effects for osteosarcoma.** Oncol Lett. 2016 Mar;11(3):2169-2175. doi: 10.3892/ol.2016.4175. Epub 2016 Feb 2. PMID: 26998143; PMCID: PMC4774596.

- Ke W, Shao K, Huang R, Han L, Liu Y, Li J, Kuang Y, Ye L, Lou J, Jiang C. **Gene delivery targeted to the brain using an Angiopep-conjugated polyethyleneglycol-modified polyamidoamine dendrimer.** Biomaterials. 2009 Dec;30(36):6976-85. doi: 10.1016/j.biomaterials.2009.08.049. Epub 2009 Sep 17. PMID: 19765819.

- Kim Y, Varn FS, Park SH, Yoon BW, Park HR, Lee C, Verhaak RGW, Paek SH. **Perspective of mesenchymal transformation in glioblastoma**. Acta Neuropathol Commun. 2021 Mar 24;9(1):50. doi: 10.1186/s40478-021-01151-4. PMID: 33762019; PMCID: PMC7992784.

- Kommareddy S., Shenoy D.B., and Amiji M.M. **Long-Circulating Polymeric Nanoparticles for Drug and Gene Delivery to Tumors.** December 2006, DOI: 10.1201/9781420006636.ch13 In book: Nanotechnology for Cancer Therapy

- Komori T. **The 2016 WHO Classification of Tumours of the Central Nervous System: The Major Points of Revision**. Neurol Med Chir (Tokyo). 2017 Jul 15;57(7):301-311. doi: 10.2176/nmc.ra.2017-0010. Epub 2017 Jun 8. PMID: 28592714; PMCID: PMC5566703.

- Kong Z, Wang Y, Ma W. **Vaccination in the immunotherapy of glioblastoma**. Hum Vaccin Immunother. 2018 Feb 1;14(2):255-268. doi: 10.1080/21645515.2017.1388481. Epub 2017 Dec 11. PMID: 29087782; PMCID: PMC5806656.

- Kroemer G, Galluzzi L, Kepp O, Zitvogel L. **Immunogenic cell death in cancer therapy.** Annu Rev Immunol. 2013;31:51-72. doi: 10.1146/annurev-immunol-032712-100008. Epub 2012 Nov 12. PMID: 23157435.
- Kumar P and Clark M. **Neurological diseases in Kumar & Clark Clinical Medicine**. 6th ed. Elsevier Saunders, (2005) Edinburgh, pp 1244-45.

- Land CA, Musich PR, Haydar D, Krenciute G, Xie Q. **Chimeric antigen receptor T-cell therapy in glioblastoma: charging the T cells to fight**. J Transl Med. 2020 Nov 11;18(1):428. doi: 10.1186/s12967-020-02598-0. PMID: 33176788; PMCID: PMC7659102.

- Lathia JD, Mack SC, Mulkearns-Hubert EE, Valentim CL, Rich JN. **Cancer stem cells in glioblastoma.** Genes Dev. 2015 Jun 15;29(12):1203-17. doi: 10.1101/gad.261982.115. PMID: 26109046; PMCID: PMC4495393.

- Lee S, Park K, Lee SY, Ryu JH, Park JW, Ahn HJ, Kwon IC, Youn IC, Kim K, Choi K. **Dark quenched matrix metalloproteinase fluorogenic probe for imaging osteoarthritis development in vivo.** Bioconjug Chem. 2008 Sep;19(9):1743-7. doi: 10.1021/bc800264z. Epub 2008 Aug 26. PMID: 18729392.

- Lee SY. **Temozolomide resistance in glioblastoma multiforme.** Genes Dis. 2016 May 11;3(3):198-210. doi: 10.1016/j.gendis.2016.04.007. PMID: 30258889; PMCID: PMC6150109.

- Lemée JM, Clavreul A, Menei P. **Intratumoral heterogeneity in glioblastoma: don't forget the peritumoral brain zone.** Neuro Oncol. 2015 Oct;17(10):1322-32. doi: 10.1093/neuonc/nov119. Epub 2015 Jul 22. PMID: 26203067; PMCID: PMC4578587.

- Li R, Tian F, Qi Y, Ma L, Zhou T, Li Y, Hui T, Zhang L, Wang S, Song Z. **Pegylated liposomal doxorubicin plus cyclophosphamide followed by docetaxel as neoadjuvant chemotherapy in locally advanced breast cancer (registration number: ChiCTR1900023052).** Sci Rep. 2019 Dec 2;9(1):18135. doi: 10.1038/s41598-019-54387-5. PMID: 31792258; PMCID: PMC6889495.

- Lim M, Xia Y, Bettegowda C, Weller M. **Current state of immunotherapy for glioblastoma**. Nat Rev Clin Oncol. 2018 Jul;15(7):422-442. doi: 10.1038/s41571-018-0003-5. PMID: 29643471.

- Liu, R., Kay, B.K., Jiang, S. *et al.* **Nanoparticle Delivery: Targeting and Nonspecific Binding.** *MRS Bulletin* 34, 432–440 (2009). https://doi.org/10.1557/mrs2009.119

- Liu XY, Gerges N, Korshunov A, Sabha N, Khuong-Quang DA, Fontebasso AM, Fleming A, Hadjadj D, Schwartzentruber J, Majewski J, Dong Z, Siegel P, Albrecht S, Croul S, Jones DT, Kool M, Tonjes M, Reifenberger G, Faury D, Zadeh G, Pfister S, Jabado N. **Frequent ATRX mutations and loss of expression in adult diffuse astrocytic tumors carrying IDH1/IDH2 and TP53 mutations.** Acta Neuropathol. 2012 Nov;124(5):615-25. doi: 10.1007/s00401-012-1031-3. Epub 2012 Aug 12. PMID: 22886134.

- Lockman PR, Mittapalli RK, Taskar KS, Rudraraju V, Gril B, Bohn KA, Adkins CE, Roberts A, Thorsheim HR, Gaasch JA, Huang S, Palmieri D, Steeg PS, Smith QR. **Heterogeneous blood-tumor barrier permeability determines drug efficacy in experimental brain metastases of breast cancer.** Clin Cancer Res. 2010 Dec 1;16(23):5664-78. doi: 10.1158/1078-0432.CCR-10-1564. Epub 2010 Sep 9. PMID: 20829328; PMCID: PMC2999649.

- Löscher W, Potschka H. **Role of drug efflux transporters in the brain for drug disposition and treatment of brain diseases**. Prog Neurobiol. 2005 May;76(1):22-76. doi: 10.1016/j.pneurobio.2005.04.006. PMID: 16011870.

- Louis DN, Ohgaki H, Wiestler OD, Cavenee WK, Burger PC, Jouvet A, Scheithauer BW, Kleihues P. **The 2007 WHO classification of tumours of the central nervous system**. Acta Neuropathol. 2007 Aug;114(2):97-109. doi: 10.1007/s00401-007-0243-4. Epub 2007 Jul 6. Erratum in: Acta Neuropathol. 2007 Nov;114(5):547. PMID: 17618441; PMCID: PMC1929165.

- Louis DN, Perry A, Reifenberger G, von Deimling A, Figarella-Branger D, Cavenee WK, Ohgaki H, Wiestler OD, Kleihues P, Ellison DW. **The 2016 World Health Organization Classification of Tumors of the Central Nervous System: a summary**. Acta Neuropathol. 2016 Jun;131(6):803-20. doi: 10.1007/s00401-016-1545-1. Epub 2016 May 9. PMID: 27157931.

- Lowther DE, Goods BA, Lucca LE, Lerner BA, Raddassi K, van Dijk D, Hernandez AL, Duan X, Gunel M, Coric V, Krishnaswamy S, Love JC, Hafler DA. **PD-1 marks dysfunctional regulatory T cells in malignant gliomas.** JCI Insight. 2016 Apr 21;1(5):e85935. doi: 10.1172/jci.insight.85935. PMID: 27182555; PMCID: PMC4864991.

- MacArthur BD, Lemischka IR. **Statistical mechanics of pluripotency.** Cell. 2013 Aug 1;154(3):484-9. doi: 10.1016/j.cell.2013.07.024. PMID: 23911316.

- Mahringer A, Fricker G. **ABC transporters at the blood-brain barrier.** Expert Opin Drug Metab Toxicol. 2016 May;12(5):499-508. doi: 10.1517/17425255.2016.1168804. Epub 2016 Apr 4. PMID: 26998936.

- Maletínská L, Blakely EA, Bjornstad KA, Deen DF, Knoff LJ, Forte TM. **Human glioblastoma cell lines: levels of low-density lipoprotein receptor and low-density lipoprotein receptor-related protein.** Cancer Res. 2000 Apr 15;60(8):2300-3. PMID: 10786698.

- Malinovskaya Y, Melnikov P, Baklaushev V, Gabashvili A, Osipova N, Mantrov S, Ermolenko Y, Maksimenko O, Gorshkova M, Balabanyan V, Kreuter J, Gelperina S. **Delivery of doxorubicin-loaded PLGA nanoparticles into U87 human glioblastoma cells.** Int J Pharm. 2017 May 30;524(1-2):77-90. doi: 10.1016/j.ijpharm.2017.03.049. Epub 2017 Mar 27. PMID: 28359811.

- Marchal S, El Hor A, Millard M, Gillon V, Bezdetnaya L. **Anticancer Drug Delivery: An Update on Clinically Applied Nanotherapeutics.** Drugs. 2015 Sep;75(14):1601-11. doi: 10.1007/s40265-015-0453-3. PMID: 26323338.

- Matsumura Y, Maeda H. **A new concept for macromolecular therapeutics in cancer chemotherapy: mechanism of tumoritropic accumulation of proteins and the antitumor agent smancs.** Cancer Res. 1986 Dec;46(12 Pt 1):6387-92. PMID: 2946403.

- Maurer N, Fenske DB, Cullis PR. **Developments in liposomal drug delivery systems**. Expert Opin Biol Ther. 2001 Nov;1(6):923-47. doi: 10.1517/14712598.1.6.923. PMID: 11728226.

- McNamara MG, Jiang H, Lim-Fat MJ, Sahebjam S, Kiehl TR, Karamchandani J, Coire C, Chung C, Millar BA, Laperriere N, Mason WP. **Treatment Outcomes in 1p19q Co-deleted/Partially Deleted Gliomas.** Can J Neurol Sci. 2017 May;44(3):288-294. doi: 10.1017/cjn.2016.420. PMID: 28488951.

- Menei P, Capelle L, Guyotat J, Fuentes S, Assaker R, Bataille B, François P, Dorwling-Carter D, Paquis P, Bauchet L, Parker F, Sabatier J, Faisant N, Benoit JP. **Local and sustained delivery of 5-fluorouracil from biodegradable microspheres for the radiosensitization of malignant glioma: a randomized phase II trial.** Neurosurgery. 2005 Feb;56(2):242-8; discussion 242-8. doi: 10.1227/01.neu.0000144982.82068.a2. PMID: 15670372.

- Miller K, Dixit S, Bredlau AL, Moore A, McKinnon E, Broome AM. **Delivery of a drug cache to glioma cells overexpressing platelet-derived growth factor receptor using lipid nanocarriers.** Nanomedicine (Lond). 2016 Mar;11(6):581-95. doi: 10.2217/nnm.15.218. Epub 2016 Mar 22. PMID: 27003178; PMCID: PMC5561905.

- Minata M, Audia A, Shi J, Lu S, Bernstock J, Pavlyukov MS, Das A, Kim SH, Shin YJ, Lee Y, Koo H, Snigdha K, Waghmare I, Guo X, Mohyeldin A, Gallego-Perez D, Wang J, Chen D, Cheng P, Mukheef F, Contreras M, Reyes JF, Vaillant B, Sulman EP, Cheng SY, Markert JM, Tannous BA, Lu X, Kango-Singh M, Lee LJ, Nam DH, Nakano I, Bhat KP. **Phenotypic Plasticity of Invasive Edge Glioma Stem-like Cells in Response to Ionizing Radiation.** Cell Rep. 2019 Feb 12;26(7):1893-1905.e7. doi: 10.1016/j.celrep.2019.01.076. PMID: 30759398; PMCID: PMC6594377.

- Miura Y, Takenaka T, Toh K, Wu S, Nishihara H, Kano MR, Ino Y, Nomoto T, Matsumoto Y, Koyama H, Cabral H, Nishiyama N, Kataoka K. **Cyclic RGD-linked polymeric micelles for targeted delivery of platinum anticancer drugs to glioblastoma through the blood-brain tumor barrier.** ACS Nano. 2013 Oct 22;7(10):8583-92. doi: 10.1021/nn402662d. Epub 2013 Sep 18. PMID: 24028526.

- Moghimi SM, Hunter AC, Murray JC. **Long-circulating and target-specific nanoparticles: theory to practice.** Pharmacol Rev. 2001 Jun;53(2):283-318. PMID: 11356986.

- Mohtashami E, Shafaei-Bajestani N, Mollazadeh H, Mousavi SH, Jalili-Nik M, Sahebkar A, Afshari AR. **The Current State of Potential Therapeutic Modalities for Glioblastoma Multiforme: A Clinical Review**. Curr Drug Metab. 2020;21(8):564-578. doi: 10.2174/1389200221666200714101038. PMID: 32664839.

- Mok H, Bae KH, Ahn CH, Park TG. **PEGylated and MMP-2 specifically dePEGylated quantum dots: comparative evaluation of cellular uptake.** Langmuir. 2009 Feb 3;25(3):1645-50. doi: 10.1021/la803542v. PMID: 19117377.

- Montcourrier P, Silver I, Farnoud R, Bird I, Rochefort H. **Breast cancer cells have a high capacity to acidify extracellular milieu by a dual mechanism.** Clin Exp Metastasis. 1997 Jul;15(4):382-92. doi: 10.1023/a:1018446104071. PMID: 9219726.

- Moreno M, Pedrosa L, Paré L, Pineda E, Bejarano L, Martínez J, Balasubramaniyan V, Ezhilarasan R, Kallarackal N, Kim SH, Wang J, Audia A, Conroy S, Marin M, Ribalta T, Pujol T, Herreros A, Tortosa A, Mira H, Alonso MM, Gómez-Manzano C, Graus F, Sulman EP, Piao X, Nakano I, Prat A, Bhat KP, de la Iglesia N. **GPR56/ADGRG1 Inhibits Mesenchymal Differentiation and Radioresistance in Glioblastoma.** Cell Rep. 2017 Nov 21;21(8):2183-2197. doi: 10.1016/j.celrep.2017.10.083. PMID: 29166609.

- Morton DB, Griffiths PH. **Guidelines on the recognition of pain, distress and discomfort in experimental animals and an hypothesis for assessment.** Vet Rec. 1985 Apr 20;116(16):431-6. doi: 10.1136/vr.116.16.431. PMID: 3923690.

- Mrugala MM. **Advances and challenges in the treatment of glioblastoma: a clinician's perspective.** Discov Med. 2013 Apr;15(83):221-30. PMID: 23636139.

- Nałęcz KA. Solute Carriers in the Blood-Brain Barier: Safety in Abundance. Neurochem Res. 2017 Mar;42(3):795-809. doi: 10.1007/s11064-016-2030-x. Epub 2016 Aug 9. PMID: 27503090.

- Neftel C, Laffy J, Filbin MG, Hara T, Shore ME, Rahme GJ, Richman AR, Silverbush D, Shaw ML, Hebert CM, Dewitt J, Gritsch S, Perez EM, Gonzalez Castro LN, Lan X, Druck N, Rodman C, Dionne D, Kaplan A, Bertalan MS, Small J, Pelton K, Becker S, Bonal D, Nguyen QD, Servis RL, Fung JM, Mylvaganam R, Mayr L, Gojo J, Haberler C, Geyeregger R, Czech T, Slavc I, Nahed BV, Curry WT, Carter BS, Wakimoto H, Brastianos PK, Batchelor TT, Stemmer-Rachamimov A, Martinez-Lage M, Frosch MP, Stamenkovic I, Riggi N, Rheinbay E, Monje M, Rozenblatt-Rosen O, Cahill DP, Patel AP, Hunter T, Verma IM, Ligon KL, Louis DN, Regev A, Bernstein BE, Tirosh I, Suvà ML. **An Integrative Model of Cellular States, Plasticity, and Genetics for Glioblastoma.** Cell. 2019 Aug 8;178(4):835-849.e21. doi: 10.1016/j.cell.2019.06.024. Epub 2019 Jul 18. PMID: 31327527; PMCID: PMC6703186.

- Newton HB, Chapter 2 - **Overview of Pathology and Treatment of Primary Brain Tumors,** Editor(s): Herbert B. Newton, Handbook of Neuro-Oncology Neuroimaging (Second Edition), Academic Press, 2016, Pages 9-22, ISBN 9780128009451, https://doi.org/10.1016/B978-0-12-800945-1.00002-1.

- Nakada M, Kita D, Watanabe T, Hayashi Y, Teng L, Pyko IV, Hamada J. **Aberrant signaling pathways in glioma.** Cancers (Basel). 2011 Aug 10;3(3):3242-78. doi: 10.3390/cancers3033242. PMID: 24212955; PMCID: PMC3759196.

- Nelson SJ, Cha S. **Imaging glioblastoma multiforme.** Cancer J. 2003 Mar-Apr;9(2):134-45. doi: 10.1097/00130404-200303000-00009. PMID: 12784879.

- Noch EK, Ramakrishna R, Magge R. **Challenges in the Treatment of Glioblastoma: Multisystem Mechanisms of Therapeutic Resistance.** World Neurosurg. 2018 Aug;116:505-517. doi: 10.1016/j.wneu.2018.04.022. PMID: 30049045.

- Ohgaki H, Kleihues P. **Genetic pathways to primary and secondary glioblastoma.** Am J Pathol. 2007 May;170(5):1445-53. doi: 10.2353/ajpath.2007.070011. PMID: 17456751; PMCID: PMC1854940.

- Ohgaki H, Kleihues P. **The definition of primary and secondary glioblastoma.** Clin Cancer Res. 2013 Feb 15;19(4):764-72. doi: 10.1158/1078-0432.CCR-12-3002. Epub 2012 Dec 3. PMID: 23209033.

- Omuro A, Vlahovic G, Lim M, Sahebjam S, Baehring J, Cloughesy T, Voloschin A, Ramkissoon SH, Ligon KL, Latek R, Zwirtes R, Strauss L, Paliwal P, Harbison CT, Reardon DA, Sampson JH. **Nivolumab with or without ipilimumab in patients with recurrent glioblastoma: results from exploratory phase I cohorts of CheckMate 143.** Neuro Oncol. 2018 Apr 9;20(5):674-686. doi: 10.1093/neuonc/nox208. PMID: 29106665; PMCID: PMC5892140.

- Ong DST, Hu B, Ho YW, Sauvé CG, Bristow CA, Wang Q, Multani AS, Chen P, Nezi L, Jiang S, Gorman CE, Monasterio MM, Koul D, Marchesini M, Colla S, Jin EJ, Sulman EP, Spring DJ, Yung WA, Verhaak RGW, Chin L, Wang YA, DePinho RA. **PAF promotes stemness and radioresistance of glioma stem cells.** Proc Natl Acad Sci U S A. 2017 Oct 24;114(43):E9086-E9095. doi: 10.1073/pnas.1708122114. Epub 2017 Oct 9. PMID: 29073105; PMCID: PMC5664518.

- Park CK, Kim J, Yim SY, Lee AR, Han JH, Kim CY, Park SH, Kim TM, Lee SH, Choi SH, Kim SK, Kim DG, Jung HW. **Usefulness of MS-MLPA for detection of MGMT promoter methylation in the evaluation of pseudoprogression in glioblastoma patients.** Neuro Oncol. 2011 Feb;13(2):195-202. doi: 10.1093/neuonc/noq162. Epub 2010 Nov 12. PMID: 21075779; PMCID: PMC3064622.

- Patel AP, Tirosh I, Trombetta JJ, Shalek AK, Gillespie SM, Wakimoto H, Cahill DP, Nahed BV, Curry WT, Martuza RL, Louis DN, Rozenblatt-Rosen O, Suvà ML, Regev A, Bernstein BE. **Single-cell RNA-seq highlights intratumoral heterogeneity in primary glioblastoma.** Science. 2014 Jun 20;344(6190):1396-401. doi: 10.1126/science.1254257. Epub 2014 Jun 12. PMID: 24925914; PMCID: PMC4123637.

- Pirmoradi L, Seyfizadeh N, Ghavami S, Zeki AA, Shojaei S. **Targeting cholesterol metabolism in glioblastoma: a new therapeutic approach in cancer therapy.** J Investig Med. 2019 Apr;67(4):715-719. doi: 10.1136/jim-2018-000962. Epub 2019 Feb 14. PMID: 30765502.

- Pisco AO, Brock A, Zhou J, Moor A, Mojtahedi M, Jackson D, Huang S. **Non-Darwinian dynamics in therapy-induced cancer drug resistance.** Nat Commun. 2013;4:2467. doi: 10.1038/ncomms3467. PMID: 24045430; PMCID: PMC4657953.

- Povlsen LK, Beli P, Wagner SA, Poulsen SL, Sylvestersen KB, Poulsen JW, Nielsen ML, Bekker-Jensen S, Mailand N, Choudhary C. **Systems-wide analysis of ubiquitylation dynamics reveals a key role for PAF15 ubiquitylation in DNA-damage bypass.** Nat Cell Biol. 2012 Oct;14(10):1089-98. doi: 10.1038/ncb2579. Epub 2012 Sep 23. PMID: 23000965.

- Prager BC, Bhargava S, Mahadev V, Hubert CG, Rich JN. **Glioblastoma Stem Cells: Driving Resilience through Chaos.** Trends Cancer. 2020 Mar;6(3):223-235. doi: 10.1016/j.trecan.2020.01.009. Epub 2020 Feb 3. PMID: 32101725.

- Preusser M, Lim M, Hafler DA, Reardon DA, Sampson JH. **Prospects of immune checkpoint modulators in the treatment of glioblastoma**. Nat Rev Neurol. 2015 Sep;11(9):504-14. doi: 10.1038/nrneurol.2015.139. Epub 2015 Aug 11. PMID: 26260659; PMCID: PMC4782584.

- Pulgar VM. **Transcytosis to Cross the Blood Brain Barrier, New Advancements and Challenges.** Front Neurosci. 2019 Jan 11;12:1019. doi: 10.3389/fnins.2018.01019. PMID: 30686985; PMCID: PMC6337067.

- Qian C, Li P, Yan W, Shi L, Zhang J, Wang Y, Liu H, You Y. **Downregulation of osteopontin enhances the sensitivity of glioma U251 cells to temozolomide and cisplatin by targeting the NF-κB/Bcl−2 pathway.** Mol Med Rep. 2015 Mar;11(3):1951-5. doi: 10.3892/mmr.2014.2951. Epub 2014 Nov 14. PMID: 25405848.

- Qian WY, Sun DM, Zhu RR, Du XL, Liu H, Wang SL. **pH-sensitive strontium carbonate nanoparticles as new anticancer vehicles for controlled etoposide release.** Int J Nanomedicine. 2012;7:5781-92. doi: 10.2147/IJN.S34773. Epub 2012 Nov 20. PMID: 23185118; PMCID: PMC3506155.

- Rafiyath SM, Rasul M, Lee B, Wei G, Lamba G, Liu D. **Comparison of safety and toxicity of liposomal doxorubicin vs. conventional anthracyclines: a meta-analysis.** Exp Hematol Oncol. 2012 Apr 23;1(1):10. doi: 10.1186/2162-3619-1-10. PMID: 23210520; PMCID: PMC3514106.

- Ramachandran RK, Sørensen MD, Aaberg-Jessen C, Hermansen SK, Kristensen BW. **Expression and prognostic impact of matrix metalloproteinase-2 (MMP-2) in astrocytomas.** PLoS One. 2017 Feb 24;12(2):e0172234. doi: 10.1371/journal.pone.0172234. PMID: 28234925; PMCID: PMC5325257.

- Rapoport BL, Anderson R. **Realizing the Clinical Potential of Immunogenic Cell Death in Cancer Chemotherapy and Radiotherapy.** Int J Mol Sci. 2019 Feb 22;20(4):959. doi: 10.3390/ijms20040959. PMID: 30813267; PMCID: PMC6412296.

- Re F, Cambianica I, Zona C, Sesana S, Gregori M, Rigolio R, La Ferla B, Nicotra F, Forloni G, Cagnotto A, Salmona M, Masserini M, Sancini G**. Functionalization of liposomes with ApoE-derived peptides at different density affects cellular uptake and drug transport across a blood-brain barrier model.** Nanomedicine. 2011 Oct;7(5):551-9. doi: 10.1016/j.nano.2011.05.004. Epub 2011 May 20. PMID: 21658472.

- Reardon DA, Brandes AA, Omuro A, Mulholland P, Lim M, Wick A, Baehring J, Ahluwalia MS, Roth P, Bähr O, Phuphanich S, Sepulveda JM, De Souza P, Sahebjam S, Carleton M, Tatsuoka K, Taitt C, Zwirtes R, Sampson J, Weller M. **Effect of Nivolumab vs Bevacizumab in Patients With Recurrent Glioblastoma: The CheckMate 143 Phase 3 Randomized Clinical Trial.** JAMA Oncol. 2020 Jul 1;6(7):1003-1010. doi: 10.1001/jamaoncol.2020.1024. PMID: 32437507; PMCID: PMC7243167.

- Reardon D, Kaley T, Dietrich J, Clarke JL, Dunn GP, Lim M, Cloughesy T, Gan HK, Park A, Schwarzenberger P, Ricciardi T, Macri M, Ryan A, Venhaus R. **ATIM-12. PHASE 2 STUDY TO EVALUATE THE CLINICAL EFFICACY AND SAFETY OF MEDI4736 (DURVALUMAB [DUR]) IN PATIENTS WITH BEVACIZUMAB (BEV)-REFRACTORY RECURRENT GLIOBLASTOMA (GBM)**. Neuro Oncol. 2017 Nov;19(Suppl 6):vi28. doi: 10.1093/neuonc/nox168.108. Epub 2017 Nov 6. PMCID: PMC5692026.

- Reardon DA, Wen PY. **Therapeutic advances in the treatment of glioblastoma: rationale and potential role of targeted agents**. Oncologist. 2006 Feb;11(2):152-64. doi: 10.1634/theoncologist.11-2-152. PMID: 16476836.

- Rideau E , Dimova R , Schwille P , Wurm FR , Landfester K . **Liposomes and polymersomes: a comparative review towards cell mimicking.** Chem Soc Rev. 2018 Nov 26;47(23):8572-8610. doi: 10.1039/c8cs00162f. PMID: 30177983.

- Robin AM, Lee I, Kalkanis SN. **Reoperation for Recurrent Glioblastoma Multiforme**. Neurosurg Clin N Am. 2017 Jul;28(3):407-428. doi: 10.1016/j.nec.2017.02.007. PMID: 28600015.

- Rooj AK, Ricklefs F, Mineo M, Nakano I, Chiocca EA, Bronisz A, Godlewski J. **MicroRNA-Mediated Dynamic Bidirectional Shift between the Subclasses of Glioblastoma Stem-like Cells.** Cell Rep. 2017 Jun 6;19(10):2026-2032. doi: 10.1016/j.celrep.2017.05.040. PMID: 28591575; PMCID: PMC5514838.

- Salah Uddin ABM, Jarmi T (2015). **Neurologic manifestations of glioblastoma multiforme clinical presentation** [online]. Available at: http://emedicine.medscape.com/ article/1156220-clinical.

- Sanchez-Covarrubias L, Slosky LM, Thompson BJ, Davis TP, Ronaldson PT. **Transporters at CNS barrier sites: obstacles or opportunities for drug delivery?** Curr Pharm Des. 2014;20(10):1422-49. doi: 10.2174/13816128113199990463. PMID: 23789948; PMCID: PMC3913737.

- Sarkaria JN, Hu LS, Parney IF, Pafundi DH, Brinkmann DH, Laack NN, Giannini C, Burns TC, Kizilbash SH, Laramy JK, Swanson KR, Kaufmann TJ, Brown PD, Agar NYR, Galanis E, Buckner JC, Elmquist WF. **Is the blood-brain barrier really disrupted in all glioblastomas? A critical assessment of existing clinical data**. Neuro Oncol. 2018 Jan 22;20(2):184-191. doi: 10.1093/neuonc/nox175. PMID: 29016900; PMCID: PMC5777482.

- Scherer RL, VanSaun MN, McIntyre JO, Matrisian LM. **Optical imaging of matrix metalloproteinase-7 activity in vivo using a proteolytic nanobeacon.** Mol Imaging. 2008 May-Jun;7(3):118-31. PMID: 19123982; PMCID: PMC2777890.

- Schindelin J, Arganda-Carreras I, Frise E, Kaynig V, Longair M, Pietzsch T, Preibisch S, Rueden C, Saalfeld S, Schmid B, Tinevez JY, White DJ, Hartenstein V, Eliceiri K, Tomancak P, Cardona A. **Fiji: an open-source platform for biological-image analysis.** Nat Methods. 2012 Jun 28;9(7):676-82. doi: 10.1038/nmeth.2019. PMID: 22743772; PMCID: PMC3855844.

- Schwendener RA. **Liposomes in biology and medicine**. Adv Exp Med Biol. 2007;620:117-28. doi: 10.1007/978-0-387-76713-0_9. PMID: 18217339.

- Scott J, Tsai YY, Chinnaiyan P, Yu HH. **Effectiveness of radiotherapy for elderly patients with glioblastoma.** Int J Radiat Oncol Biol Phys. 2011 Sep 1;81(1):206-10. doi: 10.1016/j.ijrobp.2010.04.033. Epub 2010 Aug 2. PMID: 20675068.

- Segerman A, Niklasson M, Haglund C, Bergström T, Jarvius M, Xie Y, Westermark A, Sönmez D, Hermansson A, Kastemar M, Naimaie-Ali Z, Nyberg F, Berglund M, Sundström M, Hesselager G, Uhrbom L, Gustafsson M, Larsson R, Fryknäs M, Segerman B, Westermark B. **Clonal Variation in Drug and Radiation Response among Glioma-Initiating Cells Is Linked to Proneural-Mesenchymal Transition.** Cell Rep. 2016 Dec 13;17(11):2994-3009. doi: 10.1016/j.celrep.2016.11.056. PMID: 27974212.

- Sharma A, Madhunapantula SV, Robertson GP. **Toxicological considerations when creating nanoparticle-based drugs and drug delivery systems.** Expert Opin Drug Metab Toxicol. 2012 Jan;8(1):47-69. doi: 10.1517/17425255.2012.637916. Epub 2011 Nov 19. PMID: 22097965; PMCID: PMC3245366.

- Singh SK, Hawkins C, Clarke ID, Squire JA, Bayani J, Hide T, Henkelman RM, Cusimano MD, Dirks PB. **Identification of human brain tumour initiating cells.** Nature. 2004 Nov 18;432(7015):396-401. doi: 10.1038/nature03128. PMID: 15549107.

- Smith C, Ironside JW. **Diagnosis and pathogenesis of gliomas.** Current Diagnostic Pathology, Volume 13, Issue 3, 2007, Pages 180-192, ISSN 0968-6053, https://doi.org/10.1016/j.cdip.2007.04.002.

- Soares S, Sousa J, Pais A, Vitorino C. **Nanomedicine: Principles, Properties, and Regulatory Issues.** Front Chem. 2018 Aug 20;6:360. doi: 10.3389/fchem.2018.00360. PMID: 30177965; PMCID: PMC6109690.

- Song G, Wu H, Yoshino K, Zamboni WC. **Factors affecting the pharmacokinetics and pharmacodynamics of liposomal drugs**. J Liposome Res. 2012 Sep;22(3):177-92. doi: 10.3109/08982104.2012.655285. Epub 2012 Feb 15. PMID: 22332871.

- Soni V, Kohli DV, Jain SK. **Transferrin coupled liposomes as drug delivery carriers for brain targeting of 5-florouracil.** J Drug Target. 2005 May;13(4):245-50. doi: 10.1080/10611860500107401. PMID: 16051536.

- Soukhtanloo M, Mohtashami E, Maghrouni A, Mollazadeh H, Mousavi SH, Roshan MK, Tabatabaeizadeh SA, Hosseini A, Vahedi MM, Jalili-Nik M, Afshari AR. **Natural products as promising targets in glioblastoma multiforme: a focus on NF-κB signaling pathway**. Pharmacol Rep. 2020 Apr;72(2):285-295. doi: 10.1007/s43440-020-00081-7. Epub 2020 Mar 9. PMID: 32152926.

- Sneider A, VanDyke D, Paliwal S, Rai P. **Remotely Triggered Nano-Theranostics For Cancer Applications.** Nanotheranostics. 2017;1(1):1-22. doi: 10.7150/ntno.17109. PMID: 28191450; PMCID: PMC5298883.

- Stupp R, Lukas RV, Hegi ME. **Improving survival in molecularly selected glioblastoma.** Lancet. 2019 Feb 16;393(10172):615-617. doi: 10.1016/S0140-6736(18)33211-2. Epub 2019 Feb 14. PMID: 30782332.

- Stupp R, Mason WP, van den Bent MJ, Weller M, Fisher B, Taphoorn MJ, Belanger K, Brandes AA, Marosi C, Bogdahn U, Curschmann J, Janzer RC, Ludwin SK, Gorlia T, Allgeier A, Lacombe D, Cairncross JG, Eisenhauer E, Mirimanoff RO; European Organisation for Research and Treatment of Cancer Brain Tumor and Radiotherapy Groups; National Cancer Institute of Canada Clinical Trials Group. **Radiotherapy plus concomitant and adjuvant temozolomide for glioblastoma.** N Engl J Med. 2005 Mar 10;352(10):987-96. doi: 10.1056/NEJMoa043330. PMID: 15758009.

- Swallow CJ, Grinstein S, Rotstein OD. **A vacuolar type H(+)-ATPase regulates cytoplasmic pH in murine macrophages.** J Biol Chem. 1990 May 5;265(13):7645-54. PMID: 2139663.

- Sweitzer SM, Hinshaw JE. **Dynamin undergoes a GTP-dependent conformational change causing vesiculation**. Cell. 1998 Jun 12;93(6):1021-9. doi: 10.1016/s0092-8674(00)81207-6. PMID: 9635431.

- Tamborini M, Locatelli E, Rasile M, Monaco I, Rodighiero S, Corradini I, Franchini MC, Passoni L, Matteoli M. **A Combined Approach Employing Chlorotoxin-Nanovectors and Low Dose Radiation To Reach Infiltrating Tumor Niches in Glioblastoma.** ACS Nano. 2016 Feb 23;10(2):2509-20. doi: 10.1021/acsnano.5b07375. Epub 2016 Feb 9. PMID: 26745323.

- Taylor OG, Brzozowski JS, Skelding KA. **Glioblastoma Multiforme: An Overview of Emerging Therapeutic Targets.** Front Oncol. 2019 Sep 26;9:963. doi: 10.3389/fonc.2019.00963. PMID: 31616641; PMCID: PMC6775189.

- Thakkar JP, Dolecek TA, Horbinski C, Ostrom QT, Lightner DD, Barnholtz-Sloan JS, Villano JL. **Epidemiologic and molecular prognostic review of glioblastoma.** Cancer Epidemiol Biomarkers Prev. 2014 Oct;23(10):1985-96. doi: 10.1158/1055-9965.EPI-14-0275. Epub 2014 Jul 22. PMID: 25053711; PMCID: PMC4185005.

- Torchilin VP. **Recent advances with liposomes as pharmaceutical carriers.** Nat Rev Drug Discov. 2005 Feb;4(2):145-60. doi: 10.1038/nrd1632. PMID: 15688077.

- van Vulpen M, Kal HB, Taphoorn MJ, El-Sharouni SY. **Changes in blood-brain barrier permeability induced by radiotherapy: implications for timing of chemotherapy?** (Review). Oncol Rep. 2002 Jul-Aug;9(4):683-8. PMID: 12066192.

- Verhaak RG, Hoadley KA, Purdom E, Wang V, Qi Y, Wilkerson MD, Miller CR, Ding L, Golub T, Mesirov JP, Alexe G, Lawrence M, O'Kelly M, Tamayo P, Weir BA, Gabriel S, Winckler W, Gupta S, Jakkula L, Feiler HS, Hodgson JG, James CD, Sarkaria JN, Brennan C, Kahn A, Spellman PT, Wilson RK, Speed TP, Gray JW, Meyerson M, Getz G,

Perou CM, Hayes DN; Cancer Genome Atlas Research Network. **Integrated genomic analysis identifies clinically relevant subtypes of glioblastoma characterized by abnormalities in PDGFRA, IDH1, EGFR, and NF1**. Cancer Cell. 2010 Jan 19;17(1):98-110. doi: 10.1016/j.ccr.2009.12.020. PMID: 20129251; PMCID: PMC2818769.

- Villa GR, Hulce JJ, Zanca C, Bi J, Ikegami S, Cahill GL, Gu Y, Lum KM, Masui K, Yang H, Rong X, Hong C, Turner KM, Liu F, Hon GC, Jenkins D, Martini M, Armando AM, Quehenberger O, Cloughesy TF, Furnari FB, Cavenee WK, Tontonoz P, Gahman TC, Shiau AK, Cravatt BF, Mischel PS. **An LXR-Cholesterol Axis Creates a Metabolic Co-Dependency for Brain Cancers.** Cancer Cell. 2016 Nov 14;30(5):683-693. doi: 10.1016/j.ccell.2016.09.008. Epub 2016 Oct 13. PMID: 27746144; PMCID: PMC5479636.

- Villaseñor R, Schilling M, Sundaresan J, Lutz Y, Collin L. **Sorting Tubules Regulate Blood-Brain Barrier Transcytosis.** Cell Rep. 2017 Dec 12;21(11):3256-3270. doi: 10.1016/j.celrep.2017.11.055. PMID: 29241551.

- Wadajkar AS, Dancy JG, Hersh DS, Anastasiadis P, Tran NL, Woodworth GF, Winkles JA, Kim AJ. **Tumor-targeted nanotherapeutics: overcoming treatment barriers for glioblastoma.** Wiley Interdiscip Rev Nanomed Nanobiotechnol. 2017 Jul;9(4):10.1002/wnan.1439. doi: 10.1002/wnan.1439. Epub 2016 Nov 4. PMID: 27813323; PMCID: PMC5418115.

- Wagner S, Zensi A, Wien SL, Tschickardt SE, Maier W, Vogel T, Worek F, Pietrzik CU, Kreuter J, von Briesen H. **Uptake mechanism of ApoE-modified nanoparticles on brain capillary endothelial cells as a blood-brain barrier model.** PLoS One. 2012;7(3):e32568. doi: 10.1371/journal.pone.0032568. Epub 2012 Mar 1. PMID: 22396775; PMCID: PMC3291552.

- Wahba A, Lehman SL, Tofilon PJ. **Radiation-induced translational control of gene expression.** Translation (Austin). 2016 Dec 1;5(1):e1265703. doi: 10.1080/21690731.2016.1265703. PMID: 28702276; PMCID: PMC5501380.

- Wang J, Cazzato E, Ladewig E, Frattini V, Rosenbloom DI, Zairis S, Abate F, Liu Z, Elliott O, Shin YJ, Lee JK, Lee IH, Park WY, Eoli M, Blumberg AJ, Lasorella A, Nam DH, Finocchiaro G, Iavarone A, Rabadan R. **Clonal evolution of glioblastoma under therapy.** Nat Genet. 2016 Jul;48(7):768-76. doi: 10.1038/ng.3590. Epub 2016 Jun 6. PMID: 27270107; PMCID: PMC5627776.

- Wang J, Shen F, Yao Y, Wang LL, Zhu Y, Hu J. **Adoptive Cell Therapy: A Novel and Potential Immunotherapy for Glioblastoma.** Front Oncol. 2020 Jan 31;10:59. doi: 10.3389/fonc.2020.00059. PMID: 32083009; PMCID: PMC7005203.

- Wang L, Babikir H, Müller S, Yagnik G, Shamardani K, Catalan F, Kohanbash G, Alvarado B, Di Lullo E, Kriegstein A, Shah S, Wadhwa H, Chang SM, Phillips JJ, Aghi MK, Diaz AA. **The Phenotypes of Proliferating Glioblastoma Cells Reside on a Single Axis of Variation.** Cancer Discov. 2019 Dec;9(12):1708-1719. doi: 10.1158/2159-8290.CD-19-0329. Epub 2019 Sep 25. PMID: 31554641; PMCID: PMC7161589.

- Wang Q, Hu B, Hu X, Kim H, Squatrito M, Scarpace L, deCarvalho AC, Lyu S, Li P, Li Y, Barthel F, Cho HJ, Lin YH, Satani N, Martinez-Ledesma E, Zheng S, Chang E, Sauvé CG, Olar A, Lan ZD, Finocchiaro G, Phillips JJ, Berger MS, Gabrusiewicz KR, Wang G, Eskilsson E, Hu J, Mikkelsen T, DePinho RA, Muller F, Heimberger AB, Sulman EP, Nam DH, Verhaak RGW. **Tumor Evolution of Glioma-Intrinsic Gene Expression Subtypes Associates with Immunological Changes in the Microenvironment.** Cancer Cell. 2017 Jul 10;32(1):42-56.e6. doi: 10.1016/j.ccell.2017.06.003. Erratum in: Cancer Cell. 2018 Jan 8;33(1):152. PMID: 28697342; PMCID: PMC5599156.

- Weissleder R, Tung CH, Mahmood U, Bogdanov A Jr. **In vivo imaging of tumors with protease-activated near-infrared fluorescent probes.** Nat Biotechnol. 1999 Apr;17(4):375-8. doi: 10.1038/7933. PMID: 10207887.

- Weller M, Pfister SM, Wick W, Hegi ME, Reifenberger G, Stupp R. **Molecular neuro-oncology in clinical practice: a new horizon**. Lancet Oncol. 2013 Aug;14(9):e370-9. doi: 10.1016/S1470-2045(13)70168-2. Erratum in: Lancet Oncol. 2015 May;16(5):e199. PMID: 23896276.

- Weller M, Wick W, Aldape K, Brada M, Berger M, Pfister SM, Nishikawa R, Rosenthal M, Wen PY, Stupp R, Reifenberger G. **Glioma.** Nat Rev Dis Primers. 2015 Jul 16;1:15017. doi: 10.1038/nrdp.2015.17. PMID: 27188790.

- Werfel TA, Cook RS. **Efferocytosis in the tumor microenvironment.** Semin Immunopathol. 2018 Nov;40(6):545-554. doi: 10.1007/s00281-018-0698-5. Epub 2018 Sep 5. PMID: 30187085; PMCID: PMC6223858.

- White BD, Duan C, Townley HE. **Nanoparticle Activation Methods in Cancer Treatment.** Biomolecules. 2019 May 24;9(5):202. doi: 10.3390/biom9050202. PMID: 31137744; PMCID: PMC6572460.

- Wicki A, Witzigmann D, Balasubramanian V, Huwyler J. **Nanomedicine in cancer therapy: challenges, opportunities, and clinical applications.** J Control Release. 2015 Feb 28;200:138-57. doi: 10.1016/j.jconrel.2014.12.030. Epub 2014 Dec 26. PMID: 25545217.

- Wiwatchaitawee K, Quarterman JC, Geary SM, Salem AK. **Enhancement of Therapies for Glioblastoma (GBM) Using Nanoparticle-based Delivery Systems.** AAPS PharmSciTech. 2021 Feb 11;22(2):71. doi: 10.1208/s12249-021-01928-9. PMID: 33575970; PMCID: PMC8092804.

- Wunder A, Tung CH, Müller-Ladner U, Weissleder R, Mahmood U. **In vivo imaging of protease activity in arthritis: a novel approach for monitoring treatment response.** Arthritis Rheum. 2004 Aug;50(8):2459-65. doi: 10.1002/art.20379. PMID: 15334458.

- Xavier-Magalhães A, Nandhabalan M, Jones C, Costa BM. **Molecular prognostic factors in glioblastoma: state of the art and future challenges.** CNS Oncol. 2013 Nov;2(6):495-510. doi: 10.2217/cns.13.48. PMID: 25054820; PMCID: PMC6136097.

- Xin H, Jiang X, Gu J, Sha X, Chen L, Law K, Chen Y, Wang X, Jiang Y, Fang X. **Angiopep-conjugated poly(ethylene glycol)-co-poly(ε-caprolactone) nanoparticles as dual-targeting drug delivery system for brain glioma.** Biomaterials. 2011 Jun;32(18):4293-305. doi: 10.1016/j.biomaterials.2011.02.044. Epub 2011 Mar 21. PMID: 21427009.

- Xu H, Zong H, Ma C, Ming X, Shang M, Li K, He X, Du H, Cao L. **Epidermal growth factor receptor in glioblastoma.** Oncol Lett. 2017 Jul;14(1):512-516. doi: 10.3892/ol.2017.6221. Epub 2017 May 22. PMID: 28693199; PMCID: PMC5494611.

- Yan H, Parsons DW, Jin G, McLendon R, Rasheed BA, Yuan W, Kos I, Batinic-Haberle I, Jones S, Riggins GJ, Friedman H, Friedman A, Reardon D, Herndon J, Kinzler KW, Velculescu VE, Vogelstein B, Bigner DD. **IDH1 and IDH2 mutations in gliomas.** N Engl J Med. 2009 Feb 19;360(8):765-73. doi: 10.1056/NEJMoa0808710. PMID: 19228619; PMCID: PMC2820383.

- Zanders ED, Svensson F, Bailey DS. **Therapy for glioblastoma: is it working?** Drug Discov Today. 2019 May;24(5):1193-1201. doi: 10.1016/j.drudis.2019.03.008. Epub 2019 Mar 13. PMID: 30878561.

- Zhao L, Zhang B. **Doxorubicin induces cardiotoxicity through upregulation of death receptors mediated apoptosis in cardiomyocytes**. Sci Rep. 2017 Mar 16;7:44735. doi: 10.1038/srep44735. PMID: 28300219; PMCID: PMC5353581.

- Zhao M, Ding XF, Shen JY, Zhang XP, Ding XW, Xu B. **Use of liposomal doxorubicin for adjuvant chemotherapy of breast cancer in clinical practice.** J Zhejiang Univ Sci B. 2017 Jan.;18(1):15-26. doi: 10.1631/jzus.B1600303. PMID: 28070993; PMCID: PMC5260474.

- Zhao M, van Straten D, Broekman MLD, Préat V, Schiffelers RM. **Nanocarrier-based drug combination therapy for glioblastoma**. Theranostics. 2020 Jan 1;10(3):1355-1372. doi: 10.7150/thno.38147. PMID: 31938069; PMCID: PMC6956816.

- Zhao Z, Nelson AR, Betsholtz C, Zlokovic BV**. Establishment and Dysfunction of the Blood-Brain Barrier.** Cell. 2015 Nov 19;163(5):1064-1078. doi: 10.1016/j.cell.2015.10.067. PMID: 26590417; PMCID: PMC4655822.

- Zikou A, Sioka C, Alexiou GA, Fotopoulos A, Voulgaris S, Argyropoulou MI. **Radiation Necrosis, Pseudoprogression, Pseudoresponse, and Tumor Recurrence: Imaging Challenges for the Evaluation of Treated Gliomas.** Contrast Media Mol Imaging. 2018 Dec 2;2018:6828396. doi: 10.1155/2018/6828396. PMID: 30627060; PMCID: PMC6305027.

- Zlokovic BV. **Neurovascular pathways to neurodegeneration in Alzheimer's disease and other disorders.** Nat Rev Neurosci. 2011 Nov 3;12(12):723-38. doi: 10.1038/nrn3114. PMID: 22048062; PMCID: PMC4036520.